

University of Alberta

**USE OF RADARSAT-1 SATELLITE IMAGERY AND
GEOPHYSICAL DATA FOR OIL AND KIMBERLITE
EXPLORATION**

by

Flora Paganelli



A thesis submitted to the Faculty of Graduate Studies and Research
in partial fulfillment to the requirements for the degree of
Doctor of Philosophy

Department of Earth and Atmospheric Sciences

Edmonton, Alberta

Fall 2002



National Library
of Canada

Acquisitions and
Bibliographic Services

395 Wellington Street
Ottawa ON K1A 0N4
Canada

Bibliothèque nationale
du Canada

Acquisitions et
services bibliographiques

395, rue Wellington
Ottawa ON K1A 0N4
Canada

Your file *Votre référence*

Our file *Notre référence*

The author has granted a non-exclusive licence allowing the National Library of Canada to reproduce, loan, distribute or sell copies of this thesis in microform, paper or electronic formats.

The author retains ownership of the copyright in this thesis. Neither the thesis nor substantial extracts from it may be printed or otherwise reproduced without the author's permission.

L'auteur a accordé une licence non exclusive permettant à la Bibliothèque nationale du Canada de reproduire, prêter, distribuer ou vendre des copies de cette thèse sous la forme de microfiche/film, de reproduction sur papier ou sur format électronique.

L'auteur conserve la propriété du droit d'auteur qui protège cette thèse. Ni la thèse ni des extraits substantiels de celle-ci ne doivent être imprimés ou autrement reproduits sans son autorisation.

0-612-81250-2

Canada

University of Alberta

Library Release Form

Name of Author: Flora Paganelli

Title of Thesis: Use of RADARSAT-1 satellite imagery and geophysical data for oil and kimberlite exploration

Degree: Doctor of Philosophy

Year of this degree granted: 2002

Permission is hereby granted to the University of Alberta Library to reproduce single copies of this thesis and to lend or sell such copies for private, scholarly or scientific research purposes only.

The author reserves all other publication and other rights in association with the copyright in the thesis, and except as herein before provided, neither the thesis nor any substantial portion thereof may be printed or otherwise reproduced in any material form whatever without the author's prior written permission.



Strada Tamolino, 8
Villaggio Maddalena
10020 Brusasco (TO)
ITALY

June 6th, 2002

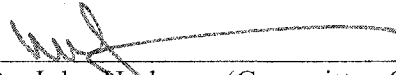
University of Alberta

Faculty of Graduate Studies and Research

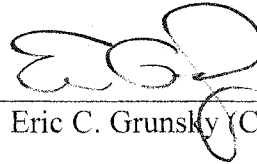
The undersigned certify that they have read, and recommend to the Faculty of Graduate Studies and Research for acceptance, a thesis entitled *Use of RADARSAT-1 satellite imagery and geophysical data for oil and kimberlite exploration* submitted by *Flora Paganelli* in partial fulfillment of the requirements for the degree of *Doctor of Philosophy*



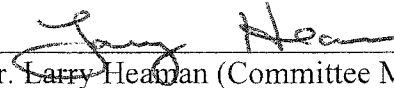
Dr. Jeremy P. Richards (Supervisor)



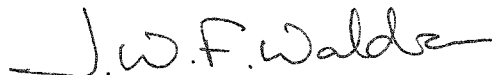
Dr. John Hodgson (Committee Chair)



Dr. Eric C. Grunsky (Committee Member)



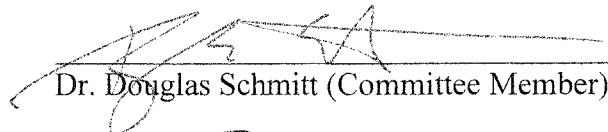
Dr. Larry Heaman (Committee Member)



Dr. John Waldron (Committee Member)



Dr. Teresa Garvin (Committee Member)



Dr. Douglas Schmitt (Committee Member)



Dr. Alexander Cruden (External Examiner)

Date May 28th, 2007

*ai miei genitori Lucia ed
Aldo, e mia sorella Marilena.*

ABSTRACT

The synergy of RADARSAT-1 and seismic imagery interpretation has been applied in the Blackstone area of the Central Alberta Foothills in the Canadian Cordillera thrust and fold belt to map the continuity of geological structures, which are of importance for oil and gas exploration. The reconstruction of the continuity of thrust-fold related major structures known in the area has been successful. Transverse faults and lineaments with ENE-WSW, NE-SW, and NNE-SSW trends have been delineated on the radar images. The ENE-WSW transverse faults have an extensional character, cut across the inner and outer Foothills and are persistent at the regional scale. The NE-SW and NNE-SSW transverse faults are wrench type faults, which are mainly localized in the inner Foothills. These structures have been identified for the first time in the area and are possibly a third generation fault-play type for oil and gas exploration.

Principal Component Analysis (PCA) of RADARSAT-1 images was applied in the Buffalo Head Hills area, in the Western Canada Sedimentary Basin (WCSB), to provide an enhanced image base for structural mapping. North- and NNE-trending lineaments bounding the eastern edge of the Buffalo Head Hills along the Loon River valley, a conjugate set of NW- and NE-trending lineaments, and ENE-trending lineaments identifying the latest features in the area were outlined. The development of these structures has been related to Precambrian terrane assemblage in the WCSB during the Early Proterozoic, the development of the Peace River Arch, and the Laramide Orogeny.

In the Buffalo Head Hills area a weights of evidence statistical approach was used to determine the spatial relationship of NNE-, NE-, -NW, and ENE-trending lineaments to known kimberlite locations. This method outlined different degrees of spatial correlation between kimberlites and lineaments, with higher correlations defined for the NNE, NE, and ENE lineament datasets. A weights of evidence model was then constructed using the structural lineament maps, the Buffalo High and Buffalo Utikuma terrane boundary, Bouguer gravity data, and magnetic characteristics of the Buffalo High and Buffalo Utikuma terranes. The model reveals maximum favourability for kimberlite exploration along the Buffalo High and Buffalo Utikuma terrane boundary in correspondence with NNE-trending lineaments and their intersections with NE and ENE lineaments. The relationship of the kimberlite occurrences along the Buffalo High-Buffalo Utikuma terrane boundary and structural lineaments seems to favour an hypothesis of kimberlite emplacement through a major zone of weakness in the basement, here characterized by the boundary between the Buffalo High and Buffalo Utikuma terranes.

ACKNOWLEDGMENTS

The research presented in this thesis was conducted at the University of Alberta in cooperation with Petro-Canada and the Geological Survey of Canada.

I wish to thank my supervisors Jeremy Richards (University of Alberta) and Eric Grunsky (Alberta Geological Survey, Edmonton) for their support and trust needed to complete this thesis.

For the work conducted in the Blackstone area I wish to thank Ken Dutchak from Alberta Environment (Edmonton) at the Alberta Geological Survey who provided the RADARSAT-1 data, and François Langlois of Petro-Canada (Calgary) who provided financial support, and Michael McDonough for access to the seismic data. I am grateful for the useful discussions and review of this work to Daniel Lebel, (Geological Survey, Quebec), Willem Langenberg (Alberta Geological Survey, Edmonton), Jeremy P. Richards, and John Waldron (University of Alberta).

For the work conducted in the Buffalo Head area I am grateful for the assistance of Ken Dutchak and Bob Sleep of the Resource Data Division of Alberta Environment (Edmonton) at the Alberta Geological Survey. The Resource Data Division and the Alberta Geological Survey provided the necessary funding that enabled the acquisition and orthorectification of the RADARSAT-1 imagery. Radarsat International Inc. provided the images that were made available through the agreement with the Canada Center for Remote Sensing (CCRS), the Canadian Space Agency, and the Alberta

Geological Survey (AGS); these organizations are gratefully acknowledged. Dave Skelton from Ashton Mining Canada Inc., and Robert Pryde from Alberta Energy Company are thanked for providing access to the additional structural maps used in this thesis. Mark Pilkington at the Geological Survey of Canada (Ottawa) is thanked for providing the recent geophysical re-redefinition of the Buffalo Head terrane, which greatly improved the statistical modeling. Larry Heaman (University of Alberta), is thanked for the useful information on the recent review of kimberlite magmatism in Canada, and the constructive comments on the revision of the discussion related to Buffalo Head Hills kimberlite field.

TABLE OF CONTENTS

Chapter 1: INTRODUCTION

1.1 Overview	1
1.2 Rationale	3
1.3 Study areas and data sets	4
1.4 Thesis outline	5
References	7

Chapter 2: CONTRIBUTION OF THE INTEGRATION OF RADARSAT-1 AND SEISMIC IMAGERY INTERPRETATION IN THE STRUCTURAL GEOLOGY OF THE CENTRAL ALBERTA FOOTHILLS, CANADA, AS AID FOR OIL AND GAS EXPLORATION

2.1 Introduction	12
2.2 Regional Geology	13
2.3 Methodology	14
2.3.1 RADARSAT-1 Beam selection	14
2.3.2 Image processing	16
2.3.3 Seismic data selection and interpretation	17
2.4 Results of integrated RADARSAT-1 and seismic structural interpretations	18
2.5 Discussion and Conclusions	22
References	25

Chapter 3: USE OF RADARSAT-1 PRINCIPAL COMPONENT IMAGERY FOR STRUCTURAL MAPPING: A CASE STUDY IN THE BUFFALO HEAD HILLS AREA, NORTHERN CENTRAL ALBERTA, CANADA

3.1 Introduction	41
3.2 Regional Geology	44
3.3 Methodology	46
3.3.1 RADARSAT-1 data selection and processing	46
3.3.2 Principal Component Analysis of RADARSAT-1 images	49
3.3.3 Structural map interpretation approach and validation	51
3.4 Results of RADARSAT-1-PC imagery interpretation	54
3.4.1 RADARSAT-1-PC2 structural interpretation	55
3.4.2 RADARSAT-1-PC1, -PC3, and -PC4 structural interpretation	58
3.4.3 Compilation RADARSAT-1-PC structural data	59
3.4.4 Comparison with AMCI, AEC, and AGS structural interpretations	61
3.5 Structural lineaments and regional geological context	64
3.6 Discussion and Conclusions	69
References	72

Chapter 4: INTEGRATION OF STRUCTURAL, GRAVITY, AND MAGNETIC DATA USING THE WEIGHTS OF EVIDENCE METHOD AS A TOOL FOR KIMBERLITE EXPLORATION IN THE BUFFALO HEAD HILLS AREA, NORTHERN CENTRAL ALBERTA, CANADA

4.1 Introduction	100
4.2 Regional Geology	101
4.3 Weights of evidence method	103
4.3.1 Weights of evidence modeling approach	103
4.3.2 Data processing and binary map generation	107
4.4 Results of the weights of evidence model in the Buffalo Head Hills	113
4.5 Discussion and Conclusions	115
References	118

Chapter 5: GENERAL DISCUSSION AND CONCLUSIONS

5.1 RADARSAT-1 contribution to structural mapping and exploration	134
5.1.1 Blackstone study area, Foothills Canadian Cordillera	135
5.1.2 Buffalo Head Hills study area, Western Canada Sedimentary Basin	136
5.1.3 Structural similarities at regional scale and their implications	138
5.2 Kimberlites in Canada	139
5.2.1 Buffalo Head Hills kimberlite emplacement model	141
5.3 Recommendations for future studies	143
References	146

BIBLIOGRAPHY	150
---------------------	-----

CURRICULUM VITAE	152
-------------------------	-----

LIST OF TABLES

CHAPTER 1

Table 1.1. RADARSAT-1 performance summary (data source Table 4, in Luscombe et al., 1993).	10
---	----

CHAPTER 3

Table 3.1. Principal components loading from Correlation Eigenvectors.	77
Table 3.2. Principal components loading expressed in % from Correlation Eigenvectors.	77
Table 3.3. Eigenvalue analysis from correlation matrix.	77
Table 3.4. Summary of lineament orientations in RADARSAT-1-PC interpretations.	77

CHAPTER 4

Table 4.1. Summary of RADARSAT-1-PC NNE total lineaments weights at variable distance from kimberlite locations.	122
Table 4.2. Summary of RADARSAT-1-PC NW total lineaments weights at variable distance from kimberlite locations.	122
Table 4.3. Summary of RADARSAT-1-PC NE total lineaments weights at variable distance from kimberlite locations.	123
Table 4.4. Summary of RADARSAT-1-PC ENE total lineaments weights at variable distance from kimberlite locations.	123
Table 4.5. Summary of weights for the RADARSAT-1-PC lineaments for modeling posterior probability of a kimberlite occurring in a 1 km ² area.	124
Table 4.6. Summary of Buffalo High and Buffalo Utikuma terranes boundary weights at variable distance from kimberlite locations.	124
Table 4.7. Boundary of the Buffalo High and Buffalo Utikuma terranes reclassified binary theme used in the weights of evidence model.	124
Table 4.8. Buffalo High and Buffalo Utikuma terranes magnetic signature weights for modeling posterior probability of a kimberlite occurring in a 1 km ² area.	125

Figure 4.5B. Buffalo Head Hills kimberlite favourability map over the Bouguer gravity field draped on the Precambrian basement DEM shading (illumination azimuth 45°, elevation 70°) with structural trend from RADARSAT-1-PC2 (legend of posterior probability as in 4.5A). 132

Figure 4.6. Buffalo Head Hills magnetic anomaly field. The blue line indicates the possible susceptibility low with NE-SW trend (base magnetic anomaly field from Pilkington et al., 2000). 133

CHAPTER 5

Figure 5.1. A) Farallon subduction sequence; B) model of Farallon subduction induced dynamic topography. The model is simulated within a confined area of 5000 km x 5000 km, defining a grid of 1000x1000 km² (from Burgess et al., 1997). 149

LIST OF FIGURES

CHAPTER 1

- Figure 1.1.** RADARSAT-1 SAR imaging modes (modified after Luscombe et al., 1993). 11

CHAPTER 2

- Figure 2.1.** Generalized tectonic map of the Canadian Cordillera thrust and fold belt western Alberta and British Columbia, showing the location of the study area (modified after Lebel et al., 1996). P: Pyramid Thrust; B: Bourgeau Thrust; PP: Pipestone Thrust; SP: Simpson Pass Thrust. 28

- Figure 2.2.** Geology of the Blackstone study area (modified after Price, 1977). PP: Paskapoo Formation; uKB, Brazeau Formation. 29

- Figure 2.3.** Schematic stratigraphic relationships across the Central Alberta Foothills and Front Ranges (modified after Lebel et al., 1996). Carbonate rocks of Cambrian and Mississippian age dominate the lower part of the sequence, and clastic marine and non-marine sedimentary rocks of Mesozoic-Cenozoic age of the foreland basin define the upper part. Thrust fault surfaces occur extensively parallel to stratigraphic horizons. 30

- Figure 2.4.** Blackstone study area. RADARSAT-1 Standard Beam Mode 1 (S1), Descending Orbit, acquired on August 5th 1997. Incidence angle 20-27°, C band, HH polarization. Nominal coverage area 100x100 km, approximate ground resolution 25 m, pixel size in range and azimuth 12.5 m. The Township & Range Grid is shown for reference. 31

- Figure 2.5.** Blackstone study area. RADARSAT-1 Fine Beam Mode 1 (F1) Near Range, Descending Orbit, acquired on July 7th 1998. Incidence angle 36.4-39.6°, C band, HH. Nominal coverage area 50x50 km, approximate ground resolution 8 m, pixel size in range and azimuth 6.25 m. The Township & Range Grid is shown for reference. 32

- Figure 2.6.** Seismic interpretation on RADARSAT-1 Standard Beam Mode 1, showing the correspondence of the topographic expression of the interpreted Ancona and Brazeau thrusts, the Pedley-Lovett and New Upper Bounding backthrusts. 33

- Figure 2.6A.** Interpretation of the seismic section B and C in the Lovett area. The Ancona thrust, Lovett anticline, and New Upper Bounding backthrust structures are shown. Their extrapolation to the surface was combined with the

structural features observed in the RADARSAT-1 Standard Beam Mode to compile the structural map in Figure 2.7. The Cardium Formation is reported in the sections as it represents the oil-productive horizon in the area. 34

Figure 2.7. Blackstone structural interpretation on RADARSAT-1 Standard Beam Mode 1. 35

Figure 2.8. Blackstone lithologic map on RADARSAT-1 Standard Beam Mode 1. Kbz: Brazeau Formation; Tpa: Paskapoo Formation. 36

Figure 2.9. Rose diagrams: **A)** transverse fault trends; **B)** lineament trends. 37

Figure 2.10A. Details of the structural interpretation of the Cardinal Hills/Lovett area on RADARSAT-1 Standard Beam Mode 1. Lower left, offset of the Brazeau thrust bounding the Cardinal Hills ridge; top center, offset of the Lovett anticline and Lovett thrusts. For symbols refer to Figure 2.7. 38

Figure 2.10B. Uninterpreted section of Cardinal Hills/Lovett area on RADARSAT-1 Standard Beam Mode 1, for reference. 39

Figure 2.11. Details of the structural interpretation of the Blackstone and Stolberg structures on RADARSAT-1 Standard Beam Mode 1. For symbols refer to Figure 2.7. 40

CHAPTER 3

Figure 3.1. Buffalo Head Hills study area and NTS coverage. GSLSZ, Great Slave Lake Shear Zone; STZ, Snowbird Tectonic Zone. The inset shows the Precambrian basement terrane boundaries (after Pilkington et al., 2000). 78

Figure 3.1A. Archean block reconstruction of the WCSB (A: Archean blocks, BH: Buffalo High terrane, BU: Buffalo Utikuma terrane; modified after Ross, 1990). 79

Figure 3.2. A) Stratigraphic correlation chart of Elk Point Group strata showing correlation across the Peace River Arch from central to northern Alberta subsurface. * are units that have biostratigraphic age-dates (from Hein, 1999); B) summary of Cretaceous strata characterizing the Buffalo Head Hills area (from Chen and Bergman, 1999). 80

Figure 3.3. Buffalo Head Hills geology draped on RADARSAT-1-PC2: Kl, Loon River Formation (Lower Cretaceous); Kp, Peace River Group (Lower Cretaceous); Ksh, Shaftesbury Formation (Lower-Upper Cretaceous); Kd, Dunvegan Formation (Upper Cretaceous); Ks, Smoky Group (Upper Cretaceous); kimberlite, red circles. Outline AMCI, AEC, and AGS structural maps. 81

Figure 3.4. Mosaic of 8 filtered RADARSAT-1 S1 Ascending scenes (MOSAIC_S1A): A, Peerless Uplands W-facing slope.	82
Figure 3.5. Mosaic of 8 filtered RADARSAT-1 S1 Descending scenes (MOSAIC_S1D): A, Buffalo Head Hills E-facing slope; B, Buffalo Head Hills NE-facing slope.	83
Figure 3.6. Mosaic of 6 filtered RADARSAT-1 S7 Ascending scenes (MOSAIC_S7A): A, Peerless Uplands W-facing slope.	84
Figure 3.7. Mosaic of 6 filtered RADARSAT-1 S7 Descending scenes (MOSAIC_S7D): A, Buffalo Head Hills E-facing slope; B, Buffalo Head Hills NE-facing slope.	85
Figure 3.8. Outline of the resulting RADARSAT-PC image coverage of the Buffalo Head Hills study area.	86
Figure 3.8A. 1) Percentage loadings of multi-beam RADARSAT-1 input channels showing the relationships of each beam mode for the first two principal components, PC1 and PC2. S1A, S1D, S7A, and S7D contribute to the overall brightness of the first principal component. For the second principal component (PC2), S1A is inversely associated with S1D, S7A, and S7D. This suggest that scene brightness and variability is controlled by incidence angle and contrast in look direction, especially imposed by the contrast of S1D and S1A, which enhance terrain features. 2) The variability in the third component (PC3) is controlled by the contrast of beam mode and look direction. S7A and S7D are inversely related to S1A and S1D. The contrast between S7A and S1D determine enhancement for drainage and quaternary features although the dark tone variability. 3) The variability in the fourth component (PC4) is controlled by the contrast in look direction defined by the inverse correlation of S7A and S7D, and minor contribution of S1D and S1A.	87
Figure 3.9. RADARSAT-1-PC1 image.	88
Figure 3.10. RADARSAT-1-PC2 image: A, Buffalo Head Hills E-facing slope; B, Buffalo Head Hills NE-facing slope; C, Peerless Uplands W-facing slope.	89
Figure 3.11. RADARSAT-1-PC3 image: A, Loon River Valley NNE-trend drainage; B, Loon River valley ENE-trend drainage; C, Buffalo Head Hills NW-trend drainage; D, Wabasca River NW-trend drainage.	90
Figure 3.12. RADARSAT-1-PC4 image: A, artifact due to processing; B, Peerless Uplands ENE-trend feature; C, Buffalo Head Hills ENE-trend features.	91

Figure 3.13. RADARSAT-1-PC2 structural interpretation and kimberlite locations.	92
Figure 3.14. Structural interpretation and kimberlite locations of: A) RADARSAT-1-PC1; B) RADARSAT-1-PC3; C) RADARSAT-1-PC4.	93
Figure 3.15. RADARSAT-PC lineament compilation: A) NNE lineaments; B) NW lineaments; C) NE lineaments; D) ENE lineaments.	94
Figure 3.16. Rose diagrams of lineaments interpreted on RADARSAT-1-PC images.	95
Figure 3.17. A) Ashton Mining of Canada Inc. (AMCI) structural interpretation map (Lockett, 1998); B) RADARSAT-1-PC2 subset structural interpretation map.	96
Figure 3.18A. Alberta Energy Company (AEC) structural interpretation map (Pryde, 2000).	97
Figure 3.18B. RADARSAT-1-PC2 subset structural interpretation map.	98
Figure 3.19. A) Alberta Geological Survey structural interpretation map (Eccles et al., 2000); B) RADARSAT-1-PC2 subset structural interpretation map.	99
 CHAPTER 4	
Figure 4.1. Buffalo Head Hills study area and NTS coverage. GSLSZ, Great Slave Lake Shear Zone; STZ, Snowbird Tectonic Zone. The inset shows the Precambrian basement terrane boundaries (after Pilkington et al., 2000).	127
Figure 4.2. Buffalo Head Hills geology and kimberlite locations: Kl, Loon River Formation (Lower Cretaceous); Kp, Peace River Group (Lower Cretaceous); Ksh, Shaftesbury Formation (Lower-Upper Cretaceous); Kd, Dunvegan Formation (Upper Cretaceous); Ks, Smoky Group (Upper Cretaceous); kimberlite, black circles.	128
Figure 4.3. Lineament binary maps used in weights of evidence modeling: A) NNE lineaments; B) NW lineaments; C) NE lineaments; D) ENE lineaments.	129
Figure 4.4. Additional predictor binary themes used in weights of evidence modeling: A) Buffalo High and Buffalo Utikuma terrane contact binary theme; B) Buffalo High and Buffalo Utikuma terranes average magnetic response; C) Buffalo Head Hills Bouguer gravity.	130
Figure 4.5A. Buffalo Head Hills kimberlite favourability map.	131

Table 4.9. Bouguer gravity anomaly weights for modeling posterior probability of a kimberlite occurring in a 1 km ² area.	125
Table 4.10. Weights for modeling posterior probability of a kimberlite occurring in a 1 km ² area.	125
Table 4.11. Table of degree of freedom independence between all pairs of 7 binary and multi-class themes.	126
Table 4.12. χ^2 values for testing conditional independence between all pairs of 7 binary and multi-class themes.	126

Chapter 1

INTRODUCTION

1.1 OVERVIEW

The advent and development of geographic information systems (GIS) and image processing systems (IPS), their converging functionality in the last decade, and the integration of multi-source remotely sensed data to provide thematic maps have had major impacts on the Earth sciences and many other land-related science disciplines.

The evolution of survey technologies from satellite to airborne sensors, and their use in GIS/IPS has enabled the development of integration techniques for independently acquired data sources that can potentially provide complementary information and insights on the geology of an area. They can be used as exploration tools and can be of guidance in field mapping and data acquisition planning (Sullivan, 1991).

The use of remotely sensed data and GIS/IPS integration techniques is particularly important in field mapping and exploration projects as a cost effective way of overcoming inaccessibility and terrain constraints (Drury, 1992; Bonham-Carter, 1994). Increasingly during the last decade, GIS/IPS integration has become the tool by which geologists complement and enhance their ability to spatially view and analyze the geology and characteristics of an area of interest (Schetselaar, 1995; Schetselaar et al., 2000).

Since 1996, RADARSAT-1 satellite Synthetic Aperture Radar (SAR) imagery has become available to the scientific community (Parashar et al., 1993) introducing

advanced options for data acquisition with multi-beam¹ (footnotes refer to glossary) operating modes (Figure 1.1), variable incidence angle² selection, and higher resolution³ depending on the beam mode⁴ selection as summarized in Table 1.1. In preparation for RADARSAT-1 (Luscombe et al., 1993; Denyer et al., 1993), the Canada Center for Remote Sensing (CCRS) acquired airborne SAR imagery with the C-CCRS airborne facility, which has similar frequency (5.3 GHz) and polarization⁵ (Horizontal-Horizontal, HH) to the European Remote Sensing Satellite Synthetic Aperture Radar (ERS-1 SAR). However, the two systems differ in resolution, incidence angle, and illumination⁶ geometry. The resolution of the C-CCRS is 15 m range⁷ and azimuth⁸ compared to the 30 m of the ERS-1. The near-range incidence angle⁹ of the C-CCRS airborne is 45°, with range variability¹⁰ 16°-90°, while the ERS-1 is 23°. Geological applications of the C-CCRS airborne SAR imagery prototype of RADARSAT-1 imaging capability, offering varying viewing geometry and spatial resolution, were demonstrated by Singhroy et al. (1993) for various areas around Canada, suggesting the suitability of RADARSAT-1 imagery for a range of topographic conditions and terrain coverage. RADARSAT-1 applications have followed in geological mapping (e.g., Paradella et al., 1997), structural mapping applications (e.g., D'Iorio and Budkewitsch, 1997; Paganelli and Rivard, 1999b, 2001; Paganelli et al., 2001a,b), geomorphological applications (e.g., Robinson et al., 1999), and image integration (e.g., Riopel et al., 1999; Grunsky, 2001; Paganelli et al., 2001b, d).

The ultimate purpose of combining spatial data from different sources in a GIS is to describe and analyze interactions between spatial patterns, in order to make predictions with statistical models that provide support for decision-making. GIS modelling applied to mineral mapping for exploration involves calculating a

suitability, or mineral favourability, from geoscientific maps (Bonham-Carter, 1994). The assignment of weights to the maps is carried out either by analyzing the importance of evidence/pattern related to known mineral occurrences, or by using subjective judgment of mineral deposits by geologists. The mineral potential is calculated by weighting and combining multiple sources of evidence using a predictive model, whose ultimate purpose is to outline new areas for exploration.

1.2 RATIONALE

This thesis presents new approaches for geological investigation by integrating multiple types of remotely sensed data, including RADARSAT-1 satellite images, gravity and aeromagnetic airborne data, as well as seismic data.

Remotely sensed data are often analyzed in isolation, which limits the amount of information that can be derived. The rationale for this research has been in the development and application of data integration techniques to improve exploration strategies. A specific objective has been to provide regional structural models applicable to oil/gas and kimberlite exploration in two specific areas of Alberta. The integration strategies presented here are intended to work with knowledge-driven and data-driven image enhancement and pattern recognition techniques.

In support of kimberlite exploration, image-derived structural maps were integrated in a GIS environment and analyzed using a weights of evidence statistical model, resulting in the identification of possible target areas for future investigation.

The statistical modelling approach enabled an objective estimation to be made of the spatial relationships between structures and kimberlite occurrences, which was then used to suggest the influence of crustal structures on kimberlite emplacement.

Where possible, field knowledge or cross-validation with available maps and ancillary data has been used to test the geological significance of the integrated interpretations.

1.3 STUDY AREAS AND DATA SETS

The integration techniques presented in this thesis are applied to two geologically distinct study areas in Alberta. The first is the Blackstone area, in the central Alberta foothills of the Rocky Mountains, which is characterized by vegetation coverage above 80% and difficult accessibility. In this area the integrated data set consisted of RADARSAT-1 Standard Beam Mode S1 descending¹¹, and Fine Beam Mode Near Range descending scenes, provided by the Resource Data Division of Alberta Environment (Edmonton), and seismic lines provided by Petro-Canada as sponsor of this project. The seismic data were made available to the author to better constrain the structural information gathered from the radar images in support of possible prospective target areas for oil/gas exploration. The main fieldwork component of the project consisted of field-testing preliminary interpretations obtained from the RADARSAT-1 imagery.

The second study site is the Buffalo Head Hills area, located in northern central Alberta, within the Western Canadian Sedimentary Basin (WCSB). In this area a more extensive data set, including RADARSAT-1 images, airborne gravity,

and aeromagnetic geophysical data, was provided by the Alberta Geological Survey (AGS). The data set was made available to the author to provide information on the structural setting of the area, and to explore a possible link between structure and kimberlite emplacement, with implications for kimberlite exploration. The Buffalo Head Hills study site area is characterized by 80-90% vegetation coverage and difficult accessibility. No fieldwork was conducted for this study; instead the structural work has been cross-validated with a structural map interpreted from well, high-resolution aeromagnetic, and seismic data, provided to the author by Rob Pryde of the Alberta Energy Company (AEC).

1.4 THESIS OUTLINE

In Chapter 2, structural interpretations from RADARSAT-1 imagery and seismic data integration are used in the Blackstone area, in the central Alberta foothills of the Rocky Mountains, to define structural features controlling oil pool separation, and outline possible target areas for light-oil exploration (Paganelli and Rivard, 1999a, 1999b). The content of this chapter is from Paganelli and Rivard (2001).

In Chapter 3, a newly developed approach (Grunsky, 2001) in the use of Principal Component Analysis (PCA), using RADARSAT-1 imagery for geological applications is illustrated, with emphasis on structural mapping in the highly vegetated terrain of the Buffalo Head Hills area (Paganelli et al., 2001a, b). The structural interpretation derived from the RADARSAT-1-PC imagery is constrained through positive cross-validation with unpublished structural maps (Lockett, 1998;

Pryde, 2000; Eccles et al., 2000), and provides an interpretation of the structural evolution of the area with possible implications for kimberlite and oil/gas exploration. The content of this chapter is from Paganelli et al. (2001b).

In Chapter 4, a quantitative geo-spatial assessment based on Bayesian statistical approach of prior and posterior probability, in a loglinear form known as weights of evidence (Spiegelhalter, 1986), is used to produce a favourability map illustrating areas for kimberlite exploration. This map is estimated using statistical weights assigned to digital spatial predictor/thematic maps (Bonham-Carter, 1994), identifying spatial patterns such as lineaments derived from the structural interpretation (Chapter 3), geology, and geophysical characteristics of the Buffalo Head Hills area basement terranes. The content of this chapter is from Paganelli et al. (2001c, 2002).

The final Chapter 5 contains general discussion and conclusions, for each of the study areas. Structural patterns identified in both the study areas are discussed in a regional tectonic context.

An outlook on the current research on kimberlite age and location in Canada is provided through work compiled by Heaman et al. (2002) to define a context in relation to the Buffalo Head Hills kimberlite field. This review enables discussion of models and environments for kimberlite magmatism that could apply to the Buffalo Head Hills kimberlite field.

Possible recommendations and some of the limitations in the methodologies applied in this thesis are discussed, with suggestions for future research.

REFERENCES

- Bonham-Carter, G.F. (1994). *Geographic Information Systems for Geoscientists: Modeling with GIS*. Pergamon Press, Oxford.
- Denyer, N., Raney, R.K., Shepherd, N. (1993). The RADARSAT SAR data processing facility. *Canadian Journal of Remote Sensing, Special Issue RADARSAT*, Vol.19, No. 4, pp. 311-316.
- D'Iorio, M. and Budkewitsch, P. (1997). Improved geological mapping in Sarawak, Malaysia, using RADARSAT-1 SAR data. *Proceedings of the Twelfth International Conference of Applied Geologic Remote Sensing*, Vol. II, p. 83.
- Drury, S.A. (1992). *Image Interpretation in Geology, Second Edition*. Chapman & Hall, London.
- Eccles, D.R., Grunsky, E.C., Grobe, M., and Weiss, J. (2000). *Structural emplacement model for kimberlitic diatremes in northern Alberta*. Report, Alberta Energy and Utilities Board, Alberta Geological Survey, March 2000, p. 116 (in press).
- Grunsky, E.C. (2001). The Application of Principal Components Analysis to Multi-beam RADARSAT-1 Satellite Imagery – A Tool for Terrain Mapping. *Canadian Journal of Remote Sensing*, (in press).
- Heaman, L.M., Kjarsgaard, B.A., and Creaser, R.A. (2002). The timing of kimberlite magmatism and implications for diamond exploration: a global perspective. *Lithos*, (in press).
- Lockett, N (1998). Ashton Mining of Canada Buffalo Head Hills Project, Alberta - Results of air photograph interpretation. Ashton Mining Ltd. Report 52214, p.10. Unpublished.
- Luscombe, A.P., Ferguson, I., Shepherd, N., Zimck, D.G., Naraine, P. (1993). The RADARSAT Synthetic Aperture Radar Development. *Canadian Journal of Remote Sensing, Special Issue RADARSAT*, Vol. 19, No. 4, pp. 298-310.
- Paganelli, F. and Rivard, B. (1999a). *Tracking geological structures in the Central Alberta Foothills, Canada, using RADARSAT imagery*. Report, Petrocanada. Unpublished.
- Paganelli, F. and Rivard, B. (1999b). Tracking geological structures in the Central Alberta Foothills, Canada, using RADARSAT imagery. *Proceedings of the Thirteenth International Conference of Applied Geologic Remote Sensing, Vol. I, p. 109*.
- Paganelli, F. and Rivard, B. (2001). Contribution of the synergy of RADARSAT-1 and seismic imagery interpretation in the structural geology of the Central Alberta Foothills, Canada, as aid for oil and gas exploration. *Canadian Journal for Remote Sensing* (in press).
- Paganelli, F., Grunsky, E.C., and Richards, J.P (2001a). *Structural interpretation of RADARSAT-1 Principal Component imagery and its potential application to kimberlite exploration in the Buffalo Head Hills area, Northern Central Alberta*.

- Alberta Geological Survey, Earth Science Report 2001-03. Edmonton, Alberta, Canada: Alberta Energy and Utilities Board (in press).
- Paganelli, F., Grunsky, E.C., and Richards, J.P. (2001b). Use of RADARSAT-1 Principal Component imagery for structural mapping: a case study in the Buffalo Head Hills area, northern central Alberta, Canada. *Canadian Journal of Remote Sensing* (in press).
- Paganelli, F., Richards, J.P., and Grunsky, E.C. (2001c). Integration of structural, gravity, and magnetic data using the weights of evidence method as a tool for kimberlite exploration in the Buffalo Head Hills area, northern central Alberta, Canada. *Natural Resources Research* (submitted).
- Paganelli, F., Grunsky, E.C., and Richards, J.P. (2001d). RADARSAT and Landsat5 TM integration for kimberlite exploration in the Buffalo Head Hills area, northern central Alberta. *Geological Association of Canada and Mineralogical Association of Canada, Joint Annual Meeting. Memorial University, St. John's, Newfoundland*, May 27-30, pp.110-111.
- Paganelli, F., Richards J.P., Grunsky E.C. (2002) - Integration of structural, gravity and magnetic data using the weights of evidence method as a tool for kimberlite exploration in the Buffalo Head Hills area, Northern Central Alberta. *Proceedings of the 2002 International Geoscience and Remote Sensing Symposium - 24th Canadian Symposium on Remote Sensing*, 24-28 June, Toronto, Ontario, Canada (in press).
- Paradella, W.R., Veneziani, P., dos Santos, A.R., Dias, R.R. (1997). Geological evaluation of RADARSAT-1 data in the Carajas mineral province (Brazil Amazon Region). *Proceedings of the Twelfth International Conference of Applied Geologic Remote Sensing*, Vol. I, pp. 490-497.
- Parashar, S., Langham, E., McNally, J., Ahmed, S. (1993). RADARSAT mission requirements and concept. *Canadian Journal of Remote Sensing*, Vol. 19, No. 4, pp. 280-288.
- Pryde, R. (2000). Buffalo Head Hills property AEC Structural Interpretation Map. Scale 1:250 000. Unpublished.
- Riopel, S., Desrouchers, A., D'Iorio, M., Budkewitsch, P., and Beauchamp, B. (1999). Stereoscopy and DEM Generation from RADARSAT-1 images for geological mapping in the Canadian High Arctic: examples from Axel Heiberg Island. *Proceedings of the Thirteenth International Conference of Applied Geologic Remote Sensing*, Vol. II, pp. 431-432.
- Robinson, C.A., Mainguet, M., and El-Baz, F. (1999). Channel morphologies observed in radar data: implication to the development of the Selima Sand Sheet. *Proceedings of the Thirteenth International Conference of Applied Geologic Remote Sensing*, Vol. II, pp. 405-410.
- Schetselaar, E.M. (1995). Computerized field data capture for geological data integration. *Proceedings Joint European Conference and Exhibition on geographical Information Systems*, The Hague, pp. 436-441.
- Schetselaar E.M., Chung, C.F., and Kim, K.E. (2000). Integration of Landsat TM, gamma-ray, magnetic, and field data to discriminate lithological units in vegetated granite-gneiss terrain. *Remote Sensing of the Environment*, Vol. 7, pp. 89-105.

- Singhroy, V.H., Slaney, R., Lowman, P., Harris, J., Moon, W. (1993). RADARSAT and radar geology in Canada. *Canadian Journal of Remote Sensing*, Vol. 19, No. 4, pp. 338-351.
- Spiegelhalter, D.J. (1986). Uncertainty in expert systems. In: *Artificial Intelligence and Statistics*, Editor: Gale, W.A., Addison-Wesley, Reading, Massachusetts, pp. 17-55.
- Sullivan, K.N.O. (1991). *A map for all reasons: the role of image processing in mineral exploration*. Minerals Industry International, January 1991.

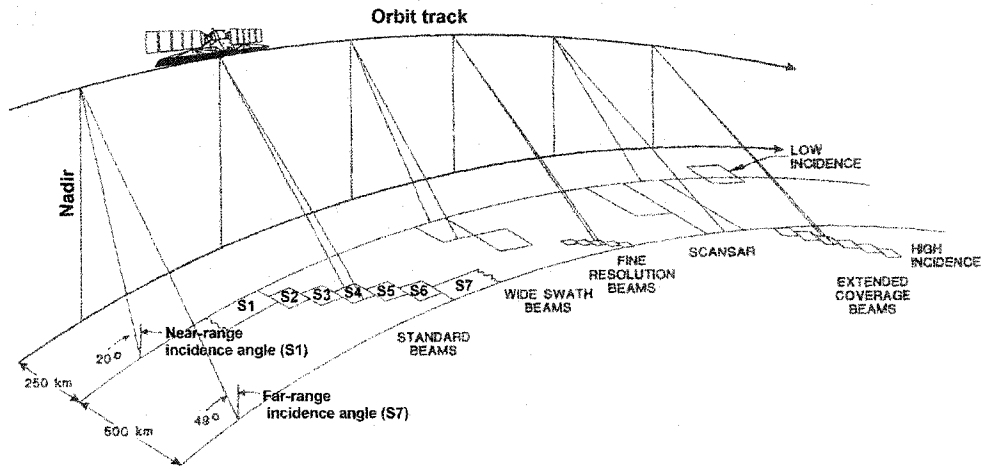
Table 1.1. RADARSAT-1 performance summary (data source Table 4, in Luscombe et al., 1993).

Mode	Resolution Range Azimuth	Number of looks	Swath width	Incidence angles
Standard Beams (7)	24 m by 26 m	4	105 km	20°-49°
Wide Swath Beams (2)	32 m by 26 m	4	158 km	20°-39°
Fine Resolution (5)	9m by 8 m	1	49 km	37°-48°
Extended Coverage Beams				
Low Incidence (1)	43 m by 26 m	4	170 km	10°-23°
High Incidence (6)	19 m by 26 m	4	75 km	49°-59°
Scan SAR				
2-Beam	35 m by 30 m 100 m by 100 m	1 14	310 km	20°-39°
4-Beam	34 m by 52 m 100 m by 100 m	1 8	520 km	20°-49°
Values are averaged performance figures across a given set of Beams				

Glossary:

- ¹ multi-beam: the minimum number of swath of around 100 km for the RADARSAT-1 Standard beam Mode that give coverage of the 500 km accessibility region while avoiding nadir ambiguity is 7 (shown in Figure 1.1).
- ² incidence angle: defines the angle between the incidence microwave signal on the surface and the perpendicular to incidence point on the surface.
- ³ resolution: is defined by the spatial resolution on the ground in range (cross-track) and azimuth (along-track).
- ⁴ beam mode: defines the specific swath width, or footprint of the radar beam, with specific incidence angle and resolution.
- ⁵ polarization: defines the planes of polarization of the emitted and received microwave signal from the emitting and receiving satellite RADARSAT-1 antenna (e.g., in the RADARSAT-1 the microwave signal is polarized horizontally for both emitted and received signal, HH).
- ⁶ illumination geometry: illumination refer to the microwave signal emitted from the radar antenna, whose geometry is defined by the combination of look direction, determined by the different selection of ascending or descending orbit, swath width, incidence angle.
- ⁷ range resolution: spatial resolution on the ground in the range (cross-track) direction (perpendicular to satellite orbit direction), which depends on the incidence angle.
- ⁸ azimuth resolution: spatial resolution on the ground in the azimuth (along-track) direction (parallel to satellite orbit direction), which depends on the incidence angle.
- ⁹ near-range incidence angle: define the smallest incidence angle for a specific beam- mode selection (e.g., in the RADARSAT-1 Standard Mode 1, the near-range incidence angle is 20° and the far-range incidence angle is 27.4°).
- ¹⁰ range variability: refer to the interval of variability of the incidence angle within a specific beam-mode (e.g., in the RADARSAT-1 Standard Mode 1 is 20°-27.4°); it can also refer to the interval of variability for the whole 500 km accessibility region of the RADARSAT-1 Standard Beam Modes 1 to 7, which covers incidence angles from 20° to 49° (shown in Figure 1.1), corresponding to the smallest near-range incidence angle for the RADARSAT-1 Standard beam Modes 1, and the far-range incidence angle for the RADARSAT-1 Standard beam Modes 7, respectively.
- ¹¹ descending orbit: defines the RADARSAT-1 satellite orbit trajectory from north to south, characterized by cross-track look direction from east to west; the ascending orbit defines instead the RADARSAT-1 satellite orbit trajectory from south to north, with cross-track look direction from west to east.

Figure 1.1. RADARSAT-1 SAR imaging modes (modified after Luscombe et al., 1993).



Chapter 2

CONTRIBUTION OF THE INTEGRATION OF RADARSAT-1 AND SEISMIC IMAGERY INTERPRETATION IN THE STRUCTURAL GEOLOGY OF THE CENTRAL ALBERTA FOOTHILLS, CANADA, AS AID FOR OIL AND GAS EXPLORATION

2.1 INTRODUCTION

The Foothills of the Central Canadian Cordillera thrust and fold belt is a known area of fossil fuel production. Currently oil companies are pursuing several Cretaceous play types in the outer Foothills, in front of the eastern limit of the foreland thrusts, in Alberta and British Columbia (Figure 2.1). The plays are identified using seismic imaging as a primary method, supported by surface geology. Often, the available surface geology is very limited, mostly based on creek outcrops with limited air photo interpolation in areas showing Quaternary overburden. In several cases, seismic images suggest that deep targeted structural features should have a surface expression. However, limited seismic coverage and poor imaging of the very shallow section (within 500 m from the surface) do not allow proper surface mapping of the structures and tracing of these elements along strike. Air photos provide limited but useful help in this highly vegetated environment when sandstone ridges outline stratigraphic contacts and fault traces. Where outcrop is limited to less than 20% the use of satellite radar imagery represents an additional tool that complements air photo interpretation and field work to achieve better data integration in areas of limited seismic coverage, and structural and geological data. The RADARSAT-1 satellite offers multiple imaging options due to varying viewing geometry and spatial resolution (Luscombe et. al, 1993; Singhroy et al., 1993; Denyer et al., 1993) and is thus

suited for imaging a range of topographic conditions. The use of RADARSAT-1 satellite SAR (Synthetic Aperture Radar) imagery in combination with seismic imagery interpretation has been investigated in the Blackstone study area (Figure 2.1) of the Central Alberta Foothills. The aim was to map the surface expression of geological structures and their continuity, and provide a comparison with previous mapping using air photo and traverse methods. The results of the integrated structural interpretation of RADARSAT-1 and seismic imagery are presented with implications and applications of this work for further oil and gas exploration in the Foothills (Paganelli and Rivard, 1999a, 1999b).

2.2 REGIONAL GEOLOGY

The Central Alberta Foothills of the Central Canadian Cordillera thrust and fold belt is characterized by an imbricated system of thrust faults that dip gently to the SW (Figure 2.1). During the Laramide Orogeny, systems of imbricated thrusts carried strata of Paleozoic rocks from above the Precambrian crystalline basement along a basal decollement (Price and Mountjoy, 1970; Price, 1981). In the thrust and fold belt, outcrops of resistant Paleozoic rocks mark the boundary between the Front Ranges and the dominantly Mesozoic-Cenozoic rocks of the Foothills. Paleozoic rocks are dominantly Middle and Upper Cambrian, Upper Devonian, and Carboniferous platformal carbonates, whose sequences are separated by mechanically weak shale units characterizing potential decollement horizons (Lebel et al., 1996). The Mesozoic-Cenozoic sequence consists

predominantly of clastic marine and non-marine sediments that were deposited in the foreland basin of the Cordilleran thrust belt (Chamberlain et al., 1989).

The Mesozoic-Cenozoic sequence of clastic marine and non-marine sediments of the foreland characterizes the surface exposure of the Blackstone study area. The area is divided into two different structural domains by the eastern limit of foreland thrusts. The Foothills represent an imbricated system of NE-vergent thrust sheets gently dipping to the SW that propagated from the Front Ranges and was underthrust beneath the Alberta Syncline. The Alberta Syncline is characterized by subtle structural features and SW-vergent backthrusts in its west limb (Figure 2.2). In the Foothills, the Ancona thrust (NE-vergent fault) defines the eastern limit of the Foothills, whereas at the west limb of the Alberta Syncline, the Pedley (Charlesworth and Gagnon, 1985) and Lovett (Lebel et al., 1996) SW-vergent backthrusts define the surface expression of the NE edge of the deformed belt. Figure 2.3 displays a schematic section of the stratigraphic relationships of the Central Alberta Foothills which apply to the Blackstone study area. The Cardium Formation, within the Cretaceous sediments of the Alberta Group, represents the most important of the productive horizons of the producing wells located in the eastern part of the area.

2.3 METHODOLOGY

2.3.1 RADARSAT-1 Beam selection

RADARSAT-1 scenes for the Standard Beam Mode 1 (S1) and Fine Beam Mode 1 (F1) were selected for this study because the character of the topography of the area shows limited elevation variations ranging from 1097 to 1680 meters, with slope values ranging from 0° to 38° . The steep incidence angle of the Standard Beam Mode 1 ($20-27^{\circ}$) is well suited to enhance subtle slope variations in this terrain and to map detailed geological structures (Figure 2.4). The steepest incidence angle available for the Fine Mode 1, at the time of data acquisition, was in the range of $36.4-39.6^{\circ}$. This viewing geometry is not as optimal as that of the Standard Mode S1 for topographic enhancement in this terrain and thus there is a trade off between spatial resolution and optimal viewing geometry (Figure 2.5).

The topography of the area is mainly controlled by the NE-vergent thrusts of the Foothills, which display characteristic scarp slopes facing NE and gentle dip slopes parallel to the bedding surfaces facing SW. These topographic elements constrained the selection of the optimal radar look direction, which should be oriented at right angles to the strike of the geological features (Graham, 1977; Elachi, 1987; Sabins, 1987; Lillesand and Kiefer, 1994). The ability to image lineaments using highlighted relief and shadows is a result of the side-looking configuration of radar imaging (Koopmans, 1985). Therefore, to maximize the illumination of topographic features described above, the RADARSAT-1 S1 and F1 scenes were acquired in a Descending Orbit which results in a westward look direction, with orientation at approximately 45° to the strike of the NE-vergent thrusts of the Foothills.

Surface roughness, soil dielectric properties, and slope attitudes (Evans et al., 1986) affect radar backscattering. With the C band radar wavelength (7.5 cm) and HH

polarization used by RADARSAT-1 most of the microwave energy interaction occurs within the top portions of a forest canopy, which often indirectly reflects topographic variation due to resistant and recessive lithological units (Brown et al., 1996) or structural escarpments.

The structural interpretation was mainly conducted using the RADARSAT-1 S1 imagery due to the enhancement of topographic features (Singhroy and Saint-Jean, 1999). The inherent properties of radar images, such as grey tone contrast and texture (Graham, 1977; Sabins, 1987; Singhroy, 1992; Lillesand and Kiefer 1994; Berger, 1994), were used to interpret the topographic variations and identify geological structures relevant for oil exploration.

2.3.2 Image Processing

RADARSAT-1 S1 and F1 data were geometrically corrected using control points extracted in UTM coordinates from National Topographic Sheets (NTS maps 83B, 83C, 83F) at 1:250,000 scale. The geocorrected images are in UTM projection (Clarke 1866 Ellipsoid). A second order polynomial transform was applied for geometric correction, and cubic interpolation resampling was used to retain edge information from the original image.

Image enhancement consisted of speckle reduction using Lee (Lee, 1980) and Enhanced Lee filters (Lee, 1981). A 3x3 kernel was used for the Lee Filter followed by three successive applications of a 3x3 kernel Enhanced Lee filter to further reduce speckle,

while maintaining edge continuity. Clearly, the effective resolution of the data was degraded by these operations, but the detection of continuous features was facilitated.

2.3.3 Seismic data selection and interpretation

Seismic prestack depth-migrated data (Gray and Maclean, 1996; Yan and Lines, 2001) were selected in key locations after a preliminary image interpretation of the RADARSAT-1 data to locate NE vergent thrusts, SW vergent backthrust, and related fold structures. The interpretation of the seismic imagery provided a documentation of the deep expression of the surface features determined from the radar. In some cases seismic imaging provided important information for the along strike characterization of structures with subtle surface expressions.

Three seismic sections with orientation parallel to the regional strike gave minimal or no contribution to the overall interpretation. Thirteen sections, with orientation perpendicular to the regional strike, yielded useful information. The structural features outlined from the seismic interpretation of these lines are reported in Figure 2.6. The interpretation of section B and C are shown in Figure 2.6A. These two seismic lines are unpublished, however are 100% property of Petro-Canada Inc., which allowed their publication in this work. The remaining 11 seismic lines are own by different companies and have not been published. A published seismic line showing analogous structures approximately 20 km NW from section A (Figure 2.6) was published by Lebel et al. (1996), and few seismic lines can be found in LeDrew (1997) approximately in the same

location as section D (DB2 in LeDrew, 1997), C and B (DB1 in LeDrew, 1997), and A (2.5 km east of LD6 in LeDrew, 1997).

2.4 RESULTS OF INTEGRATED RADARSAT-1 AND SEISMIC STRUCTURAL INTERPRETATIONS

The integrated RADARSAT-1 S1 and seismic interpretation allowed the reconstruction along strike of the continuity and characterization of the major NE vergent Ancona and Brazeau thrusts, the Pedley-Lovett (Lebel et al., 1996) backthrust, and the New Upper Bounding Backthrust (LeDrew, 1997), the Lovett anticline representing the surface culmination of the Lovett Triangle Zone (LeDrew, 1997), a convergence zone between the Ancona and Pedley-Lovett thrusts, and the Stolberg anticline-syncline ramp fold structures in the Ancona thrust sheet (Price et al., 1977). These features are shown in the structural interpretation map in Figure 2.7 and the lithological interpretation map shown in Figure 2.8. In the lithological interpretation map the radar image allowed a good differentiation of the Brazeau and Paskapoo Formation based on texture, and tone variations. The predominant coarse-grained sandstone and conglomerate of the Brazeau Formation result in a coarse texture and light grey tones in the image, while the Paskapoo Formation characterized by fine-grained sandstone and shale displays a smoother texture and darker grey tones. The Coalspur Formation defined by sandstone, shale, and coal seams, is present with limited extent in the area between the Lovett and Cardinal Hills structures, and between the Ancona and Brazeau thrust fronts. However, the radar

response of the Coalspur Formation is defined by the same texture and tone characteristics observed for the Paskapoo Formation, and therefore in the lithological interpretation map the Paskapoo and Coalspur Formation were not differentiated. For a detailed lithological mapping of the area refer to LeDrew (1997), and the published map of Langenberg and Ledrew (2001).

The Lovett and Stolberg fold structures together with the Blackstone structure, this last characterized by imbricated panels within the Ancona thrust sheet, host major thrust-fold related oil plays and are of relevance for oil and gas exploration in the area. In the structural interpretation map (Figure 2.7) the reconstruction of the structural continuity of these major known structures along strike is consistent with published maps (Price et al., 1977; Lebel et al., 1996; Langenberg and LeDrew, 2001), and the work of LeDrew (1997). However, additional transverse faults and lineament structures have been identified from this study.

In the RADARSAT-1 S1 interpretation (Figure 2.7) major transverse faults and lineaments are shown. The observable offset along fault sets is a combined effect due to the topography, textural variation, and contrast in tone of the lithology (Graham, 1977; Lillesand and Kiefer, 1994; Rossignol, 1996). Lineaments typically do not show observable offset but are identified as linear trends detected by texture or tonal variations in the image. These faults and lineaments were not detected in the seismic data, possibly because of their vertical nature or superficial extent. Faults with approximately ENE-WSW, NE-SW, and NNE-SSW trends have been identified across the area (Figure 2.9, A), as well as structural lineaments with NE-SW, EW, NNW-SSE, and NNE-SSW trends (Figure 2.9, B). The ENE-WSW faults (Figure 2.9, A) are mainly distributed in the

Ancona thrust sheet and Alberta Syncline. They cut across the main features of the Foothills and through the Alberta Syncline attesting their regional scale. The NE-SW and NNE-SSW faults are preferentially located in the Foothills within the Brazeau thrust sheet, although a few are imaged in the Alberta Syncline within the Lovett structure.

A set of approximately ENE-WSW faults cut across the Lovett anticline, intersect the Pedley-Lovett backthrust in the west limb of the Alberta Syncline, and the Ancona thrust front in the Foothills (Figure 2.7). The brighter tone and different texture of the lithology at the core of the Lovett anticline (Brazeau Formation) contrast with that of the surrounding lithology (Paskapoo Formation) allowing the detection of structural steps resulting from the motion along these faults. The type of offset imaged along the faults suggests that they could represent transverse extensional faults as shown in the enlarged section of the Lovett area in Figure 2.10A. For clarity and comparison the same section without interpretation is shown in Figure 2.10B. The motion along the faults is compatible with lateral extensional faults associated with the propagation of the Ancona and Lovett thrusts during and after thrust faulting. The density of the transverse lateral extensional faults increases across the southeast-plunging nose of the Lovett anticline, which suggests relaxation of the structure along a probable oblique ramp. A series of transverse ENE-WSW faults cuts across the Ancona frontal thrust southeast of the Blackstone structure and at the northwest plunging nose of the Stolberg anticline-syncline pair (Figure 2.11). The motion along the faults may also be due to the presence of lateral extensional faults along oblique ramps of the Blackstone culmination and the Stolberg anticline-syncline structure.

A set of NE-SW faults intersects the Lovett structure in the Alberta Syncline. Structural steps of the Pedley-Lovett backthrusts are outlined and a consistent dislocation of the plunging nose of the Lovett anticline is imaged (Figure 2.10A). The imaged offset along the faults suggests they might represent right-lateral transverse tear faults (Dahlstrom, 1970), in which a differential movement occurred during the translation of the Pedley-Lovett thrust. The ENE-WSW extensional faults dislocate and postdate the NE-SW faults.

In the inner foothills, NE-SW faults dislocate the Brazeau thrust fault which bounds the Cardinal Hills thrust-fold structure (Figure 2.10A). The brighter tone and rough texture of the Brazeau Formation of the Cardinal Hills show a distinct contrast with the dark grey tone and smooth texture of the Paskapoo Formation lying in the footwall of the Brazeau thrust. These features outline structural steps in the Cardinal Hills structure with predominant left-lateral dislocations of the Brazeau thrust front. The imaged offset along the faults suggests they might represent transverse wrench type faults, in which the direction of slip is concurrent with the translation of the Brazeau thrust and is parallel to it. This system of transverse tear faults strikes approximately 90° to the Brazeau thrust fault. Other probable transverse tear faults are displayed in the Brazeau thrust sheet further southwest where they terminate within the Brazeau thrust sheet (Figure 2.7).

None of the identified fault sets is reported on published maps. However, Schmidt (1955) has previously documented evidence of local tear faults in the Central Foothills of Alberta. Documented transverse tear faults cutting across strike are also reported in the Front Ranges of the Southern Cordillera in the Banff area (Price et al., 1972), Canmore area (Price et al., 1970), Rundle Thrust Sheet (Bielenstein, 1969) and Mount Bryant area

(Zolnai, 1987), and in the Foothills where they have been documented in the Nordegg (Douglas, 1956) and Chungo Creek maps (Douglas, 1958).

Structural lineaments with NE-SW, EW, NNW-SSE, NNE-SSW orientation were also identified in this study (Figure 2.9, B). Lineaments can represent the continuity of fault structures where no clear displacement is present but where a linear trend is still detectable, as shown in the area between the Cardinal Hills ridge and the Lovett anticline in Figure 2.10A. In the Plains/Alberta Syncline, fault structures commonly displace lineaments. East of the Lovett anticline, the intersection between ENE-WSW transverse faults and the NNE-SSW lineaments outline a subtle fault-block ridge. A few ENE-WSW lineaments have been identified along the Brazeau River valley, which extends for several kilometers across the inner and outer Foothills. Although no clear intersection relationships have been identified with the Ancona and Brazeau thrusts (Figure 2.7), these features could represent surface evidence of deeper structures related to the basement, whose characterization might be corroborated through interpretation of high resolution aeromagnetic images of the area.

2.5 DISCUSSIONS AND CONCLUSIONS

The results obtained in this work show that satellite radar data can enhance the structural and lithological mapping of the Canadian Rocky Mountain. RADARSAT-1 S1 proved to be particularly good in this type of terrain for structural and lithological mapping. At a regional scale, the main known structural features have been identified and

mapped along strike with the assistance of seismic data. Additional structural features, namely transverse faults and lineaments, have been delineated. The topographic expression of deep-seated structures such as thrust and backthrusts has been successfully documented and verified with the integrated seismic data. The deep extension of the transverse faults and lineaments identified in the radar data was not visible using the seismic data, possibly because the small offsets observed at the surface (in the order of tens of meters) cannot be resolved. The integration of radar interpretation with aeromagnetic imaging may provide further documentation of these faults and insights for the detection of those faults with important displacement.

ENE-WSW transverse extensional faults, which cut across the inner and outer foothills, are mainly localized at the termination of the major structural culmination of the Lovett structure in the outer Foothills and the Blackstone and Stolberg structures within the Ancona thrust sheet. Their localization suggest that they could be related to the presence of deep structures such as oblique ramps lateral to the Lovett, Blackstone and Stolberg culmination. Although this hypothesis remains untested, such transverse faults could play a role in the structural separation of the main thrust-fold related oil plays located in the Lovett, Blackstone, and Stolberg structures. Moreover, these structures may characterize third- generation fault-play types of fractured reservoirs (Newson, 2001; MacDonald et al., 1981; Rumsey, 1976) and represent potential targets for light-oil exploration in the area.

The NE-SW transverse tear faults, localized in the inner foothills, cutting through the Brazeau thrust sheet, determine left-lateral offsets of the Brazeau thrust in the Cardinal Hills area. The observable displacement of the Brazeau thrust demonstrates that transverse

tear faults propagated throughout the Foothills, and are not restricted to the Front Ranges. A similar result was found by Douglas (1956) in the Nordegg area within the Bighorn thrust sheet.

This work illustrates that satellite radar data can be used to improve the structural and lithological mapping of terrains with dense vegetation cover and limited outcrop, such as the Foothills of the Central Alberta Cordillera thrust and fold belt. In this study, the interpreted features have been verified, where possible, with seismic imaging interpretations, and the interpretations of radar imagery were used to fill mapping gaps in the existing seismic coverage.

REFERENCES

- Berger, Z. (1994). *Satellite hydrocarbon Exploration: Interpretation and Integration Techniques*. Springer-Verlag Publishers.
- Bielenstein, H.U. (1969). *The Rundle Thrust Sheet, Banff, Alberta*. PhD Thesis, Queen's University, Kingston, Ontario, Canada.
- Brown, R.J., Brisco, B., D'Iorio, M.A., Prevost, C., Ryerson, R. A., Singhroy, V. (1996). RADARSAT applications: review of GlobeSAR Program. *Canadian Journal of Remote Sensing*, Vol. 22, No. 4, pp. 404-419.
- RADARSAT applications: review of GlobeSAR Program. *Canadian Journal of Remote Sensing*, Vol. 22, No. 4, pp. 404-419.
- Chamberlain, V.E., Lambert, R.S.J., and McKerrow, W.S. (1989). Mesozoic sedimentation rates in the Western Canada Basin as indicator of the time and place of tectonic activity. *Basin Research*, Vol. 2, pp. 189-202.
- Charlesworth, H.A.K., and Gagnon, L.G. (1985). Intercutaneous wedges, the triangle zone, and structural thickening of the Mynheer Coal seam at Coal Valley in the Rocky Mountain Foothills of central Alberta. *Bulletin of Canadian Petroleum Geology*, Vol. 33, pp. 22-30.
- Dahlmstrom, C.D.A. (1970). Structural geology in the eastern margin of the Canadian Rocky Mountains. *Bulletin of Canadian Petroleum Geology*, Vol. 18, pp. 332-406.
- Denyer, N., Raney, R.K., Shepherd, N. (1993). The RADARSAT SAR data processing facility. *Canadian Journal of Remote Sensing, Special Issue RADARSAT*, Vol.19, No. 4, pp. 311-316.
- Douglas, R.J.W. (1956). Nordegg, Alberta. *Geological Survey of Canada*, Paper 55-34.
- Douglas, R.J.W. (1958). Chunco Creek map area, Alberta. *Geological Survey of Canada*, Paper 58-3.
- Douglas, R.J.W., and Lebel, D. (1993). Geology and structure cross-section, Cardinal River. Alberta. *Geological Survey of Canada*, Map 1828A.
- Elachi, C (1987). *Spaceborn Radar Remote Sensing: application and Techniques*. IEEE Press, New York.
- Evans, D.L., Farr, T.G., Ford, J.P., Thompson, T.W., Werner, C.L. (1986). Multipolarization Radar Images for geologic mapping and vegetation discrimination. *IEEE Transaction on Geoscience and Remote Sensing*, Vol. GE-24, No. 2, pp. 246-257.
- Graham, L. C. (1977). Synthetic aperture radar geologic interpretation techniques. *Microwave Remote Sensing Symposium*, NASA /JSC, Huston Texas, pp. 129-140.

- Gray, S.H., and Maclean, G. (1996). In the Foothills, Prestack Depth Migration IS Interpretive Processing. In *Geophysics, a reservoir of knowledge*, (Calgary, Alta Ed), Canadian Society of Exploration Geophysicists & 23rd annual meeting, pp. 7-18.
- Koopmans, B.N. (1985). Side looking radar, a tool for geological survey. *Remote Sensing Reviews*, Academic Publishers GmbH, Great Britain, pp. 19-70.
- Langenberg, C.W., and LeDrew, J. (2001). Coal Valley. *Geological Survey of Canada*, Map 273.
- Lebel, D., Langenberg, C.W., Mountjoy, E.W. (1996). Structure in the central Canadian Cordillera thrust and fold belt, Athabasca-Brazeau area, Alberta: a large, complex intercunaneous wedge. *Bulletin of Canadian Petroleum Geology*, Vol. 44, No. 2, pp.282-298.
- Lee, J. S. (1980). Digital Image Enhancement and Noise Filtering by Use of Local Statistics. *IEEE Transactions on Pattern Analysis and Machine Intelligence*, Vol. PAM1-2, No. 2.
- Lee, J. S. (1981). Refined Filtering of Image Noise Using Local Statistics. *Computer Graphic and Image Processing*, Vol. 15, pp. 380-389.
- LeDrew, J. (1997). *Three-dimensional geometry and evolution of the Lovett River Triangle Zone, Central Alberta Foothills*. Master's Thesis, Department of Geology, University of Calgary.
- Lillesand, T.M., and Kiefer, R.W. (1994). *Remote sensing and image interpretation*. John Wiley & Sons Inc., Toronto, ON, Canada.
- Luscombe, A.P., Ferguson, I., Shepherd, N., Zimck, D.G., Naraine, P. (1993). The RADARSAT Synthetic Aperture Radar Development. *Canadian Journal of Remote Sensing, Special Issue RADARSAT*, Vol. 19, No. 4, pp. 298-310.
- MacDonald, H.C (1980). Techniques and applications of imaging radars. In Siegal, B.S. and Gillespie, A.R. Eds., *Remote sensing in geology*. John Wiley & Sons, New York.
- MacDonald, H.C., Waite, W., Elachi, C., Borengasser, M., and Tolman, D. (1981). Exploration for fractured reservoirs using radar/LANDSAT merge combinations. *Geoscience and Remote sensing Symposium, Proceedings*, Washington, D.C., pp. 312-317.
- Newson, A.C. (2001). The future of natural gas exploration in the Foothills of the Western Canadian Rocky Mountains. *The Leading Edge*, The Society of Exploration Geophysicists, Vol. 20, No. 1, pp. 74-79.
- Paganelli, F. and Rivard, B. (1999a). *Tracking geological structures in the Central Alberta Foothills, Canada, using RADARSAT imagery*. Report Petrocanada. Unpublished
- Paganelli, F. and Rivard, B. (1999b). Tracking geological structures in the Central Alberta Foothills, Canada, using RADARSAT imagery. *Proceedings of the Thirteenth International Conference of Applied Geologic Remote Sensing*, Vol. I, p. 109.

- Price, R.A. (1981). The Cordilleran foreland thrust and fold belt in the southern Canadian Rocky Mountains. In *Thrust and Nappe Tectonics* (K.C. McClay and N.J. Price Ed), Geological Society of London, Special Publication Vol. 9, pp. 427-448.
- Price, R.A., and Mountjoy, E.W. (1970). Geologic structure of the Canadian Rocky Mountains between Bow and Athabasca Rivers - a progress report. In *Structure of the Southern Canadian Cordiller* (J.O. Wheeler Ed.), Geological Association of Canada, Special Paper 6, pp. 7-25.
- Price, R.A., Mountjoy, E.W. , Eitken, J.D., Bielenstein, H.U., Cook, D.G., Leech, G.B. (1970). Canmore (West Half). *Geological Survey of Canada*, Map 1266A.
- Price, R.A., Mountjoy, E.W. , Eitken, J.D., Bielenstein, H.U., Cook, D.G., Leech, G.B. (1972). Banff (East Half). *Geological Survey of Canada*, Map 1294A.
- Price, R.A., Scott, D.E., Campbell, R.B., Mountjoy, E.W., and Ollerenshaw, N. C. (1977). Athabasca River. *Geological Survey of Canada*, Map 1339A.
- Rossignol, S., and Corbley, K.P. (1996). Reconnaissance by Radar. *Canadian Mining Journal* , Vol. 117, No. 6, pp. 13-16.
- Rumsey, I.A.P. (1976). Airborne radar finds deep fracture-controlled pools. *World Oil*, Vol. 182, No. 1, pp. 1-4.
- Sabins, F.F. Jr. (1987). *Remote Sensing: Principles and Interpretation*, W.H. Freeman and Company, 3rd Ed., New York.
- Singhroy, V.H. (1992). Radar Geology: Techniques and Results. *Episodes*, Vol. 15, pp. 15-20.
- Singhroy, V.H., Slaney, R., Lowman, P., Harris, J., Moon, W. (1993). RADARSAT and radar geology in Canada. *Canadian Journal of Remote Sensing*, Vol. 19, No. 4, pp. 338-351.
- Singhroy, V. and Saint-Jean, R. (1999). Effect of relief on the selection of RADARSAT-1 incidence angle for geological applications. *Canadian Journal of Remote Sensing*, Vol. 25, No. 3, pp. 211-217.
- Schmidt, R.G. (1955). Joint patterns in relation to local tear faults in the central foothills of Alberta. *Master's Thesis, Columbia University, Teachers College. New York, NY, United States.*
- Wheeler, J.O., and McFeely, P. (1991). Geotectonic Assemblage Map of the Canadian Cordillera and adjacent parts of the United States of America. *Geological Survey of Canada*, Map 1712A.
- Yan, L., and Lines, L. (2001). Imaging of an Alberta foothills seismic survey. *The Leading Edge*, The Society of Exploration Geophysicists, Vol. 20, No. 1, pp. 80-84.
- Zolnai, A.I. (1987). Structure and stratigraphy, Mount Bryant area, eastern Rocky Mountain Front Ranges, Alberta. *Geological Survey of Canada*, Vol. 87-1A, pp. 323-330.

Figure 2.1. Generalized tectonic map of the Canadian Cordillera thrust and fold belt western Alberta and British Columbia, showing the location of the study area (modified after Lebel et al., 1996). P: Pyramid Thrust; B: Bourgeau Thrust; PP: Pipestone Thrust; SP: Simpson Pass Thrust.

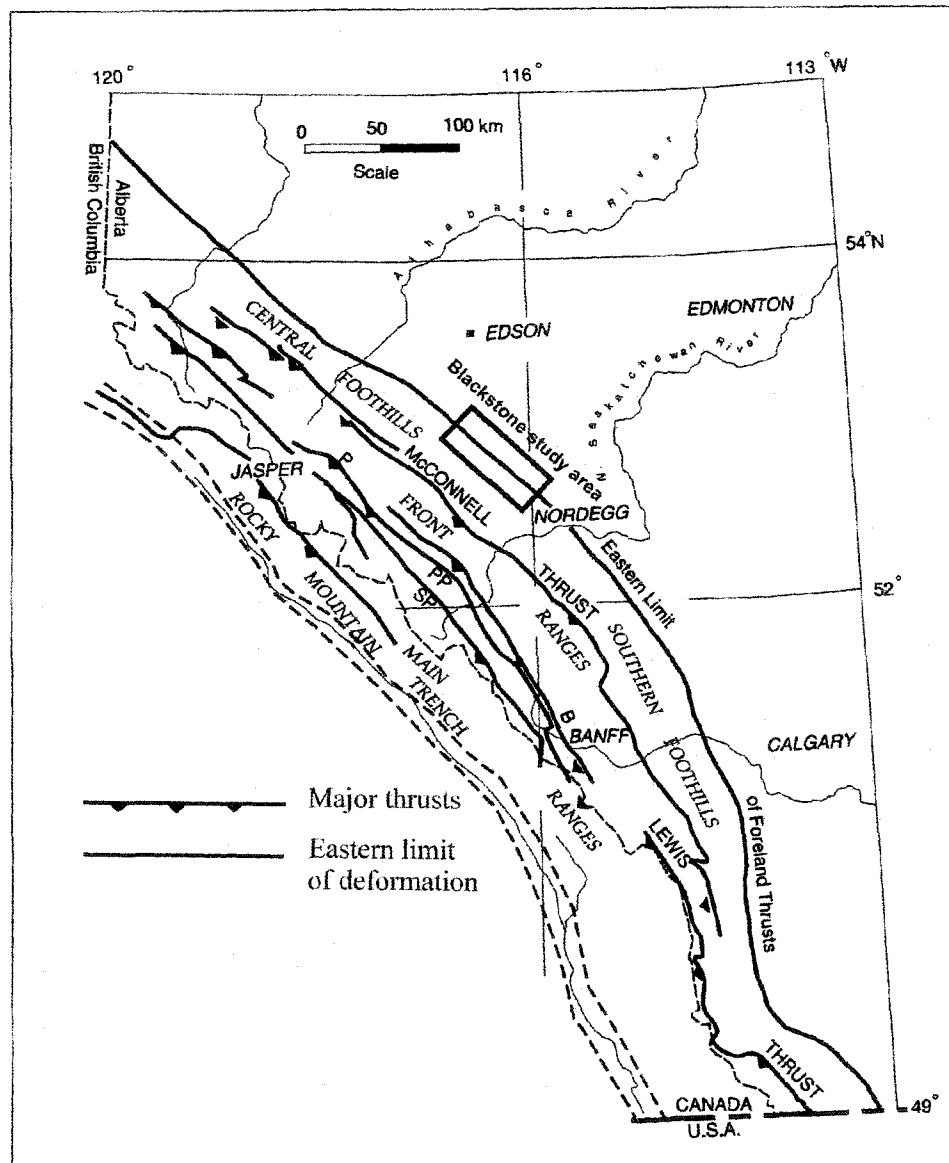


Figure 2.2. Geology of the Blackstone study area (modified after Price, 1977). PP: Paskapoo Formation; uKB, Brazeau Formation.

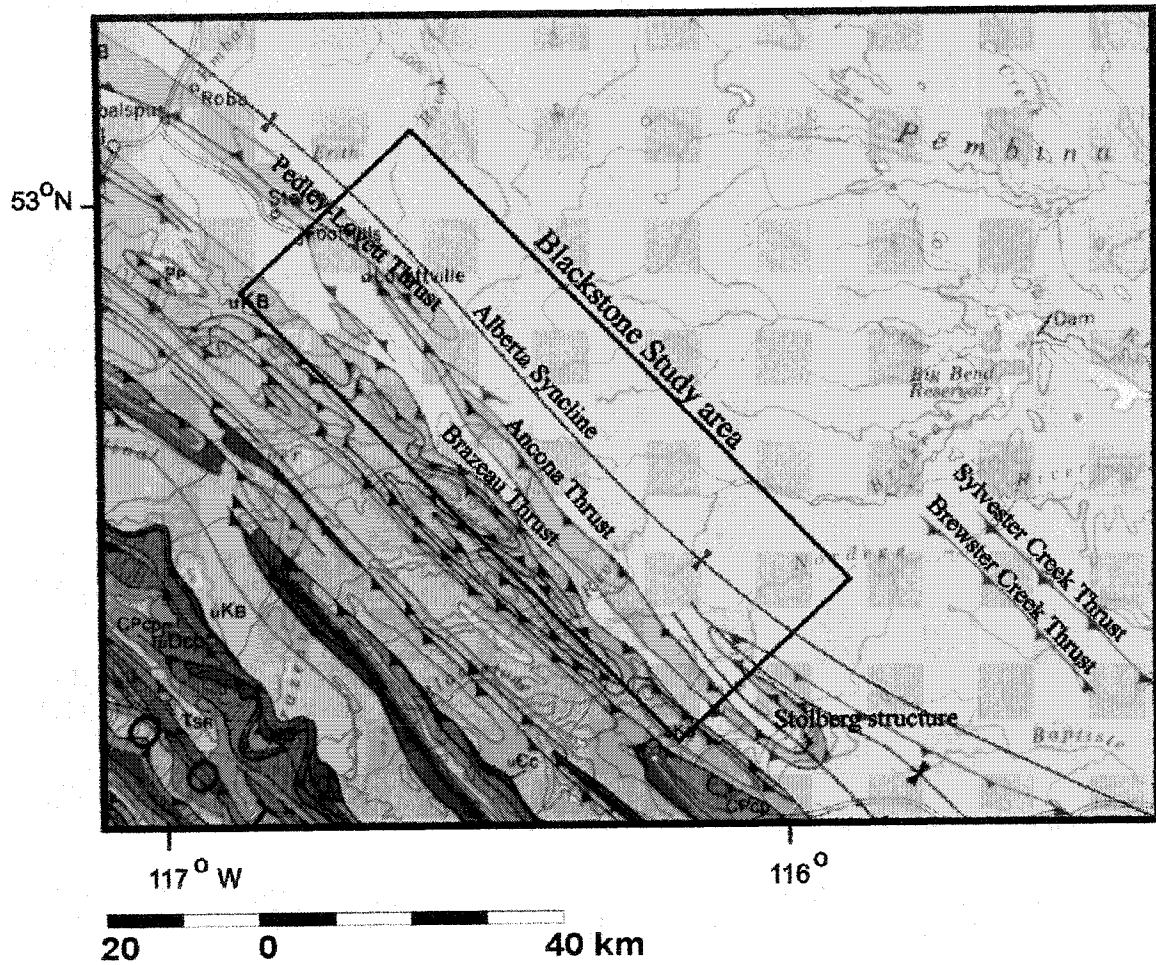


Figure 2.3. Schematic stratigraphic relationships across the Central Alberta Foothills and Front Ranges (modified after Lebel et al., 1996). Carbonate rocks of Cambrian and Mississippian age dominate the lower part of the sequence, and clastic marine and non-marine sedimentary rocks of Mesozoic-Cenozoic age of the foreland basin define the upper part. Thrust fault surfaces occur extensively parallel to stratigraphic horizons. Vertical scale (Vertical exaggeration approximately 10 times)

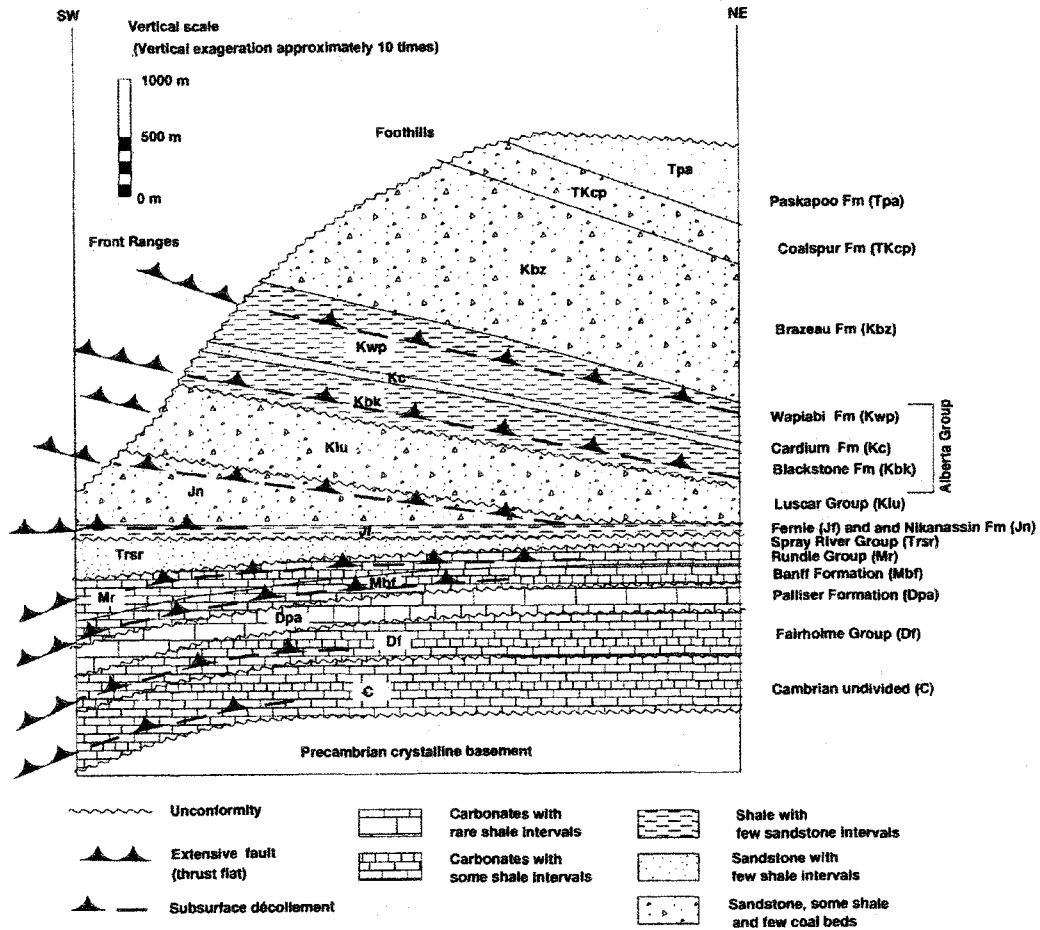


Figure 2.4. Blackstone study area. RADARSAT-1 Standard Beam Mode 1 (S1), Descending Orbit, acquired on August 5th 1997. Incidence angle 20-27°, C band, HH polarization. Nominal coverage area 100x100 km, approximate ground resolution 25 m, pixel size in range and azimuth 12.5 m. The Township & Range Grid is shown for reference.

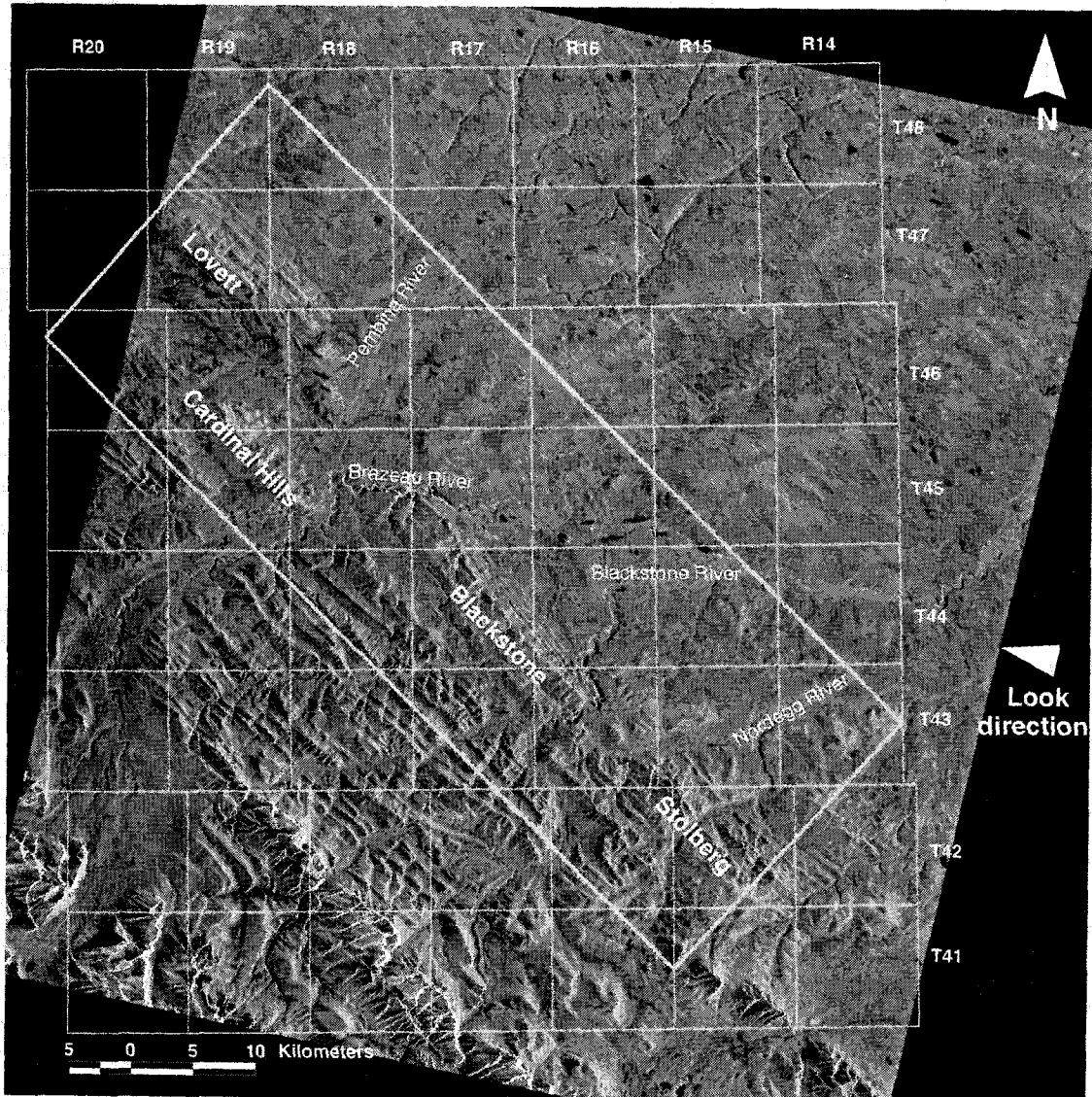


Figure 2.5. Blackstone study area. RADARSAT-1 Fine Beam Mode 1 (F1) Near Range, Descending Orbit, acquired on July 7th 1998. Incidence angle 36.4-39.6°, C band, HH. Nominal coverage area 50x50 km, approximate ground resolution 8 m, pixel size in range and azimuth 6.25 m. The Township & Range Grid is shown for reference.

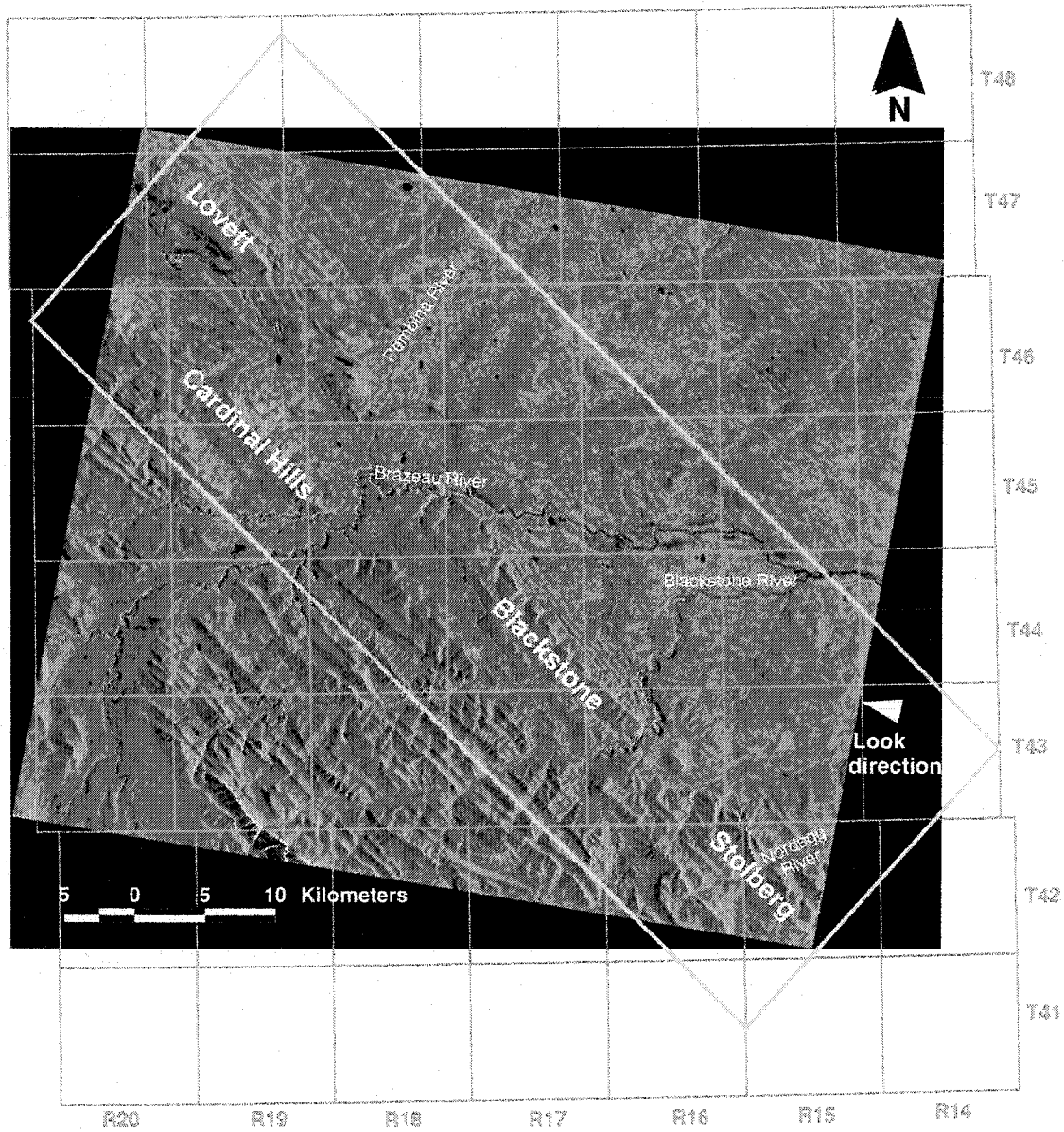


Figure 2.6. Seismic interpretation on RADARSAT-1 Standard Beam Mode 1, showing the correspondence of the topographic expression of the interpreted Ancona and Brazeau thrusts, the Pedley-Lovett and New Upper Bounding backthrusts.

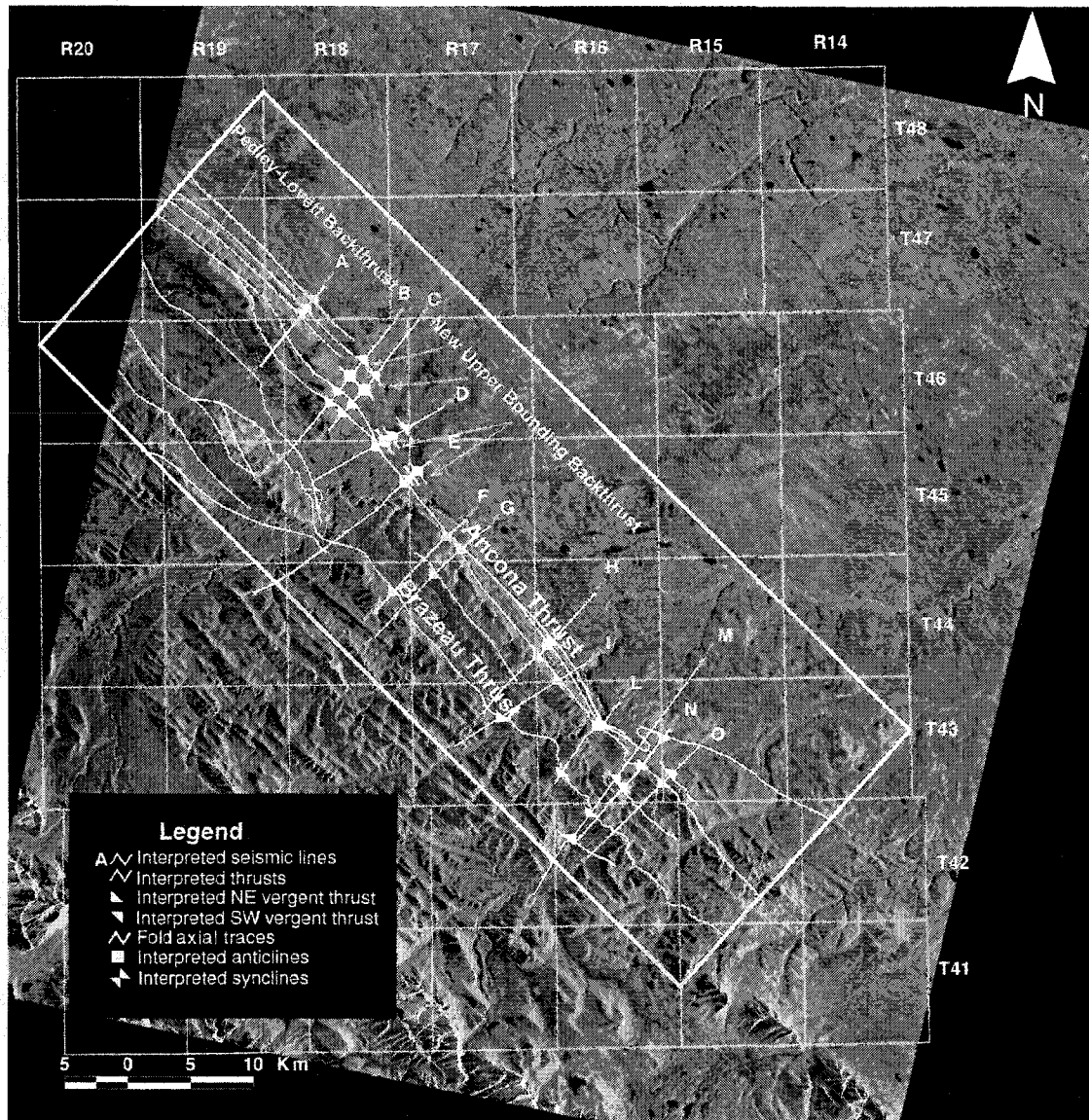


Figure 2.6A. Interpretation of the seismic section B and C in the Lovett area. The Ancona thrust, Lovett anticline, and New Upper Bounding backthrust structures are shown. Their extrapolation to the surface was combined with the structural features observed in the RADARSAT-1 Standard Beam Mode to compile the structural map in Figure 2.7. The Cardium Formation is reported in the sections as it represents the oil-productive horizon in the area.

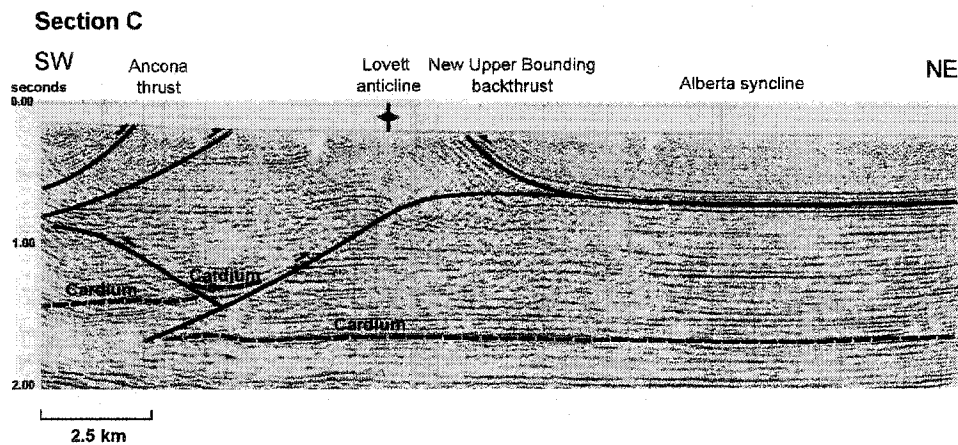
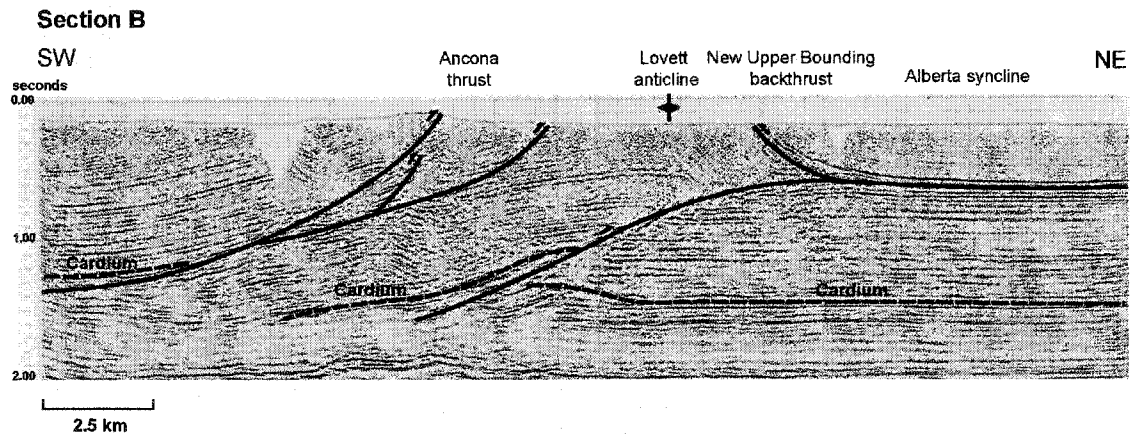


Figure 2.7. Blackstone structural interpretation on RADARSAT-1 Standard Beam Mode 1.

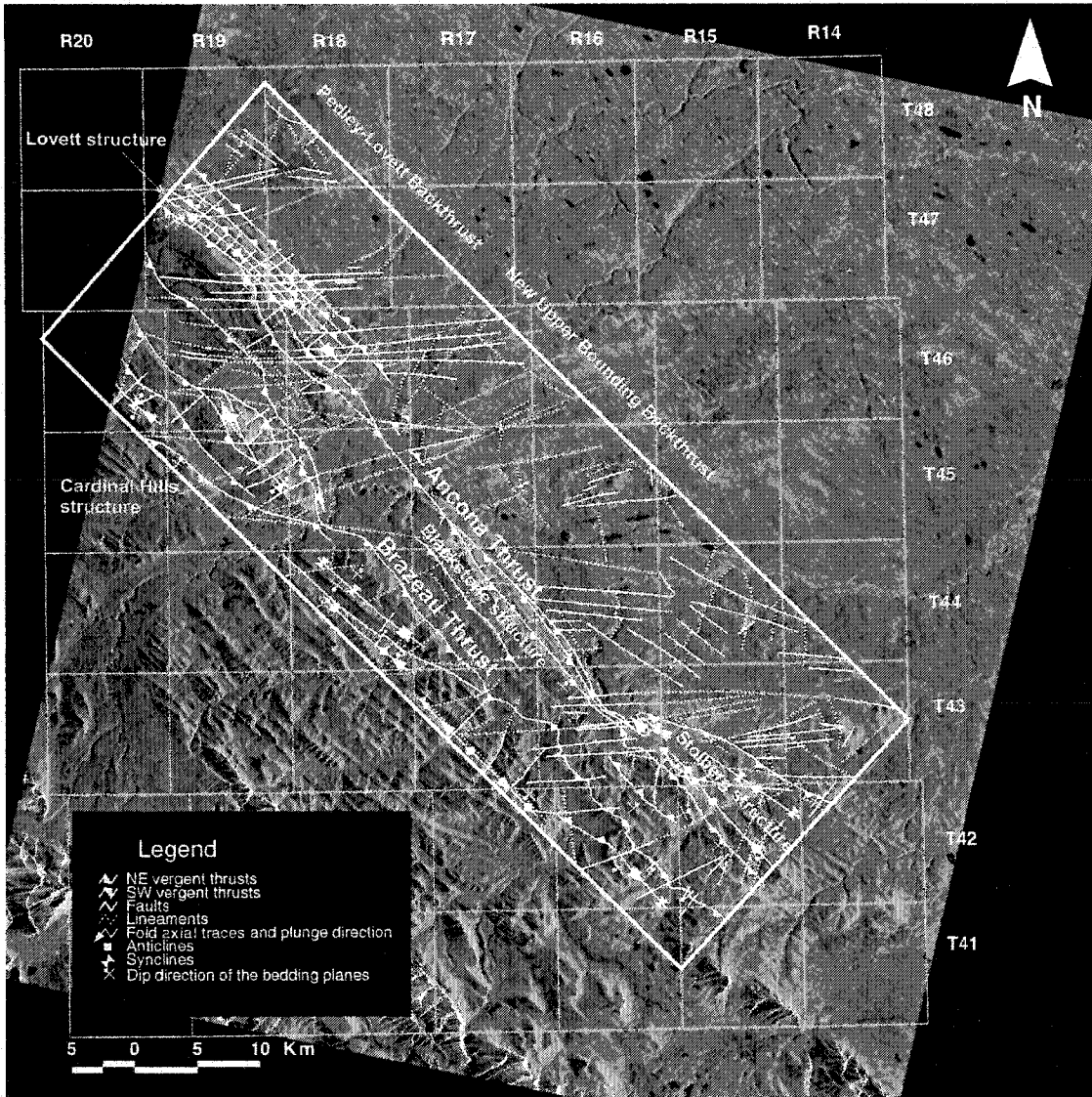


Figure 2.8. Blackstone lithologic map on RADARSAT-1 Standard Beam Mode 1. Kbz: Brazeau Formation; Tpa: Paskapoo Formation.

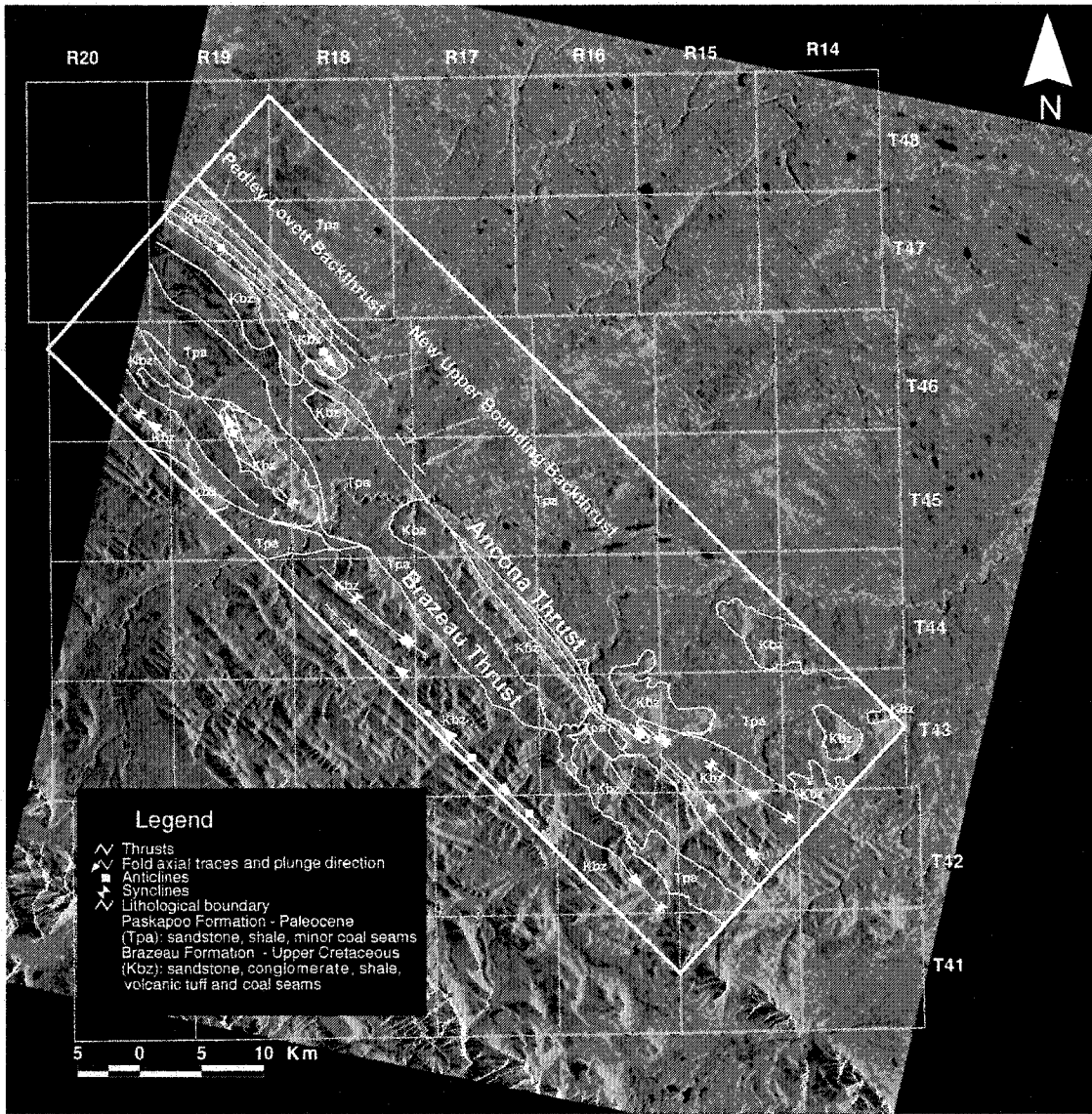


Figure 2.9. Rose diagrams: **A)** transverse fault trends; **B)** lineament trends.

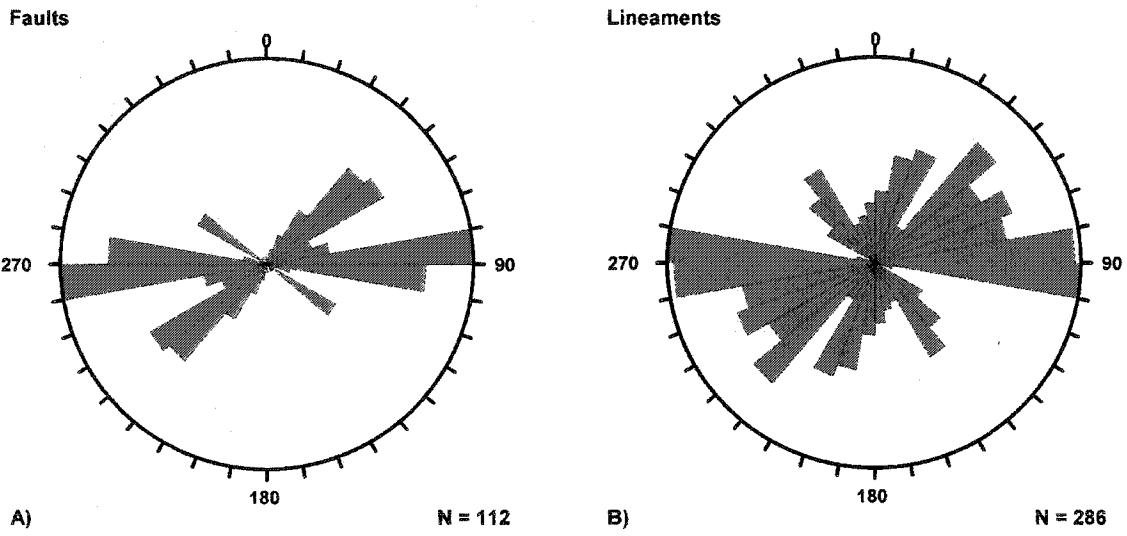


Figure 2.10A. Details of the structural interpretation of the Cardinal Hills/Lovett area on RADARSAT-1 Standard Beam Mode 1. Lower left, offset of the Brazeau thrust bounding the Cardinal Hills ridge; top center, offset of the Lovett anticline and Lovett thrusts. For symbols refer to Figure 2.7.

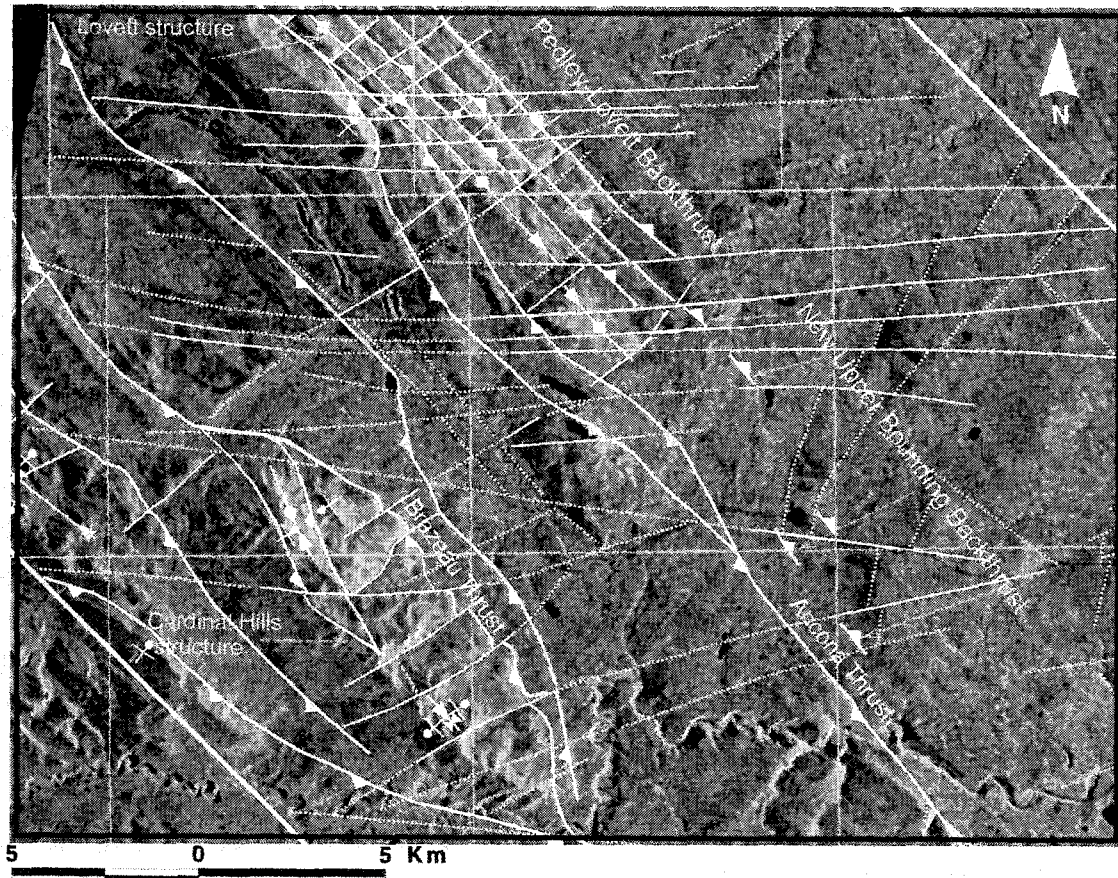


Figure 2.10B. Uninterpreted section of Cardinal Hills/Lovett area on RADARSAT-1 Standard Beam Mode 1, for reference.

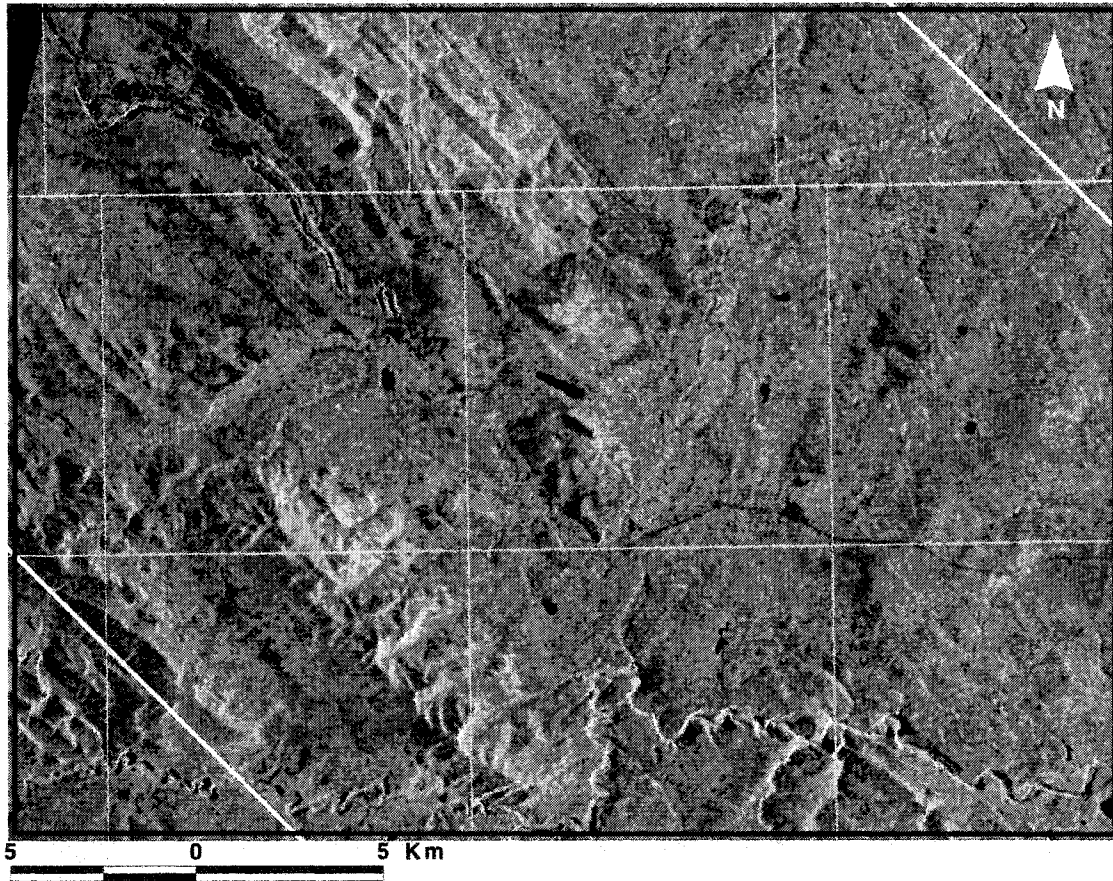
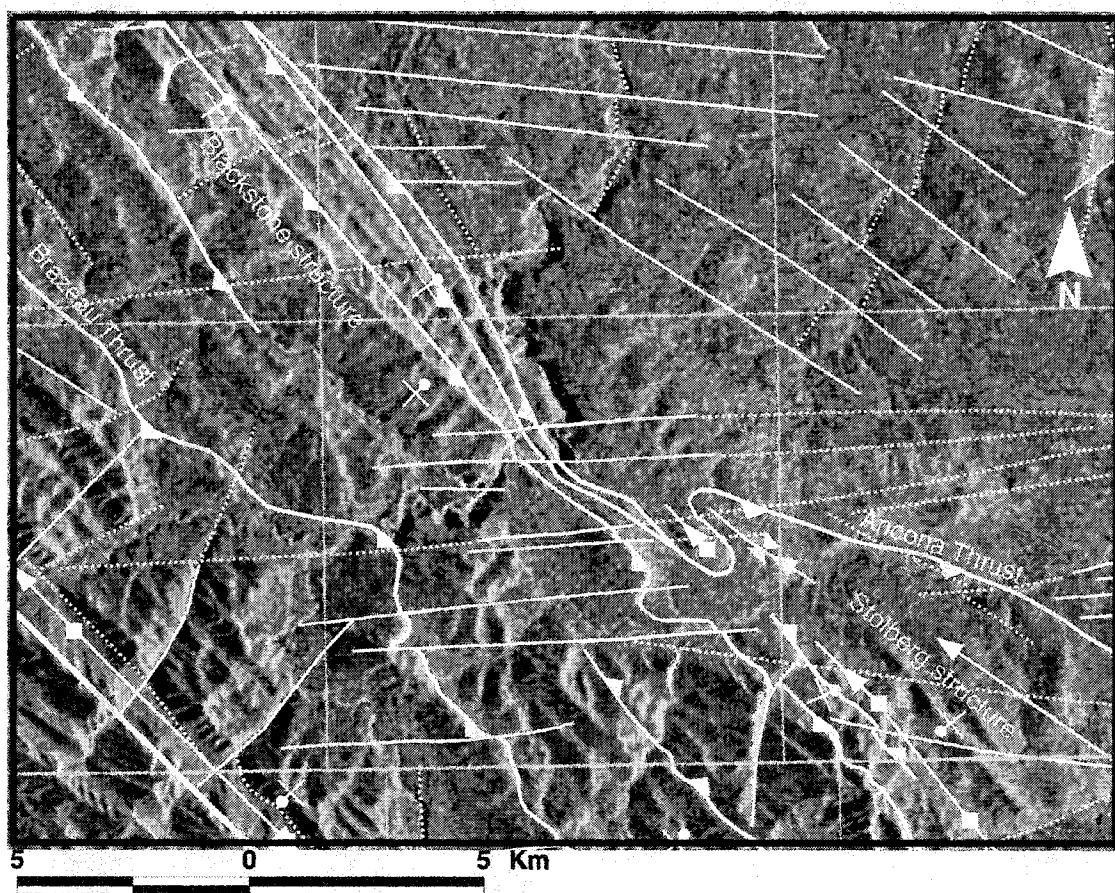


Figure 2.11. Details of the structural interpretation of the Blackstone and Stolberg structures on RADARSAT-1 Standard Beam Mode 1. For symbols refer to Figure 2.7.



Chapter 3

USE OF RADARSAT-1 PRINCIPAL COMPONENT IMAGERY FOR STRUCTURAL MAPPING: A CASE STUDY IN THE BUFFALO HEAD HILLS AREA, NORTHERN CENTRAL ALBERTA

3.1 INTRODUCTION

Principal Component Analysis (PCA) is a classical method used to express linear combinations of multi-band images in order to analyze and reduce redundancy in the input data set. PCA of multi-band quad-polarimetric radar images acquired during the SIR-C/X-SAR mission has previously yielded useful results for lithological mapping (e.g., Price, 1999), and analysis of visible and infrared bands from Landsat TM images have been used for alteration mineral mapping (Loughlin, 1991; Crosta and Moore, 1989; Tangestani and Moore, 2001). Recently, Geostationary Operational Environmental Satellite (GOES) images have also been used for meteorological applications (Hillger, 1996b; Hillger and Ellrod, 2000).

Based on the same multi-band processing approach, we applied PCA to a multi-band image containing four mosaic images from RADARSAT-1 Standard Beam Mode S1/S7 scenes in ascending and descending orbit. The four different geometrical configurations of the input images/bands determine the backscattering variability of surface targets within each scene. These differences are the independent contributions which are mapped in the PCA as linear combinations in the resulting principal components image.

The first objective of this study is to assess the quantitative and qualitative information present in the RADARSAT-1 principal component images using the Feature Oriented Principal Components Selection (FPCS) method of Crosta and McMoore (1989), and to explore their applicability for structural mapping in highly vegetated terrains.

Radar topographic perception and response to surface geometry, roughness, and dielectric properties have been widely used for structural and geological mapping in desert (Blom et al., 1984; Rudant et al., 1994; Price, 1999), and vegetated (Sabins, 1983; Berger, 1994) environments. The use of RADARSAT-1 synoptic properties has also contributed to geological and structural mapping applications (Singhroy et al., 1993; Berger, 1994; Paganelli and Rivard, 1999a, 1999b, 2001). RADARSAT-1 Principal Component Analysis (PCA) based on the extraction of image components from a multi-band image of RADARSAT-1 S1/S7 Mode in ascending/descending orbit (Paganelli et al., 2001b; Grunsky, 2001) has also been used successfully for structural mapping. In particular, the RADARSAT-PC2 image has been shown to be characterized by improved topographic perception and surface texture information. In the present study, RADARSAT-1-PC1, -PC2, -PC3, and -PC4 images have been used to outline linear features interpreted to be related to underlying bedrock structures. Therefore, the second objective of this study is to evaluate RADARSAT-1 PC imagery for structural mapping in the Buffalo Head Hills area within a regional geological context as a contribution to geological mapping and mineral exploration.

A significant regional structural study using remotely sensed data was carried out previously by Misra et al. (1991). In that study, Landsat MSS, TM, and Seasat satellite

radar images were used to prepare a lineament map of the entire western plains region of Alberta, Saskatchewan, part of British Columbia, and a portion of North Western Territories. The satellite images were interpreted visually to outline fractures and bedding trends. Two main lineament datasets with NW and NE trend were outlined, which revealed basement structures in northern central Alberta attributed to the Peace River Arch, a Devonian flexural-isostatic crustal thinning (Ross, 1990). These NW- and NE-trending lineaments have been clearly identified in the present study, and two additional NNE- and ENE-trending lineament sets have also been found.

The structural interpretation in this study has been compared with unpublished independent studies by Ashton Mining Canada Inc. (Lockett, 1998), and Alberta Energy Corp. (Pryde, 2000). These studies, although focused on a restricted portion of the Buffalo Head Hills, represent structural compilations from various datasets, and have been used to add constraints to the interpretation in this paper. An additional study and reference map was provided by the Alberta Geological Survey for the south-eastern corner the Buffalo Head Hills, representing a subset area within the AGS report of the Peerless Lake study by Eccles et al. (2000). The comparison with these datasets is purely qualitative, because the data are protected by proprietary agreements, and are not published at this time. However, at a regional scale the various studies show similarity with the structural trends extracted using the RADARSAT-1-PC imagery, thus giving confidence to the use of RADARSAT-1-PC imagery for regional structural mapping.

3.2 REGIONAL GEOLOGY

The Buffalo Head Hills in north-central Alberta (Figure 3.1) has been an area of intense oil and gas exploration, and recently also kimberlite exploration (Carlson et al., 1998). It is part of the cratonic platform whose tectonic evolution has been influenced by the uplift and extensional episodes of the Peace River Arch (Cant, 1988; O'Connell et al., 1990; Ross, 1990). These episodes have determined the development since the Phanerozoic of N- and NE-trending horst-graben block structures in the Precambrian basement (O'Connell et al., 1990), which affected the sedimentation of a Middle Devonian to Upper Cretaceous succession of platform carbonates, shale, and sandstone (Figure 3.2 A).

The Precambrian crystalline metamorphic basement is characterized by Archean crust, tectono-thermally reworked during the Proterozoic (Edwards et al., 1995). The Buffalo High and Buffalo Utikuma accreted terranes are distinguished, based on a recent re-interpretation of the magnetic high of the Buffalo Head High, and magnetic medium-low of the Buffalo Utikuma (Pilkington et al., 2000). These terranes are largely characterized by 2.0 to 2.3 Ga metaplutonic and metavolcanic rocks (Ross, 1990; Ross, 1991; Villeneuve et al., 1993). The Sm-Nd isotope systematics along with recent Lithoprobe Program results indicate that the Proterozoic terranes in northern Alberta may represent thin-skinned thrust slices emplaced over a composite Archean-Early Proterozoic basement during the Paleo-Proterozoic, as has been proposed for the Taltson, Ksituan, and western Buffalo Head terranes (Ross, 1990). West and southwest of the Buffalo High lies the Chinchaga Low, which consists of metasedimentary and

metaplutonic gneisses with U-Pb crystallization ages of 2.08 to 2.17 Ga (Ross, 1990). Based on geophysical, Nd isotopic, and geochronological data, Theriault and Ross (1991) and Villeneuve et al. (1993) speculated that the Buffalo Head terrane (now Buffalo High-Buffalo Utikuma terranes) and Chinchaga Low may be composite Archean crustal blocks, which amalgamated between 2.0 and 2.1 Ga. They also suggested that the presence of 2.00-1.99 Ga granite rocks in the Buffalo Head Domain may have been generated by collision with the Chinchaga Low. The schematic tectonic model proposed by Ross (1990) for the assembly and growth of continental crust in northern Alberta is reported here in Figure 3.1A, with the addition of the Buffalo High, and Buffalo Utikuma terranes.

The Middle Devonian to Late Cretaceous sedimentary sequence and its depositional history have been locally affected and/or structurally controlled by the Peace River Arch structures (Figure 3.2, A; Cant, 1988; Ross, 1990; Hein, 1999). These structures provide oil and gas traps and reservoirs within the Granite Wash and Keg River formations (Mossop and Shetsen, 1994; Hein, 1999). A summary stratigraphic sequence of the Cretaceous sediments in the study area is shown in Figure 3.2 (B), and their areal distribution is shown in Figure 3.3.

The Buffalo Head Hills area has recently attracted interest for kimberlite exploration (Carlson et al., 1998). Kimberlite pipes intrude the recessive Cretaceous sediments of the Smoky Group, Dunvegan Formation, and Shaftesbury Formation (Figure 3.3), and are characterized by crater facies lithologies, mainly of lapilli-bearing olivine crystal tuffs. Crustal xenoliths consist of shales of the Shaftesbury Formation, while mantle derived xenoliths include peridotite, pyroxenite, eclogite, and corundum-

spinel-bearing lithologies (Carlson et al., 1998). U-Pb perovskite dates of 86 ± 3 and 88 ± 5 Ma (Carlson et al., 1998) suggest that the pipes were emplaced in mid to late Cretaceous (Cenomanian to Campanian).

3.3 METHODOLOGY

3.3.1 RADARSAT-1 data selection and processing

A data set of 28 RADARSAT-1 scenes in Standard Beam S1 and S7 Modes (12.5 m pixel resolution) in ascending and descending orbit were acquired to provide full coverage for the Buffalo Head Hills area. The data set provides four different geometric configurations that combine different incidence angles characteristic of the S1 (20-27.4°) and S7 (44.9-49.4°) Standard Beam Modes (Luscombe et al., 1993), and different look directions (east or west) depending on the geometry of the acquisition mode in ascending and/or descending orbit.

The pre-processing of the multi-beam RADARSAT-1 imagery consisted in orthorectification using a digital elevation data in grid form, at 100 m resolution, provided by the Resource Data Division of the Alberta Department of Sustainable Development. The orthorectification is a necessary step in order to minimize the effects of foreshortening and layover associated with the difference in incidence angles of the S1 and S7 beam modes. The data set was georeferenced using the Universal Transverse Mercator (UTM) projection, Zone 11, National A Datum 83 (NAD83) ellipsoid.

The RADARSAT-1 scenes were pre-processed for speckle reduction using a 11x11 Gaussian filter with Standard Deviation of 1.6. In order to conduct the regional investigation of the Buffalo Head Hills area, mosaics of the RADARSAT-1 filtered scenes were constructed. Linear stretch matching and adaptive average filtering were applied to smooth image edge effects and image-to-image tone variations. Four mosaic scenes MOSAIC_S1A (Figure 3.4), MOSAIC_S1D (Figure 3.5), MOSAIC_S7A (Figure 3.6), and MOSAIC_S7D (Figure 3.7) were generated, and have been respectively assigned to bands 1, 2, 3, and 4 in a multi-band image MOSAIC_S1-S7. The multi-band image was then used for Principal Component Analysis. The extent of the resulting RADARSAT-1-PC images reflects the intersection area of the analyzed input bands, and is outlined by the RADARSAT-PC mask in Figure 3.8. Statistical analysis has been limited to the area within the mask (RADARSAT-PCmask) in order strictly to evaluate and compare the resulting images from the PCA to the input image bands.

The Feature Oriented Principal Component Selection (FPCS) technique (Crosta and McMoore, 1989) has been applied to analyze the information content of the RADARSAT-1-PC images. The FPCS was developed by Crosta and McMoore (1989) for analysis of Landsat Thematic Mapper (TM) data, but it is equally applicable to radar images (Price, 1999). In this study we used the FPCS technique to examine the PCA eigenvector loadings of the correlation matrix to select which of the principal component images concentrate and highlight information directly related to the theoretical backscattering signature of specific surface targets. The sign of the eigenvector loadings indicates whether a target surface type is characterized by dark or bright pixels and how this will affect its topographic perception, in relation to the radar backscattering response

as a combination of geology/vegetation, topography, and slope orientation observable in the input RADARSAT-1 image/bands. At the C band radar wavelength and HH polarization used by RADARSAT-1, most of the microwave backscatter is a result of interactions from primarily the top portion of the forest canopy. Image tone, contrast, and texture variation are enhanced by the appropriate look direction and incidence angle inherent in the RADARSAT-1 image acquisition. Topographic feature perception observable in such images therefore reflects either changes in slope, such as erosional escarpments due to variation of resistant and recessive lithological units (Evans et al., 1986; Brown et al. 1996; Paganelli and Rivard, 1999a, 1999b, 2001), or structural escarpments. In the study area, the Buffalo Head Hills topographic high defines east- and northeast-facing slopes towards the Loon River valley, best seen in the westward-looking RADARSAT-1 S1 and S7 descending mode scenes (Figures 3.5 and 3.7). In contrast, the Peerless Uplands are characterized by westward-facing slopes towards the Loon River Valley, and are highlighted in the eastward-looking RADARSAT-1 S1 and S7 ascending mode scenes (Figures 3.4 and 3.6). Both the Buffalo Head Hills and Peerless Uplands define N-trending topographic highs whose perception can be either emphasized or suppressed by the different look directions of the images. The steepest incidence angles (S1 scenes) provide the best enhancement of the gentle topography of the area (e.g., MOSAIC_S1D; Figure 3.5), whereas images characterized by shallower angles (e.g., MOSAIC_S7D, Figure 3.7) provide less topographic enhancement (Singhroy and Saint-Jean, 1999). These geometric factors affect the backscattering response from surface targets and therefore provide unique input to the RADARSAT-1-PC imagery.

3.3.2 Principal Component Analysis of RADARSAT-1 images

The principal component correlation eigenvectors in Table 3.1 define the loadings that each input band provides to the principal components. The original eigenvector values have been recalculated as a percentage of loading from the input bands and are shown in Table 3.2. This transformation allows a more straightforward understanding of the original band contributions to each RADARSAT-1-PC image. The relationships of each RADARSAT-1 beam mode with the four principal components as a function of the recalculated percentage loadings are shown in Figure 3.8A. The eigenvalues defining the relative proportion of the overall scene variance encompassed by each component are shown in Table 3.3.

The analysis of the RADARSAT-1-PC1 image and eigenvectors shown in Figure 3.9 reveals a significant positive mixture of all the input bands, with the greatest proportion provided by the MOSAIC_S7A and MOSAIC_S7D bands, this is also shown by the percentage loadings relationships in Figure 3.8A (1). This image highlights intensity information and tone variation related to radar backscattering in response to topographic changes, vegetation, and superficial terrain distribution. As can be observed in Table 3.3, the RADARSAT-1-PC1 image is characterized by the highest percentage of total variance (53.55%).

In the RADARSAT-1-PC2 image shown in Figure 3.10, a highly negative loading from band S1A (-58.02%) determines an inverse contribution to the image in terms of tone variability, and inverse topographic perception of the surface features facing to the west. Positive loadings are derived from band S7D (22.88%), S1D (11.82%), and S7A

(7.28%) as shown in Figure 3.8A (1). The image accounts for a total variance of 20.13%. The S7D and S1D band contributions greatly enhance the topographic perception of E- and NE-facing surface features of the Buffalo Head Hills, whereas the contribution of band S7A imparts perception of the W-facing slopes of the Peerless Uplands (Figure 3.10). The inverse relationship of the S1D and S1A band contributions optimizes topographic perception of surface targets with different orientation, contrast, and textural variability, making it particularly useful for the identification of surface topographic features related to structural patterns in the underlying bedrock.

The RADARSAT-1-PC3 image shown in Figure 3.11 contains two positive loadings with 38.40% contribution from band S7A, and 8.25% from S7D. The remaining loadings are negative, with -2.32% from band S1A, and -51.03% from band S1D. The image is characterized by 17.65% of total variance, with variance reduction of approximately 3% compared to the RADARSAT-1-PC2 image. In the RADARSAT-1-PC3 image the topographic perception is still appreciable due to the positive loadings of band S7D and S7A, and their inverse relationship with the negative loadings of band S1A and S1D as shown in Figure 3.8A (2), which results in an overall darker image tone. The bands S1D and S1A account for the higher intensity of backscattering response in the original images in relation to major topographic targets, due to the steeper incidence angle used by RADARSAT-1 Standard Mode 1 data acquisition. The negative contributions of these bands determine the presence of darker pixels corresponding to topographic targets such as the Buffalo Head Hills and Peerless Uplands, resulting in a subdued and/or inverse topographic perception. However, this effect combined with the positive contributions of bands S7A and S7D results in emphasis of brightness contrast

along the drainage patterns. Examples of well defined drainage with NNE- and ENE-trends are observable in the Loon River Valley, whereas NW-trending drainage patterns are defined by the Wabasca River, and in the Buffalo Head Hills (Figure 3.11).

The RADARSAT-1-PC4 image shown in Figure 3.12 contains two positive loadings, with 18.42% from band S1D, and 32.75% from band S7A. The two negative loadings are from band S1A with -8.12%, and band S7A with -40.71%. The contrast in the image is derived by the inverse relationship of band S7A and S7D as shown in Figure 3.8A (3). These loadings produce a total image variance of only 8.68%, and this image therefore contains the least correlated information. Nevertheless, useful geological information may still be recognized, despite the noisy appearance of the image. For example, abrupt tone variations that may be related to structural features are observable in the Peerless Uplands, across the Loon River Valley, and in the northern and central parts of the Buffalo Head Hills (Figure 3.12); these features do not appear in any of the other components or original input bands.

3.3.3 Structural map interpretation approach and validation

Interpretation of the RADARSAT-1-PC imagery involved visual pattern recognition of surface features resulting from the radar backscattering distribution, foreshortening and shadowing effects, tone, contrast, and textural variations enhancing the topographic perception in the RADARSAT-1 scenes (Paganelli et al., 2001b). The RADARSAT-1-PC1, -PC2, -PC3, and -PC4 images have been interpreted separately to allow independent identification of structural features, which may have variable degrees

of accuracy or certainty in each image as an effect of the different input contributions from the mosaic RADARSAT-1 scenes. The resulting lineaments have been analyzed in their regional geological context, compiled and plotted on rose-diagrams to outline the strike variability of the depicted features and the possible bias inherent in the interpretation of the individual RADARSAT-1-PC images.

The offset relationships of the outlined structural features have been used as a means to reconstruct the structural evolution of the Buffalo Head Hills. Identified features have been compared with known regional structural trends, attributed to the Peace River Arch development (Cambrian-Late Devonian), and the Laramide orogeny (Cretaceous).

Qualitative comparisons of the structural trends outlined in this study have also been made with unpublished independent studies conducted by Ashton Mining of Canada Inc. (AMCI; Lockett, 1998), Alberta Energy Company (AEC; Pryde, 2000), and Alberta Geological Survey (AGS; Eccles et al., 2000). These studies cover specific areas of known kimberlite occurrences within the regional Buffalo Head Hills study area of this paper. Nevertheless, they provide substantial support for the proposed interpretation. The outline of the AMCI, AEC, and AGS maps is shown in Figure 3.3.

The AMCI structural interpretation was compiled from 15 black and white aerial photographs at nominal scale of 1: 60 000. The interpretation was conducted visually by stereoscope to identify lineaments derived from drainage, topography, and Quaternary features (Lockett, 1998). The hand drafted compilation at 1: 50 000 scale was then scanned and vectorized to a final digital version at 1: 100 000 scale.

The AEC structural interpretation was compiled from three data sets that included structural data from oil/gas wells, aeromagnetic depth-solution analysis, and structural interpretation data from compiled 2D-3D seismic sections (Pryde, 2000). Subsurface structural data were derived for the Keg River Formation carbonate surface from oil well, along with isopachs from the top of the Keg River Formation to the Precambrian basement, which was used to define the morphology of the basement. This procedure enabled the definition of the isopach of the Keg River Formation to the Precambrian. These data were then compared with the high resolution aeromagnetic dataset, to estimate the features' depths into the basement and produce a map of the intrabasement-Precambrian lineaments. The high resolution aeromagnetic data were processed using the vertical dyke model and Euler depth determination (Reid et al., 1990; Gumm, 1997). Intra-sedimentary lineaments were also interpreted from the subsurface maps and the aeromagnetic data. The seismic data set consisting of 2-D lines and 3-D data cubes was then used, where available, to develop a complete interpretation of the Precambrian basement and to verify the trends established by regional subsurface mapping and the aeromagnetic data. A minimum of four 3-D seismic cubes, and numerous 2-D seismic lines orientated NE-SW (line spacing of approximately 2 miles) were used. The line density diminishes northward from Swan Lake, and did not cover the northern part of the map, for which only oil well and aeromagnetic data were used. The seismic interpretation provided information through the entire stratigraphic sequence. The accuracy of the seismic interpretation in the central portion of the study area has been estimated at 70% (Pryde, pers. comm.). This estimate represents a correlation coefficient derived from the

interpretation of all the data sets, on a density of 800 control points (wells) in the central part of the map. The final structural interpretation map was produced at 1: 250 000 scale.

The AGS structural interpretation (Eccles et al., 2000) was compiled using a mosaic of a RADARSAT-1 Standard Mode S7 scene (12.5 m pixel resolution, incidence angle 47° at beam centre) and a RADARSAT-1 Fine Mode F5 scene (6.5 m pixel resolution, incidence angle 46° at beam centre) draped on surface topography digital elevation model (DEM, 10 meters resolution). The interpretation was conducted visually and resulted in a map of approximately 1:212 000 scale.

3.4 RESULTS OF RADARSAT-1-PC IMAGERY STRUCTURAL INTERPRETATION

Four lineament trends have been recognized in each of the RADARSAT-1-PC images: NNE, NW, NE, and ENE. The intersection and offset relationships between the various lineament groups enabled definition of a relative succession of events in which the NNE lineaments are recognized as the oldest features bounding the main topographic high of the Buffalo Head Hills and Peerless Uplands. This event was followed by the NW and NE lineaments, which probably define a conjugate set. These lineaments are well developed throughout the region, and cross-cut the earlier NNE lineaments. The ENE-trending lineaments show cross-cutting relationships with all the previous lineaments and are therefore interpreted to be the latest features.

Readily recognized structures were observed using the RADARSAT-1-PC2 image due to the enhanced topographic perception, which aids visualization and interpretation of structural features expressed by physiographic features, surface geology transitions and/or associated vegetation coverage variation. This image is described below in detail to illustrate examples of lineament intersections, offsets, and inferred relative movements. Positive contribution in the lineament data compilation was derived also from the interpretation of the RADARSAT-1-PC1, -PC2, and -PC3 images.

3.4.1 RADARSAT-1-PC2 structural interpretation

In the RADARSAT-1-PC2 image (Figure 3.13) the NNE-trending lineaments are readily traced along the eastern boundary of the Buffalo Head Hills because of the very good topographic perception due to contrasts in brightness, texture, and tone between the Buffalo Head Hills E-facing scarp and the Loon River Valley. These contrasts are probably due to the combined effects of the E-facing topographic slope and lithological variations. Along the northern portion of the Buffalo Head Hills eastern boundary, these features have a clear structural control on the path of the Wabasca River. NNE lineaments that bound the W-facing slope of the Peerless Uplands, extend into the Loon River Valley where they appear to control the drainage pattern. Additional NNE-lineaments are observable in the central and southern portion of the area, and the SE corner of the Buffalo Head Hills.

The NW-trending lineaments intersect and offset the NNE-trending lineaments as described above, suggesting a relative age relationship. The NW lineaments set can be

traced throughout the study area from the SE in the western boundary of the Peerless Uplands, through the Loon River Valley, to the NW across the Buffalo Head Hills. The offset induced by the NW lineaments is mainly observable in the northern portion of the Buffalo Head Hills and Wabasca River, and across the Loon River Valley. Here, the Wabasca River drainage is structurally controlled by NW-trending lineaments, and the east-facing slope of the Buffalo Head Hills is truncated by a NW-trending trough. This trough is emphasized by both topographic perception and brightness contrast, and the texture and tone variation induced by a lithological transition between the Shaftesbury Formation (in the trough), and the Dunvegan Formation/Smoky Group in the topographic highs to the side. Other block-fault structures defined by the intersection of NW-trending lineaments offsetting the Buffalo Head Hills NNE-bounding lineaments can be observed in the central portion of the Buffalo Head Hills eastern scarp. Here again, the emphasized topographic perception, brightness contrast, texture, and tone variations between the Shaftesbury Formation (in the Loon River Valley), and the Dunvegan Formation/Smoky Group in the topographic highs, is interpreted to be a response to lithological changes and structural escarpments. In the SE corner of the Buffalo Head Hills, the NW lineaments define a series of step-faults propagating towards the SW, which can be observed due to subtle topographic perception along the NW-trending lineaments, and the texture and tone variation induced by lithologic transition of the Dunvegan Formation (medium grey) and the Smoky Group (light grey tone). These features have probably determined the down-throw of the SE corner and southern boundary of the Buffalo Head Hills to the SW.

The NE-trending lineaments intersect and offset the NNE-trending lineaments, again indicating relative age. This lineament set can be traced mainly across the central

part of the Buffalo Head Hills and extends through the Loon River Valley. The offset induced by the NE lineaments is observable along the Buffalo Head Hills eastern boundary, mainly due to texture and tone variations in response to lithological transitions between the Shaftesbury Formation and Dunvegan Formation/Smoky Group. The highest concentration of NE lineaments is observed in the Buffalo Head Hills near its eastern and northern boundaries. In the northern portion of the Buffalo Head Hills, a series of NE-lineaments is outlined by topographic features and brightness contrasts induced by shadowing effects. This response is associated with texture and tone variation caused by the lithologic transition between the Loon River Formation (dark grey), Shaftesbury (medium light grey), and Dunvegan Formations (light grey). Their geometry suggest step-faults propagating towards the northwest, which have down-thrown the Buffalo Head Hills northern boundary towards the NW.

The ENE-trending lineaments intersect and offset the NNE-, NW-, and NE-trending lineaments, and are therefore interpreted to be the youngest structural features in the area. They are regionally distributed from north to south, almost regularly spaced, and can be traced throughout the Buffalo Head Hills, the Loon River Valley, and part of the western limit of the Peerless Uplands. The highest concentration of ENE lineaments is observed in the SE corner, southern boundary, and NE portion of the Buffalo Head Hills. In the SE portion of the Buffalo Head Hills, the offset induced by the ENE-trending lineaments is mainly observable along the eastern boundary as textural and tone variations in response to lithological transitions from the Shaftesbury Formation (within the Loon River Valley), and the Dunvegan Formation and Smoky Group of the Buffalo Head Hills topographic high. These lineaments seem to define step-faults that down-

throw the southern boundary towards the SE. In the NE portion of the Buffalo Head Hills, ENE-trending lineaments are at times identified by abrupt deviations of the drainage pattern of the Wabasca River along its path parallel to the NE-edge of the Buffalo Head Hills. Here the enhanced topographic perception of the Buffalo Head Hills eastern edge and the shadowing effect and brightness contrast along the Wabasca River provide a clear outline of the ENE-trending lineaments. In the NE corner of the Buffalo Head Hills, the ENE-trending lineaments seem to define step-faults that down-throw the northern portion of the Buffalo Head Hills towards the NNW.

3.4.2 RADARSAT-1-PC1, -PC3, and -PC4 structural interpretation

The structural interpretations of RADARSAT-1-PC1, -PC3, and -PC4 are illustrated in Figure 3.14, A, B, and C respectively. The RADARSAT-1-PC1 lacks topographic perception (Figure 3.14, A), although good contrast and tone variation, clearly outline the NNE-trending lineaments in the Loon River valley. The NW-trending lineaments are emphasized by detailed drainage pattern in the western side of the Buffalo Head Hills, and the Wabasca drainage in the Loon River valley. The NE-trending lineaments are mainly observable in the south-central portion of the Buffalo Head Hills eastern edge, and the ENE-trending lineaments are readily observable in the Buffalo Head Hills southern portion.

In the RADARSAT-1-PC3 image (Figure 3.14, B), high contrast and darker tone emphasize the main drainage patterns. The moderate topographic perception highlights

the Buffalo Head Hills east-facing scarp. Drainage patterns reveal additional NNE-trending lineaments within the Loon River Valley, the western boundary of the Peerless Uplands, and in the central and southern portion of the Buffalo Head Hills. The NW-trending lineaments were traced along the Wabasca drainage, and the western side of the Buffalo Head Hills. The NE-trending lineaments are not readily observable in this image, whereas the ENE-trending lineaments are very well enhanced by high contrast and textural variations across the Loon River valley and Buffalo Head Hills central and southern portions.

In the RADARSAT-1-PC4 image (Figure 3.14, C) the surface target features are poorly constrained by topographic perception, although the outlined lineaments in the RADARSAT-1-PC2 and -PC3 images can be resolved by brightness contrast and texture variation. The main features visible in this image are the ENE-trending lineaments, which are defined as dark-grey ENE-trending corridors in the southern portion of the Buffalo Head Hills, and extending across the Loon River valley into the Peerless Uplands.

3.4.3 Compilation of RADARSAT-1-PC structural data

The compilation of the lineaments extracted from all the RADARSAT-1-PC images outlines well defined trends, with strike variations from north to south, throughout the study area; this is most clearly shown in the NW- and NE-trending lineaments shown respectively in Figure 3.15 (B) and 3.15 (C), the rose diagrams representation in Figure 3.16, and the relative standard deviation reported in Table 3.4. The minimal strike variation is shown by the ENE lineaments.

From the compiled data sets, it is clear that the NNE, NW and NE lineaments represent the most prominent linear trends in the area (Figures 3.15, A, B, and C). The ENE lineaments show a well defined trend that is superimposed on the previously defined structural features (Figure 3.15, D).

The NW-trending lineaments have the highest strike variability, and separate the study area in two structural domains: the southern part, in which there is a general WNW-trend, and the northern part with a NNW-trend. This could imply variability and/or rotation of the stress field over time during the development of the NW lineaments, or may reflect a refraction effect imposed by the Buffalo Head Hills block. The NE-trending lineaments also show a strike variation from south to north, which is consistent with that observed in the NW lineaments data set. A more clear refraction effect imposed by the Buffalo Head Hills block is observable in the NE-trending lineaments, especially in the NE-corner of the Buffalo Head Hills block. These observations lead to the possibility that the two trends may form a conjugate joint set suggesting E-W compression. The latest ENE-trending lineaments exhibit an extensional character, suggesting a stress field to a near E-W compression.

Geological causes for the strike variability of the NNE-, NW, and NE-trending lineaments are possibly related to tilting effects of fault block interaction, and refraction imposed by the Buffalo Head Hills block. In addition, although not quantifiable, the different geometric properties inherent to the RADARSAT-1-PC images due to the variable proportion of the RADARSAT-1 source images from the Principal Component Analysis (Paganelli et al., 2001b) could be an additional cause for such a variability. This effect is not accountable or minimal for the ENE-trending lineaments because their

orientation is parallel to the look direction of the ascending and descending orbit mode (W to E, and E to W look direction respectively) of the RADARSAT-1 source scenes. Therefore, a minimal geometric variation induced by the processing would affect the ENE-trending lineaments and their extraction from the RADARSAT-1-PC images.

3.4.4 Comparison with AMCI, AEC, and AGS structural interpretations

Similarities to the outlined lineament trends have been found in studies conducted by Aston Mining of Canada Inc. (Figure 3.17, A; Lockett, 1998), Alberta Energy Company (Figure 3.18A; Pryde, 2001), and the Alberta Geological Survey (Figure 3.19, A; Eccles et al., 2000). Subsets of the RADARSAT-1-PC2 structural interpretation matching the areas of the AMCI, AEC, and AGS maps are shown for comparison in Figure 3.17 (B), 3.18B, and 3.19 (B) respectively.

NNE-lineaments defined by RADARSAT-1-PC analysis (Figure 3.17, B) are observed in the structural interpretation derived from aerial photos and drainage patterns in the AMCI study (Figure 3.17, A). In the AEC map (Figure 3.18A), well structural data interpretation defined NNW-trending Precambrian lineaments that controlled the sedimentation as shown by the NNW-trending isopachs of the Keg River Formation. The seismic data provided verification of the NNW intra-sedimentary lineaments through the Granite Wash and Keg River formations and the top of the basement, while the high-resolution aeromagnetic data enabled the identification of NNW intrabasement lineaments (intrabasement- Precambrian in legend). All these lineaments fan towards a more N-NNE oriented trend northwards, and at the eastern boundary of the AEC map.

Looking closely at the orientation of the north-trending lineaments in the RADARSAT-1-PC2 image (Figure 3.18B), within the sub-area covered by AEC map, the Buffalo Head Hills eastern boundary is delimited by more NNW oriented lineaments, which fan northwards towards more N-NNE oriented features. This similarity with the NNW-trending lineaments in the AEC map constrains evidence that N-trending lineaments have a deep-seated origin within the basement and sedimentary sequence of the Granite Wash and Keg River formations (Middle Devonian), and influenced the sedimentation during the Cretaceous. Evidence of N-trending lineaments (Figure 3.19, B) has also been found in the AGS map (Figure 3.19, A), and these have been interpreted as delimiting the eastern edge of the Buffalo Head Hills from the Loon River graben (Eccles et al., 2000). This interpretation was derived from borehole stratigraphic reconstructions covering the Devonian-Cretaceous sedimentary sequence to the Precambrian basement at approximately 100 m depth, along an EW section between the eastern edge of the Buffalo Head Hills and the Peerless Uplands.

The NW-trending features delineated in the RADARSAT-1-PC interpretation (Figure 3.17, B) are comparable to NW lineaments identified from drainage and aerial photos in the AMCI interpretation map (Figure 3.17, A). NW-lineaments (Figure 3.18B) also find analogy with intrabasement-Precambrian and intrasedimentary lineaments derived from wells, aeromagnetic and seismic data in the AEC map (Figure 3.18A). In the latter map, a wide strike variability in the NW lineaments is present, which seems to follow the trend observed in the NW-lineaments outlined in this study, and rotates to more northerly-trending orientation progressively from south to north within the map area.

The NE-trending features delineated in the RADARSAT-1-PC interpretation (Figure 3.17, B) are comparable to NE lineaments identified from drainage and aerial photos delineated in the AMCI interpretation map (Figure 3.17, A). NE-lineaments (Figure 3.18B) find analogy with wrench, intrasedimentary, and Precambrian lineaments delineated from wells, aeromagnetic and seismic data interpretation in the AEC map (Figure 3.18A). In the latter map, the inferred kinematics of the NE-lineaments seems to involve left-lateral movement defining a series of en-echelon grabens along the eastern boundary of the Buffalo Head Hills. In the present study, a dip-slip with down-drop movement to the SE has been associated to the NE-lineaments, however a combined dip-slip and strike-slip left-lateral movement cannot be excluded. The isopach of the Keg River Formation (Middle Devonian) follows to some extent the NE-trend, which clearly shows the influence of this lineament trend on the Keg River deposition. The NE-trending lineaments (Figure 3.19, B) have been documented as surface linear trends in the AGS map as shown in Figure 3.19 (A).

The ENE-trending features delineated in the RADARSAT-1-PC interpretation (Figure 3.17, B) are comparable to ENE lineaments outlined from air photo interpretations in the AMCI structural map (Figure 3.17, A). ENE-lineaments (Figure 3.18B) find analogy with a few wrench, intrasedimentary, and intrabasement-Precambrian lineaments delineated in the AEC map (Figure 3.18A). Similar ENE lineaments are locally defined by isopachs of the Keg River Formation in the central portion of the Buffalo Head Hills, and within the Loon River section. These comparisons suggest that the ENE-trending lineaments extracted from the RADARSAT-1-PC

interpretation have deep-seated origin within the sedimentary sequence, and are possibly associated with intrabasement-Precambrian lineaments.

3.5 STRUCTURAL LINEAMENTS AND REGIONAL GEOLOGICAL CONTEXT

The structural lineaments identified in this study are analyzed in the context of the regional tectonic history from published literature. This comparison suggests a possible relationship between the identified structural trends in the Buffalo Head Hills area and the development of the Peace River Arch structures, and the onset of the Laramide orogeny.

NNE-trending lineaments

The NNE-trending lineaments define a persistent pattern bounding the Buffalo Head Hills and Peerless Uplands, and have been identified as the oldest features in the area. Magnetic data within the Buffalo Head Hills Precambrian basement outline a well-defined fabric with NNE trend within the Buffalo High terrane, and NNW and NNE trends within the Buffalo Utikuma terrane (Pilkington et al., 2000). Along the Peace River Arch northern margin, NNE-trending lineaments identified in the underlying Precambrian surface (O'Connell et al., 1990) have affected the deposition of the Granite Wash siliciclastics to the east, interbedded with Leduc dolomite. These observations suggest that the NNE-trending lineaments may have been originally Precambrian

(O'Connell et al., 1990; Ross et al., 1991; Pilkington et al., 2000), and have influenced and/or partially controlled the Peace River Arch structural development. From this interpretation and analogy with previous work, it is suggested that the NNE lineaments in the Buffalo Head Hills are related to steep, deep-seated Precambrian faults, sub-parallel to the boundary between the Buffalo High and Buffalo Utikuma terranes, and which have possibly been reactivated in the Phanerozoic (because they can be detected through the Phanerozoic sedimentary cover).

NW-trending lineaments

The NW-trending lineaments define a well developed regional pattern which clearly post-dates and offsets the NNE-lineaments bounding the eastern edge of the Buffalo Head Hills. These lineaments had structural control on the drainage path development of the Wabasca River, as can be observed in the northern part of the Loon River Valley. NW lineaments have been recorded in the Peace River Arch area from a combined study of the Precambrian basement surface and the Granite Wash (Devonian) isopach (Cant, 1988). Based on the thickness patterns of the Granite Wash, Cant (1988) suggested these were normal faults with down-throw to the west-southwest. This type of movement is similar to the SW down-throw of the SE corner of the Buffalo Head Hills observed in this study. The NW-trending lineaments are attributed in the literature to the Mid- to Late Devonian faulting phase of the Peace River Arch (Cant, 1988). More recently, Pilkington et al. (2000) outlined NW-trending preferential strike orientation within the gravity data of the Buffalo High and Buffalo Utikuma terranes, which have been suggested to characterize the fabric of the Precambrian terranes. This suggests that

the NW lineaments outlined in this study might have a Precambrian origin, and have been reactivated during Proterozoic and Phanerozoic time. Evidence within the Buffalo Head Hills of the timing of NW-trending fault reactivation, as in the Peace River Arch region, is derived from evidence of intrasedimentary lineaments in the Keg River formation (Middle Devonian) in the AEC map (Figure 3.18A). On the southeast flank of the Peace River Arch, the NW-trending Dunvegan normal fault seems to define the Cretaceous Fox Creek Escarpment (O'Connell, 1988) and appears to coincide with underlying basement structures defined by the shear zone boundary between the Ksituan and Chinchaga domains (Ross and Eaton, 1999).

NE-trending lineaments

The NE-trending lineaments define a persistent regional pattern throughout the Buffalo Head Hills. Their development clearly post-dates and offsets the NNE-trending lineaments, as observed along the eastern edge of the Buffalo Head Hills. NE-trending structures have previously been recorded in the basement and overlying sedimentary sequences of the Peace River Arch area (O'Connell et al., 1990). In the Peace River Arch area, the lineaments are parallel to the Arch axis, and are therefore interpreted to be associated with its formation (Cant, 1988; O'Connell et al., 1990). The best known structure, is the "Axial Graben", which is clearly defined in the uppermost Devonian Wabamun unit (Cant, 1988), and is also identifiable in the isopach of the Delbot Formation of the Rundle Group (uppermost Mississippian). The NE-trending lineaments have been documented on the exposed shield in Saskatchewan, and under the thin cover of eastern Alberta (Garland and Bower, 1959), as well as in the Precambrian basement at

the eastern edge of the Peace River Arch (O'Connell et al., 1990). These observations suggest that the NE lineaments may originally have been Precambrian in age, and have been reactivated repeatedly during the Paleozoic (O'Connell et al., 1990). A synthesis of electromagnetic studies in the Lithoprobe Alberta Basement Transect (Boerner et al., 2000) outlined the presence of conductive structures (Kiskatinaw conductor) with inferred NE strike direction bounding the Buffalo Head High terrane. Evidence within the Buffalo Head Hills of the timing and characterization of NE-trending fault reactivation, as in the Peace River Arch region, is derived from evidence of wrench intrasedimentary faults in the Keg River formation (Middle Devonian) in the AEC map (Figure 3.18A).

ENE-trending lineaments

The ENE-trending lineaments have been recognized as products of the latest tectonic event in the area, which post-dates and offsets the NNE-, NW-, and NE-trending structures and Cretaceous sediments. They define a persistent regional pattern throughout the Buffalo Head Hills. Evidence of ENE-lineaments in the Buffalo Head Hills from seismic interpretations in the AEC map (Figure 3.18A) suggests the possible association of these features with wrench faults.

Evidence for structures with ENE-WSW trend has been documented in the southeast flank of the Peace River Arch within the lower Cretaceous sediments of the Bluesky Formation (Cant, 1988; Rouble and Walker, 1994; Chen and Bergman, 1997). These structures are perhaps related to the final subsidence of the Peace River Arch, parallel the trend of the arch axis. Development of graben structures with dominantly E-W oriented axes are documented in the northern edge of the western part of the Peace

River Arch by O'Connell et al. (1990). Late Cretaceous strata reorientations have been observed in the southeast flank of the Peace River Arch by Chen and Bergman (1999) from isopach maps of the Colorado Shales and Lea Park Formation, changing from NW-SE in Santonian (84-87.5 Ma) to E-W (NE-SW) in the Campanian (74.5-84 Ma). Chen and Bergman (1999) suggested that this situation resembles the process in the Lower Cretaceous of the U.S. foreland basin, which involved flexural subsidence and eastwards forebulge migration during the Laramide orogeny (Currie, 1998). The Campanian tectonic event may therefore be related to Laramide-style basement uplift (Chen and Bergman, 1999).

The above suggests that the ENE-trending lineaments are probably the result of extensional tectonics in the foreland due to horizontal translation of the terranes accumulating on the western North American margin during the Laramide orogeny. This convergence occurred at an angle with the orientation of the Buffalo High and Buffalo Utikuma terranes boundary, which might have caused differential reactivation of pre-existing structures. A kinematic reconstruction of the Laramide orogeny at 80 Ma (Bird, 1998b) suggests convergence with approximately N-S orientation. In the Buffalo Hills, this kinematic scenario would suggest possible development of extensional faults with ENE orientation, probably favoured by the existence of previous structures with NE-ENE trend associated with the Peace River Arch. The timing of these lineaments appears to coincide with kimberlitic magmatism in the area, a relationship which is further analyzed using the statistical approach of weights of evidence in Paganelli et al. (2001c, 2002).

3.6 DISCUSSION AND CONCLUSIONS

This study has focused on evaluating the potential of RADARSAT-1-PC imagery to contribute to geological mapping and mineral exploration in the highly vegetated and moderate relief environment of northern central Alberta.

When applying PCA the relative image variance is a measure of the amount of information observable in each image. It appears that useful information, in particular for structural mapping, can be obtained using the RADARSAT-1-PC2 and -PC3 images, which are characterized by 20.13% and 17.65% respectively of the total image variance from the input bands. In the RADARSAT-1-PC4 image the noise level is high and most of the image characteristics are lost, but 8.65% of image variance remains and structural information may still be present. The signal-to-noise ratio cannot be considered to be evenly distributed in the principal components (Mather, 1987), and therefore higher noise level does not necessarily make the image useless.

The RADARSAT-1-PC1 image is shown to be a good source of information for tone and texture variations derived from surface and canopy contrast in the original radar images, suggesting that this image could be used to improve automatic classification schemes and data integration for surface terrain mapping.

The improved topographic perception in the RADARSAT-1-PC2 and -PC3 images provides optimal interpretability of structural features. In particular, RADARSAT-1-PC2 could provide valuable data for structural interpretation/mapping

and data integration. In comparison, RADARSAT-PC3 provides optimal response and enhancement of drainage patterns.

The evaluation of RADARSAT-1-PC imagery for structural mapping in the highly vegetated environment and moderate relief of the Buffalo Head Hills area, has shown that topographic perception in the RADARSAT-1-PC2 provides valuable synoptic properties together with texture and tone information.

The structural analysis provided sufficient information suggesting that the NNE-, NE- and NW-trending lineaments have Precambrian origin, and have been shown to have also effected the Phanerozoic sedimentary sequence. Those basement structures were therefore possibly reactivated producing splays of analogous trends throughout the sedimentary sequence. The latest ENE lineaments intersect all the above and it has been suggested that they formed in an extensional regime associated with the Laramide orogeny.

The outlined structural lineaments and their tectonic/geologic implications provide a basis for kimberlite, as well as oil/gas exploration in the area. The NNE, NW, and NE lineaments in the area have been associated with originally Precambrian basement trends. The NNE lineaments reflect the general N-S trend of accreted terranes defining the north central Western Canadian Sedimentary Basin. The NE and NW trends are probably associated to the Peace River Arch development, and form a conjugate set which suggests an E-W-trending compression regime during Mid to Late Devonian. The ENE lineaments show extensional character probably developed in a near E-W compression regime, which has been associated with the Cretaceous convergence induced by the Laramide Orogeny.

Ultimately, the distribution of the N-, NE-, and ENE-trending lineaments outlined possible spatial interrelationships with the kimberlite emplacement, which have been analyzed using the statistical approach of weights of evidence method in Paganelli et al.(2001c, 2002).

REFERENCES

- Berger, Z. (1994). *Satellite Hydrocarbon Exploration: interpretation and integration techniques*. Springer-Verlag.
- Bird, P. (1998b). Kinematic history of the Laramide orogeny in latitudes 35°-49° N, western United States. *Tectonics*, Vol. 17, pp. 780-801. http://element.ess.ucla.edu/publications/1998_Laramide/1998_Laramide.htm (December 2001)
- Blom, R.G., Crippen, R.E., and Elachi, E. (1984). Detection of subsurface features in SEASAT radar images of Means Valley, Mojave Desert, California. *Geology*, Vol. 12, pp. 346-349.
- Boerner, D.E., Kurtz, R.D., Craven, J.A., Ross, G.M. and Jones, F.W. (2000). A synthesis of electromagnetic studies in the Lithoprobe Alberta Basement Transect: constraints on Paleoproterozoic indentation tectonics. *Canadian Journal of Earth Science*, Vol. 37, pp. 1509-1534.
- Brown, R.J., Brisco, B., D'Iorio, M.A., Prevost, C., Ryerson, R.A., Singhroy, V. (1996). RADARSAT applications: review of GlobeSAR Program. *Canadian Journal of Remote Sensing*, Vol. 22, No. 4, pp. 404-419.
- Burwash, R.A., Baadsgaard, H., and Peterman, Z.E. (1962). Precambrian K-Ar dates from the Western Canadian Sedimentary Basin. *Journal of Geophysical Research*, Vol. 67, pp. 1617-1625.
- Cant, D.J. (1988). Regional structure and development of the Peace River Arch, Alberta: a Paleozoic failed-rift system? *Bulletin of Canadian Petroleum Geology*, Vol. 36, pp. 284-295.
- Carlson, S.M., Hillier, H.D., Hood, C.T., Pryde, R.P., and Skelton, D.N. (1998). The Buffalo Head Hills kimberlite province, north central Alberta, Canada. In: *Seventh International Kimberlite Conference: Extended Abstracts*. Cape Town, April 1998, pp. 138-140.
- Chen, D. and Bergman, K.M. (1997). High-resolution stratigraphic analysis of Cretaceous formations in the Peace River Arch area of the Western Canada Sedimentary Basin: depositional processes and possible controlling mechanisms. *Lithoprobe Report 59*, pp. 129-162.
- Chen, D. and Bergman, K.M. (1999). Stratal reorientation, depositional processes, and sequence evolution of the Cretaceous in the Peace River Arch region of the Western Canada Sedimentary Basin. *Bulletin of Canadian Petroleum Geology*, Vol. 47, No. 4, pp. 594-620.
- Crosta, A.P. & McM. Moore, J. (1989). Enhancement of Landsat Thematic Imagery for residual soil mapping in SW Minas Gerais State, Brazil: a prospecting case history in Greenstone Belt Terrain. *Proceedings of the 7th (ERIM) Thematic Conference: Remote Sensing for Exploration Geology 2-6th October*, Calgary, Vol. II, pp. 1173-1187.
- Drury, S.A. (1993). *Image Interpretation in Geology*. Chapman & Hall Publisher, Second Edition. London.

- Currie, B.S. (1998). Upper Jurassic-Lower Cretaceous Morrison and Cedar Mountain formations, NE Utah-NW Colorado; relationships between non-marine deposition and early Cordilleran foreland-basin development. *Journal of Sedimentary Research*, Vol. 68, pp.632-652.
- Dredge, L.A., Kjarsgaard, I.M., Ward, B.C., Kerr, D.E., Stirling, J.A.R. (1995). Distribution and chemistry of kimberlite indicator minerals, Aylmer Lake map area (76C), Northwest Territories. Geological Survey of Canada, Open File 3080.
- Eccles, D.R., Grunsky, E.C., Grobe, M. and Weiss, J. (2000). *Structural emplacement model for kimberlitic diatremes in northern Alberta*. Report, Alberta Energy and Utilities Board, Alberta Geological Survey, March 2000, p. 116. (in press).
- Edwards, D.J., Lyatsky, H.V. and Brown, R.J. (1995). Basement fault control on Phanerozoic stratigraphy in the Western Canada Sedimentary Province; integration of potential-field and lithostratigraphic data. In: G.M. Ross Ed., *Alberta Basement Transects Workshop, Lithoprobe Report 47*, pp. 181-224.
- Evans, D.L., Farr, T.G., Ford, J.P., Thompson, T.W., Werner, C.L. (1986). Multipolarization Radar Images for geologic mapping and vegetation discrimination. *IEEE Transactions on Geoscience and Remote Sensing*, Vol. GE-24, No. 2, pp. 246-257.
- Garland, G.D. and Bower, M.E. (1959). Interpretation of aeromagnetic anomalies in the northeastern Alberta. Fifth World Petroleum Congress, Section 1-Paper 42, pp. 787-800.
- Grunsky, E.C. (2001). The Application of Principal Components Analysis to Multi-beam RADARSAT-1 Satellite Imagery – A Tool for Terrain Mapping. *Canadian Journal of Remote Sensing* (in press).
- Gunn, P.J. (1997). Quantitative methods for interpreting aeromagnetic data: a subjective review. *Australian Journal of Geology & Geophysics*, Vol. 17, No. 2, pp. 105-113.
- Hillger, D.W. (1996b). Meteorological features from principal component image transformation of GOES imagery. *International Symposium of Optical Science, Engineering, and Instrumentation (GEOS-8 and Beyond Conference)*, SPIE, pp. 111-121.
- Hillger, D.W., and Ellrod, G.P. (2000). Detection of unusual atmospheric and surface features by employing Principal Component Image transformation of GOES imagery. *Tenth Conference on Satellite Meteorology and Oceanography*, AMS, pp. 461-464.
- Hein, F.J., (1999). Mixed (“multi”) fractal analysis of Granite Wash fields/pools and structural lineaments, Peace River Arch area, northwestern Alberta, Canada: A potential approach for use in hydrocarbon exploration. *Canadian Society of Petroleum Geologists*, Vol. 47, No. 4, p.556- 572.
- Leckie, D.A., Kjarsgaard, B.A., Pierce, J.W., Grist, A.M., Collins, A., Sweet, A., Stasiuk, L., Tomica, M.A., Eccles, R., Dufresne, M., Fenton, M.M., Pawlowicz, J.G., Blazer, S.A., McIntyre, D., McNeil D. (1997a). Geology of Late Cretaceous possible kimberlite at Mountain Lake, Alberta – Chemistry, petrology, indicator minerals, aeromagnetic signature, age, stratigraphic position and setting. Geological Survey of Canada, Open File 3441.

- Leckie, D.A., Kjarsgaard, B.A., and Bloch, J., McIntyre, D., McNeil D., Stasiuk, L., Heaman, L. (1997b). Emplacement and reworking of Cretaceous, diamond-bearing, crater facies kimberlite of central Saskatchewan, Canada. *Geological Society of America Bulletin*, Vol. 109, No. 8, pp. 1000-1020.
- Lemieux, S. (1999). Seismic reflection expression and tectonic significance of the Late Cretaceous extensional faulting of the Western Canada Sedimentary Basin in Southern Alberta. *Bulletin of Canadian Petroleum Geology*, Vol. 47, No. 4, pp. 375-390.
- Lenhart-Thiel, K., Loewer, R., Orr, R.G., and Robertshaw, P. (1992). Diamond-bearing kimberlites in Saskatchewan, Canada: The Fort a la Corne case history. *Exploration and Mining Geology*, Vol. 1, pp. 391-403.
- Lockett, N (1998). Ashton Mining of Canada Buffalo Head Hills Project, Alberta - Results of air photograph interpretation. Ashton Mining Ltd. Report 52214, p.10. Unpublished.
- Loughlin, W.P. (1991). Principal Component Analysis for Alteration Minerals. *Photogrammetric Engineering and Remote Sensing*, Vol. 57, No. 9, pp. 1163-1169.
- Luscombe, A.P., Ferguson, I., Shepherd, N., Zimck, D.G., Naraine, P. (1993). The RADARSAT synthetic aperture radar development. *Canadian Journal of Remote Sensing*, Vol. 19, No. 4, pp. 298-310.
- Mather, P.M. (1987). *Computer Processing of Remotely-Sensed Images*. John Wiley & Sons Publisher. New York.
- Misra, K.S, Slaney, V.R., Graham, D., Harris, J.(1991). Mapping of Basement and other tectonic features using SEASAT and Thematic Mapper in hydrocarbon-producing areas of the Western Sedimentary Basin of Canada. *Canadian Journal of Remote Sensing*, Vol. 17, No. 2, pp. 137-151.
- Mitchell, R.H. (1986). *Kimberlites and Related Rocks. Their composition, occurrence origin and emplacement*. Geological Society of Australia, Special Publication No. 14.
- Mitchell, R.H. (1995). *Kimberlites Orogenites and Related Rocks*. Plenum Press, New York.
- Mossop, G.D. and Shetsen, I. (1994). *Geological Atlas of the Western Canada Sedimentary Basin*. Canadian Society of Petroleum Geologists & Alberta Research Council, Alberta Geological Survey.
- O'Connell, S.C., Dix, G.R. and Barclay, J.E. (1990). The origin, history and regional structural development of the Peace River Arch, Western Canada. *Bulletin of Canadian Petroleum Geology*, Vol. 38A, pp. 4-24.
- Paganelli, F. and Rivard, B. (1999a). *Tracking geological structures in the Central Alberta Foothills, Canada, using RADARSAT imagery*. Report PetroCanada. Unpublished.
- Paganelli, F. and Rivard, B. (1999b). Tracking geological structures in the Central Alberta Foothills, Canada, using RADARSAT imagery. *Proceedings of the Thirteenth International Conference of Applied Geologic Remote Sensing*, Vol. I, p. 109.

- Paganelli, F. and Rivard, B. (2001). Contribution of the synergy of RADARSAT-1 and seismic imagery interpretation in the structural geology of the Central Alberta Foothills, Canada, as aid for oil and gas exploration. *Canadian Journal of Remote Sensing* (in press).
- Paganelli, F., Grunsky, E.C., and Richards, J.P. (2001a). Structural interpretation of RADARSAT-1 Principal Component imagery and its potential application to kimberlite exploration in the Buffalo Head Hills area, Northern Central Alberta. *Alberta Geological Survey, Earth Science Report 2001-03*. Edmonton, Alberta, Canada: Alberta Energy and Utilities Board. (in press).
- Paganelli, F., Grunsky, E.C., and Richards, J.P. (2001b). Use of RADARSAT-1 Principal Component imagery for structural mapping: a case study in the Buffalo Head Hills area, northern central Alberta, Canada. *Canadian Journal of Remote Sensing* (in press).
- Paganelli, F., Richards, J.P., and Grunsky, E.C. (2001c). Integration of structural, gravity and magnetic data using the weights of evidence method as a tool for kimberlite exploration in the Buffalo Head Hills area, northern central Alberta, Canada. *Natural Resources Research* (submitted).
- Paganelli, F., Richards J.P., Grunsky E.C. (2002) - Integration of structural, gravity and magnetic data using the weights of evidence method as a tool for kimberlite exploration in the Buffalo Head Hills area, Northern Central Alberta. *Proceedings of the 2002 International Geoscience and Remote Sensing Symposium - 24th Canadian Symposium on Remote Sensing*, 24-28 June, Toronto, Ontario, Canada (in press).
- Pilkington, M., Miles, W.F., Ross, G.M., and Roest, W.R. (2000). Potential-field signatures of buried Precambrian basement in the Western Canada Sedimentary Basin. *Canadian Journal of Earth Science*, Vol. 37, pp. 1453-1471.
- Price, M.H. (1999). Integration of Landsat TM and SIR-C polarimetric radar for lithological mapping near Goldfield, Nevada. *Proceeding of the Thirteenth International Conference on Applied Geologic Remote Sensing*, Vol. I, pp. 452-459.
- Pryde, R. (2000). Buffalo Head Hills property AEC Structural Interpretation Map. Scale 1:250 000. Unpublished.
- Reid, A.B., Allsop, J.P., Granser, H., Millet, A.J., and Somerton, I.W. (1990). Magnetic interpretation in three dimensions using Euler deconvolution. *Geophysics*, Vol. 55, pp. 80-91.
- Ross, G.M. (1990). Deep crust and basement structure of the Peace River Arch: constraints on mechanism of formation. *Bulletin of Canadian Petroleum Geology*, Vol. 38A, pp. 25-35.
- Ross, G.M., Parrish, R.R., Villeneuve, M.E., and Bowring, S.A. (1991). Geophysics and geochronology of the crystalline basement of the Alberta Basin, western Canada. *Canadian Journal of Earth Sciences*, Vol. 28, pp. 512-522.
- Ross, G.M., Eaton, D.W. (1999). Basement reactivation in the Alberta Basin: Observational constraints and mechanical rationale. *Bulletin of Canadian Petroleum Geology*, Vol. 47, No. 4, pp. 391-411.

- Rouble, R.G. and Walker, R.G. (1994). Sequence stratigraphy and controls of barrier-strandplain systems in Falher Members A and B of the Lower Cretaceous Spirit River Formation, north-western Alberta, Canada. *American Association of Petroleum Geologist Annual Meeting Abstract*, p. 247.
- Rudant, J.P., Deroin, J.P., and Polidori, L. (1994). Multi-resolution analysis of radar images and its application to lithological and structural mapping; Larzac (southern France) test site. *International Journal of Remote Sensing*, Vol. 15, pp. 2451-2468.
- Sabins, F.F. (1983). Geologic interpretation of Space Shuttle radar images in Indonesia. *American Association of Petroleum Geologists*, Vol. 64, pp. 612-628.
- Singhroy, V., Slaney, R., Lowman, P., Harris, J. and Moon, W. (1993). RADARSAT and radar geology in Canada. *Canadian Journal of Remote Sensing*, Vol. 19, No. 4, pp. 338-351.
- Singhroy, V. and Saint-Jean, R. (1999). Effect of relief on the selection of RADARSAT-1 incidence angle for geological applications. *Canadian Journal of Remote Sensing*, Vol. 25, No. 3, pp. 211-217.
- Skelton, D. and Bursey, T. (1998). *Assessment Report, Buffalo Hills property (ALO1)*. Ashton Mining of Canada Inc., Public as October 1999.
- Theriault, R.J. and Ross, G.M. (1991). Nd isotopic evidence for crustal recycling in the ca.2.0 Ga subsurface of western Canada. *Canadian Journal of Earth Sciences*, Vol. 28, pp. 1140-1147.
- Villeneuve, M.E., Ross, G.G., Parrish, R.R., Theriault, R.J., Miles, W., and Broome, J. (1993). Geophysical subdivision, U-Pb geochronology and Sm-Nd isotope geochemistry of the crystalline basement of the Western Canadian Sedimentary Basin, Alberta and Northeastern British Columbia. *Geological Survey of Canada, Bulletin 447*.
- Ulaby, F.T., Moore, R.K., Fung, A.K. (1982). *Microwave Remote Sensing, Active and Passive. From Theory to Applications*, Volume III. Artech House, Inc. London.
- Ward, B.C., Kjarsgaard, I.M., Dredge, L.A., Kerr, D.E., Stirling, J.A.R. (1995). Distribution and chemistry of kimberlite indicator minerals, Lac de Gras map area (76D), Northwest Territories. Geological Survey of Canada, Open File 3080.

Table 3.1. Principal components loading from Correlation Eigenvectors.

Corr. Eigenvectors	PC1	PC2	PC3	PC4
S1A	0.391	-0.908	-0.036	-0.145
S1D	0.479	0.185	-0.792	0.329
S7A	0.538	0.114	0.596	0.585
S7D	0.573	0.358	0.128	-0.727

Table 3.2. Principal components loading expressed in % from Correlation Eigenvectors.

%Corr. Eigenvectors	PC1	PC2	PC3	PC4
S1A	19.74	-58.02	-2.32	-8.12
S1D	24.18	11.82	-51.03	18.42
S7A	27.16	7.28	38.40	32.75
S7D	28.92	22.88	8.25	-40.71

Table 3.3. Eigenvalue analysis from correlation matrix.

PC	Eigenvalue	Difference	Proportion	% Total variance Corr. Matrix	% Cumulative Total variance	Ratio eigenvalue
PC1	2.142	1.337	0.536	53.55	53.55	1
PC2	0.805	0.099	0.201	20.13	73.68	2.66
PC3	0.706	0.359	0.177	17.65	91.33	3.03
PC4	0.347	0.000	0.087	8.68	100.00	6.17

Table 3.4. Summary of lineament orientations in RADARSAT-1-PC interpretation.

RADARSAT-1-PC lineaments trend	Total lineaments	Mean (°)	Std (°)
NNE	395	12.7	12.0
NW	564	310.0	13.6
NE	321	56.7	13.9
ENE	251	83.7	3.5

Figure 3.1. Buffalo Head Hills study area and NTS coverage. GSLSZ, Great Slave Lake Shear Zone; STZ, Snowbird Tectonic Zone. The inset shows the Precambrian basement terrane boundaries (after Pilkington et al., 2000).

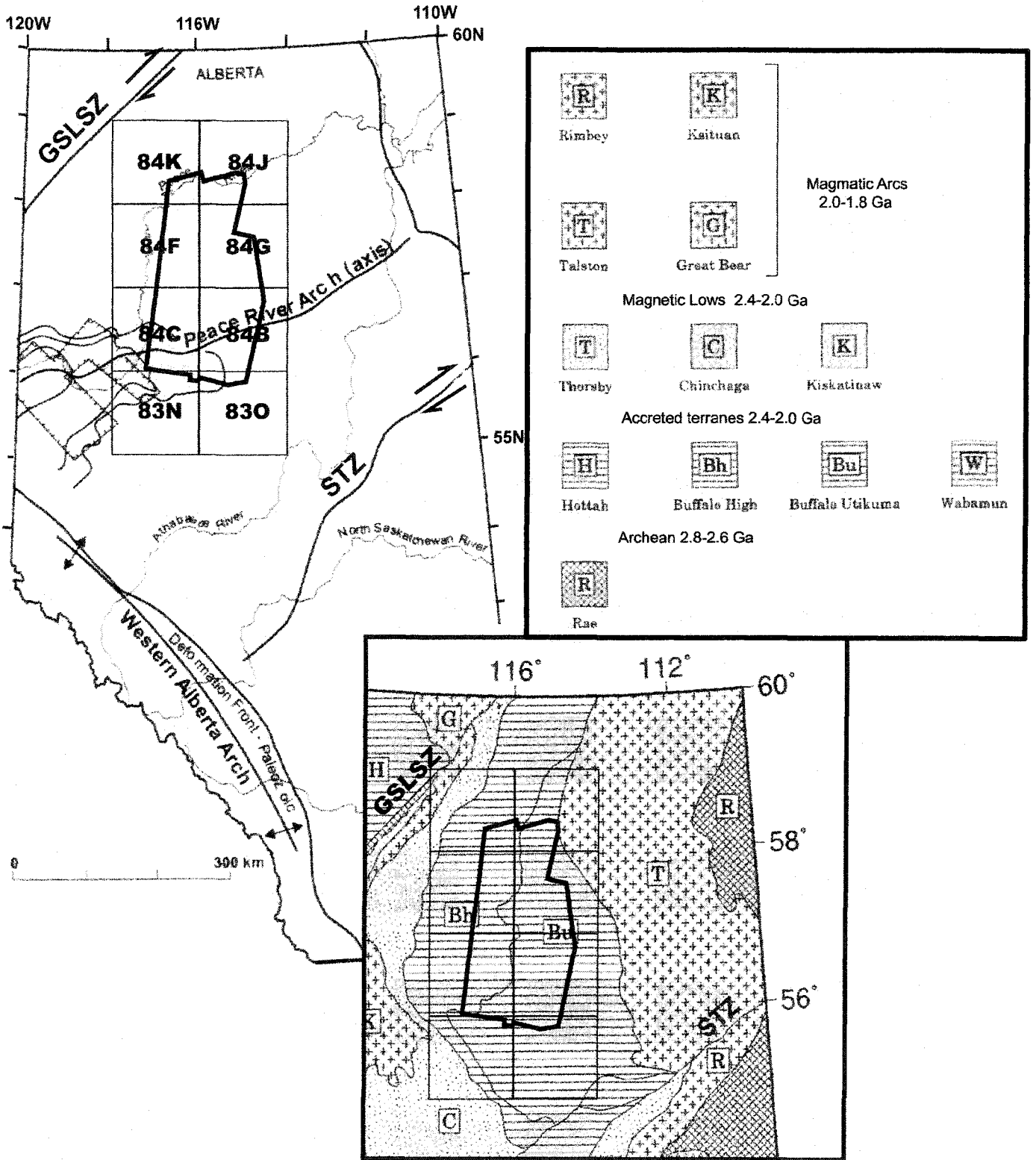
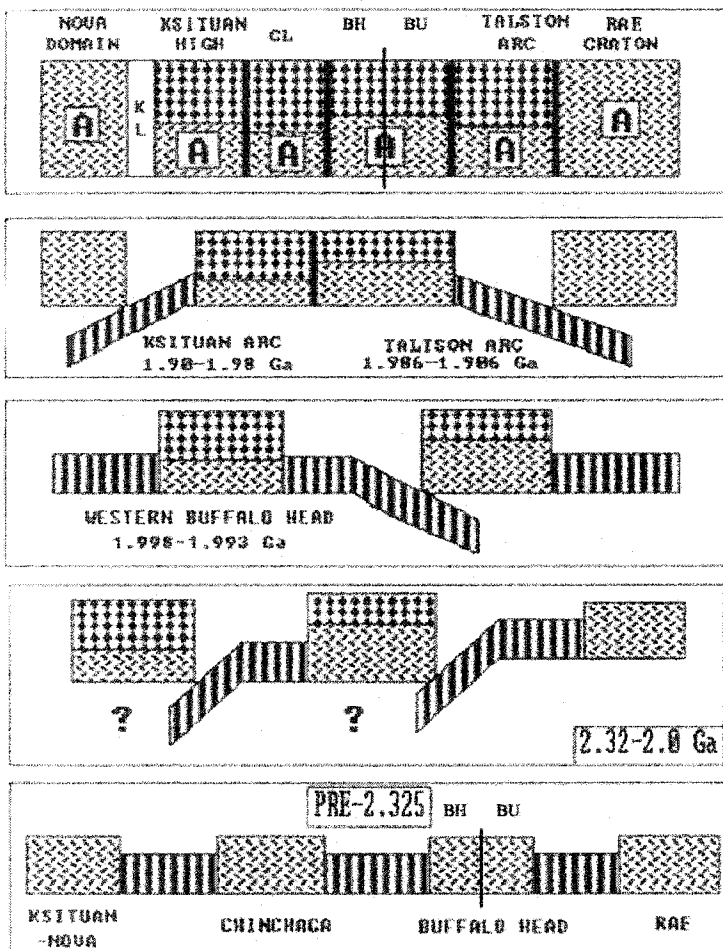


Figure 3.1A. Archean block reconstruction of the WCSB (A: Archean blocks, BH: Buffalo High terrane, BU: Buffalo Utikuma terrane; modified after Ross, 1990).



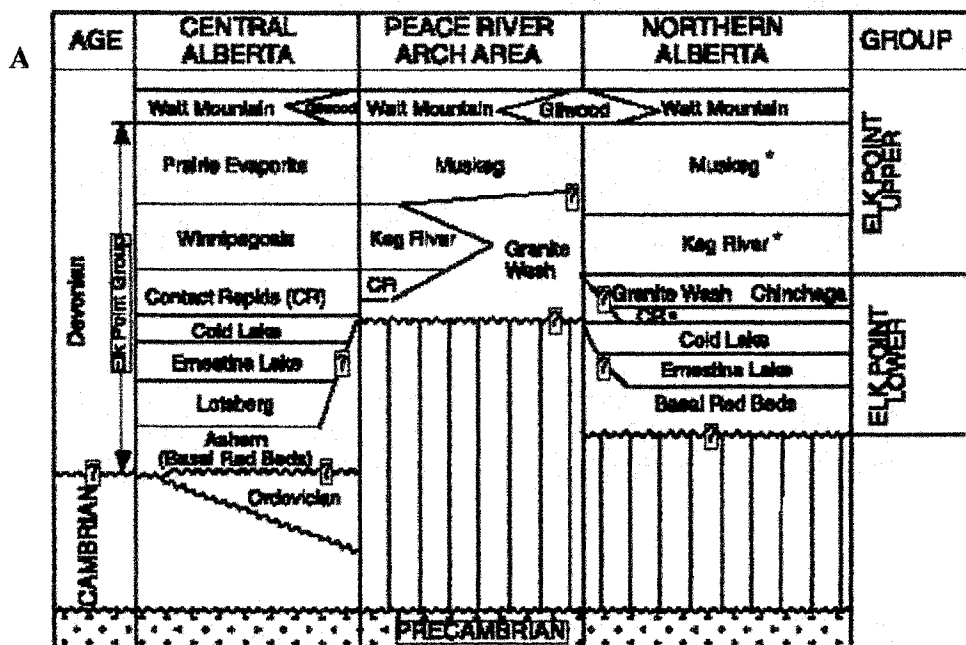


Figure 3.2. A) Stratigraphic correlation chart of Elk Point Group strata showing correlation across the Peace River Arch from central to northern Alberta subsurface. * are units that have biostratigraphic age-dates (from Hein, 1999); B) summary of Cretaceous strata characterizing the Buffalo Head Hills area (from Chen and Bergman, 1999).

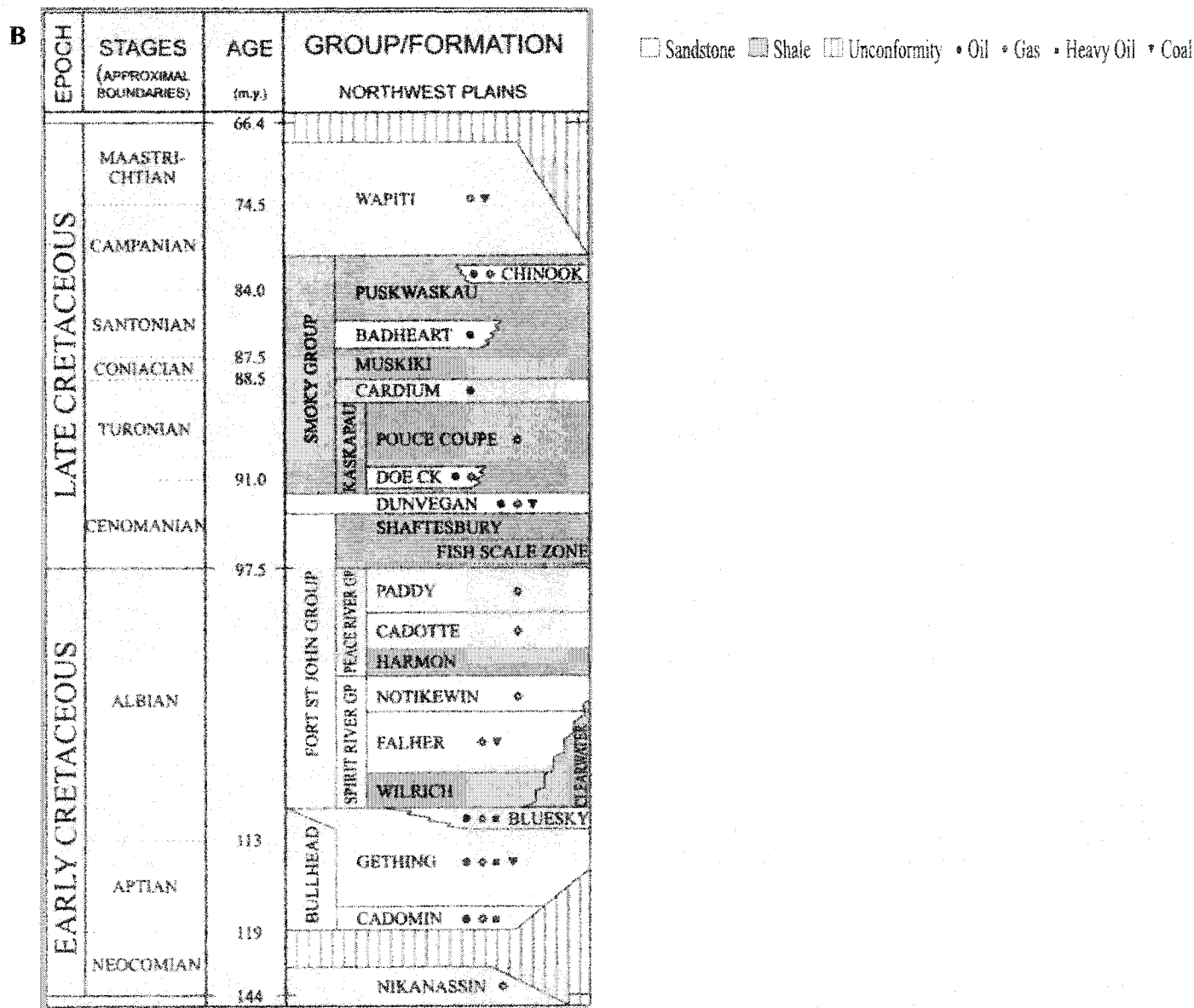


Figure 3.3. Buffalo Head Hills geology outlined on RADARSAT-1-PC2: K1, Loon River Formation (Lower Cretaceous); Kp, Peace River Group (Lower Cretaceous); Ksh, Shaftesbury Formation (Lower-Upper Cretaceous); Kd, Dunvegan Formation (Upper Cretaceous); Ks, Smoky Group (Upper Cretaceous); kimberlite, black circles. Outline AMCI, AEC, and AGS structural maps.

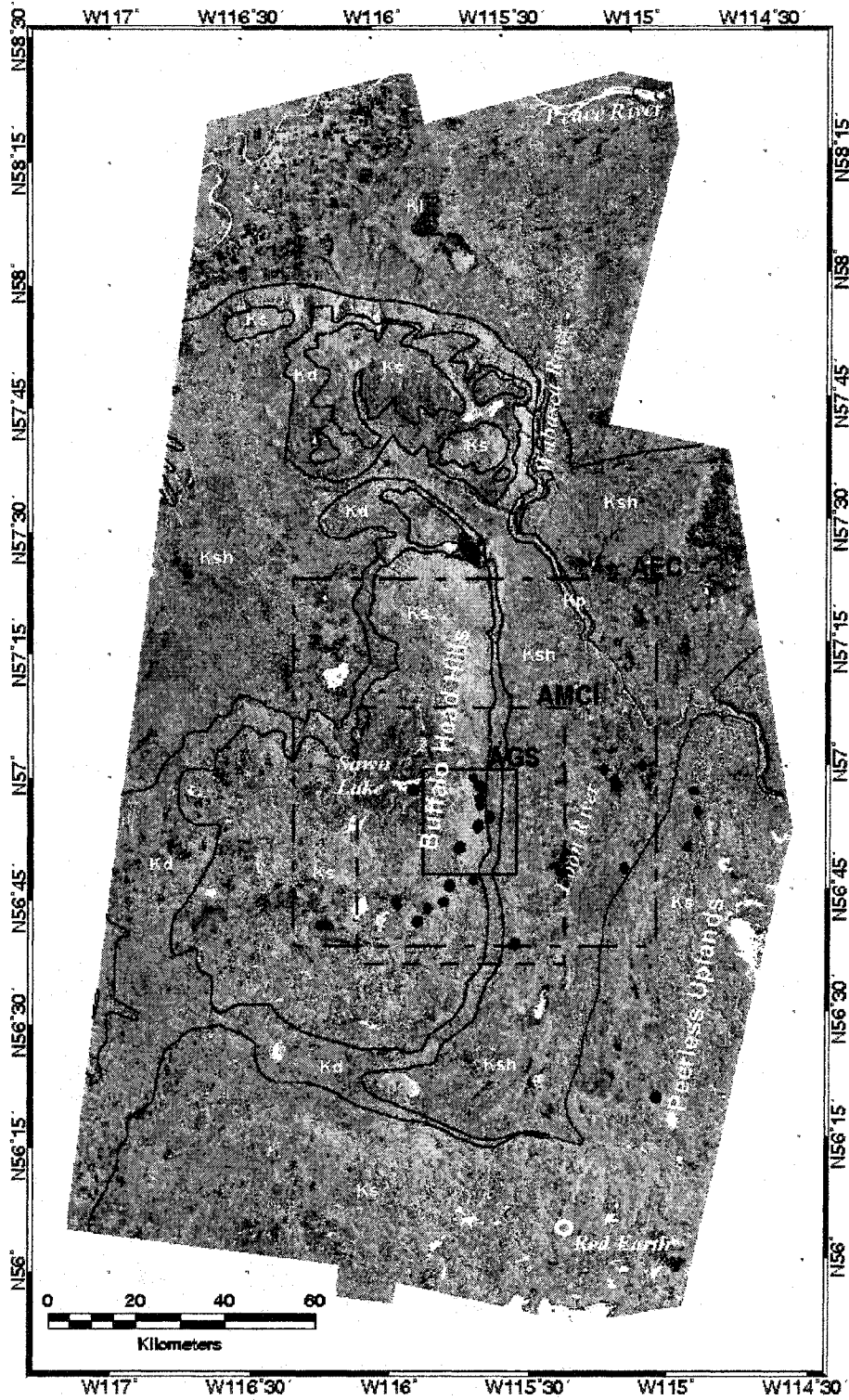


Figure 3.4. Mosaic of 8 filtered RADARSAT-1 S1 Ascending scenes (MOSAIC_S1A):
A, Peerless Uplands W-facing slope.

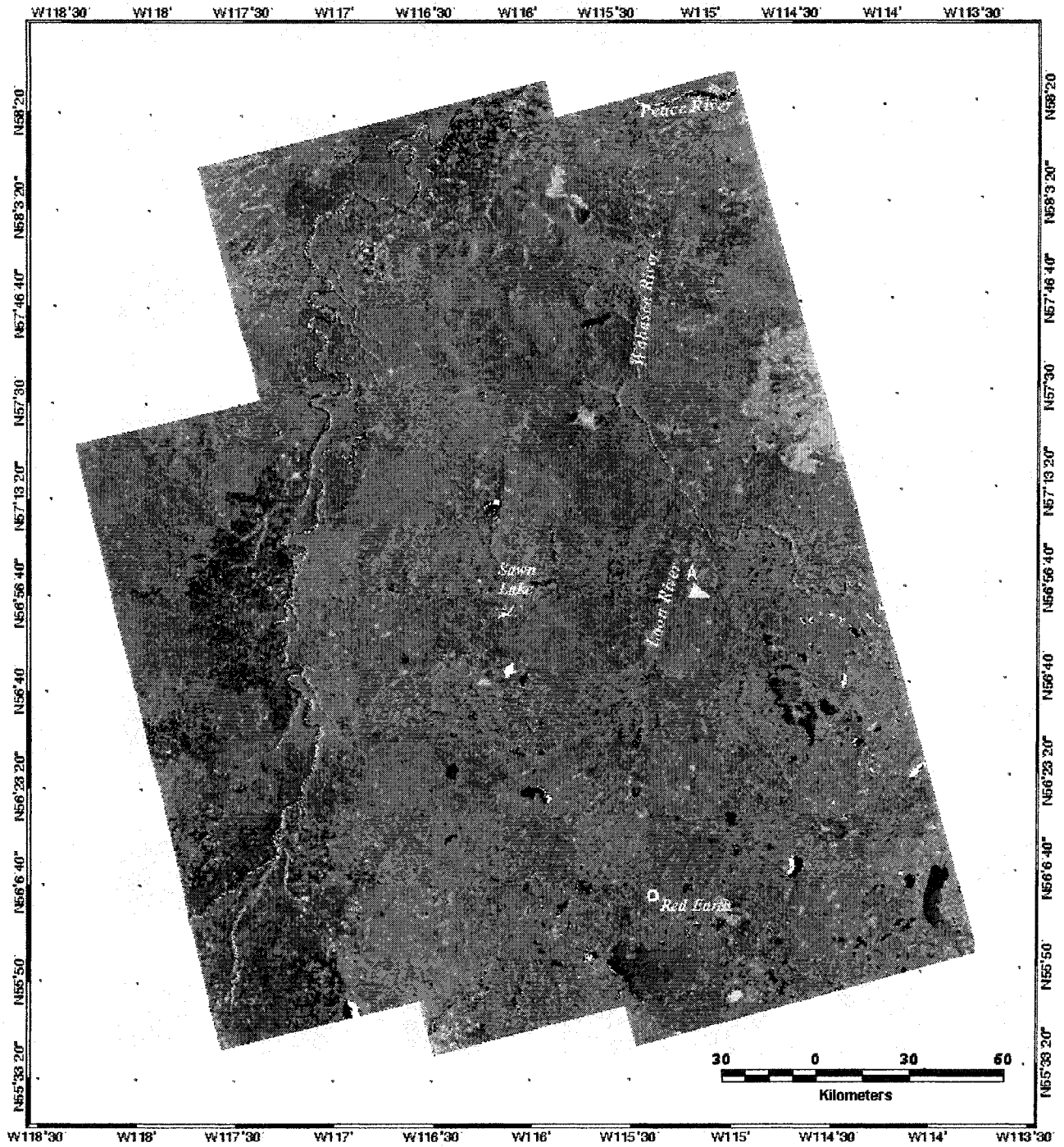


Figure 3.5. Mosaic of 8 filtered RADARSAT-1 S1 Descending scenes (MOSAIC_S1D):
A, Buffalo Head Hills E-facing slope; B, Buffalo Head Hills NE-facing slope.

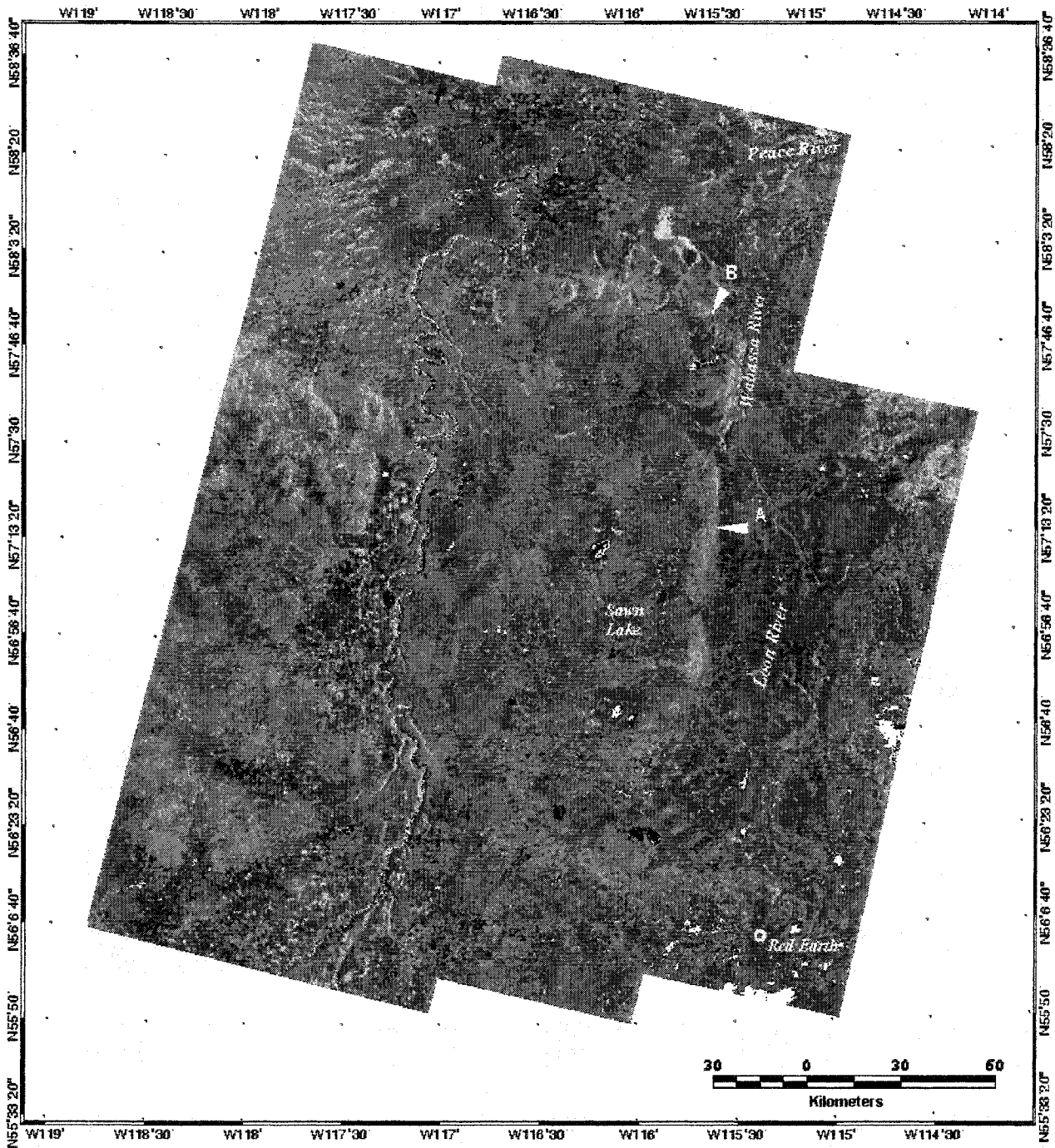


Figure 3.6. Mosaic of 6 filtered RADARSAT-1 S7 Ascending scenes (MOSAIC_S7A):
A, Peerless Uplands W-facing slope.

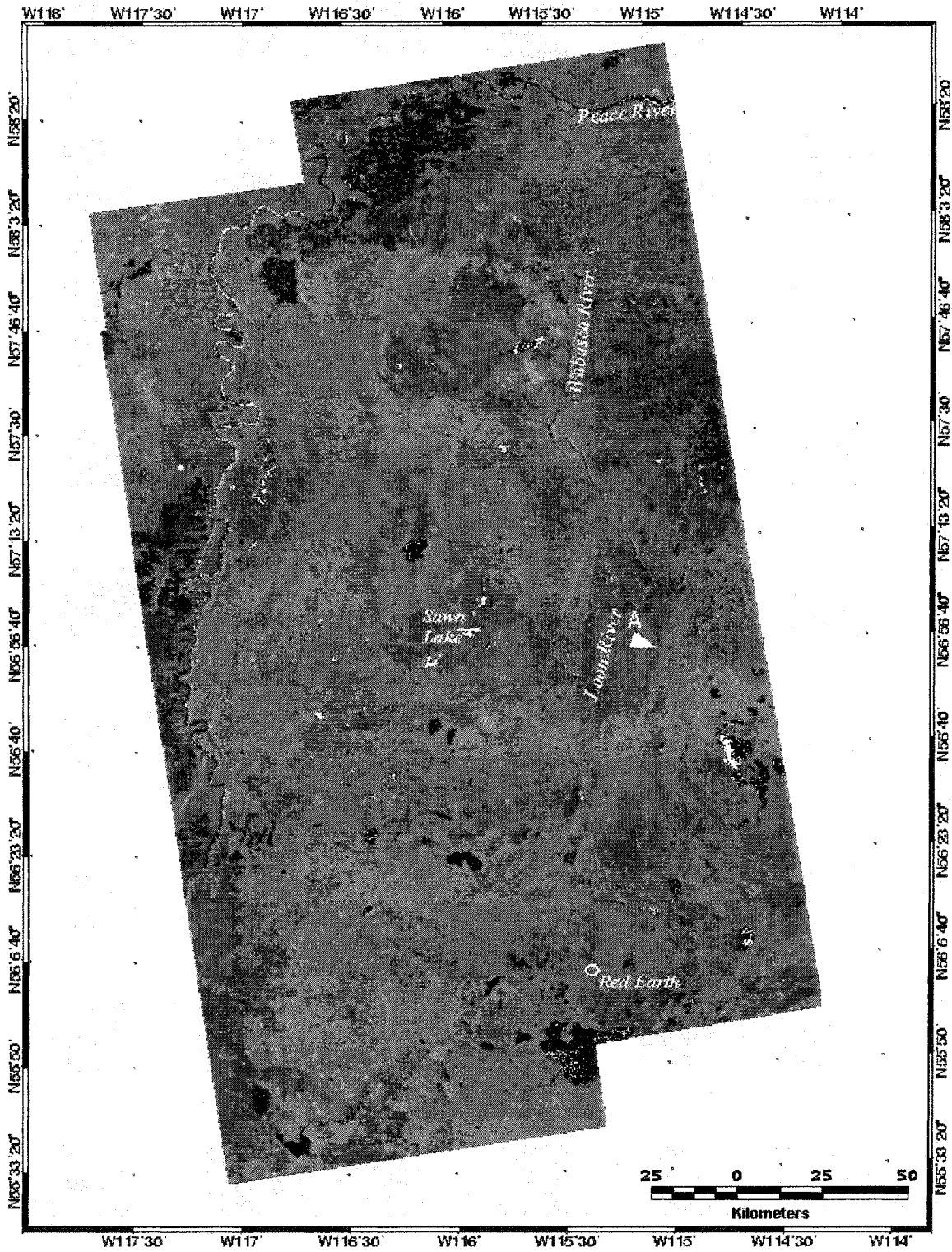
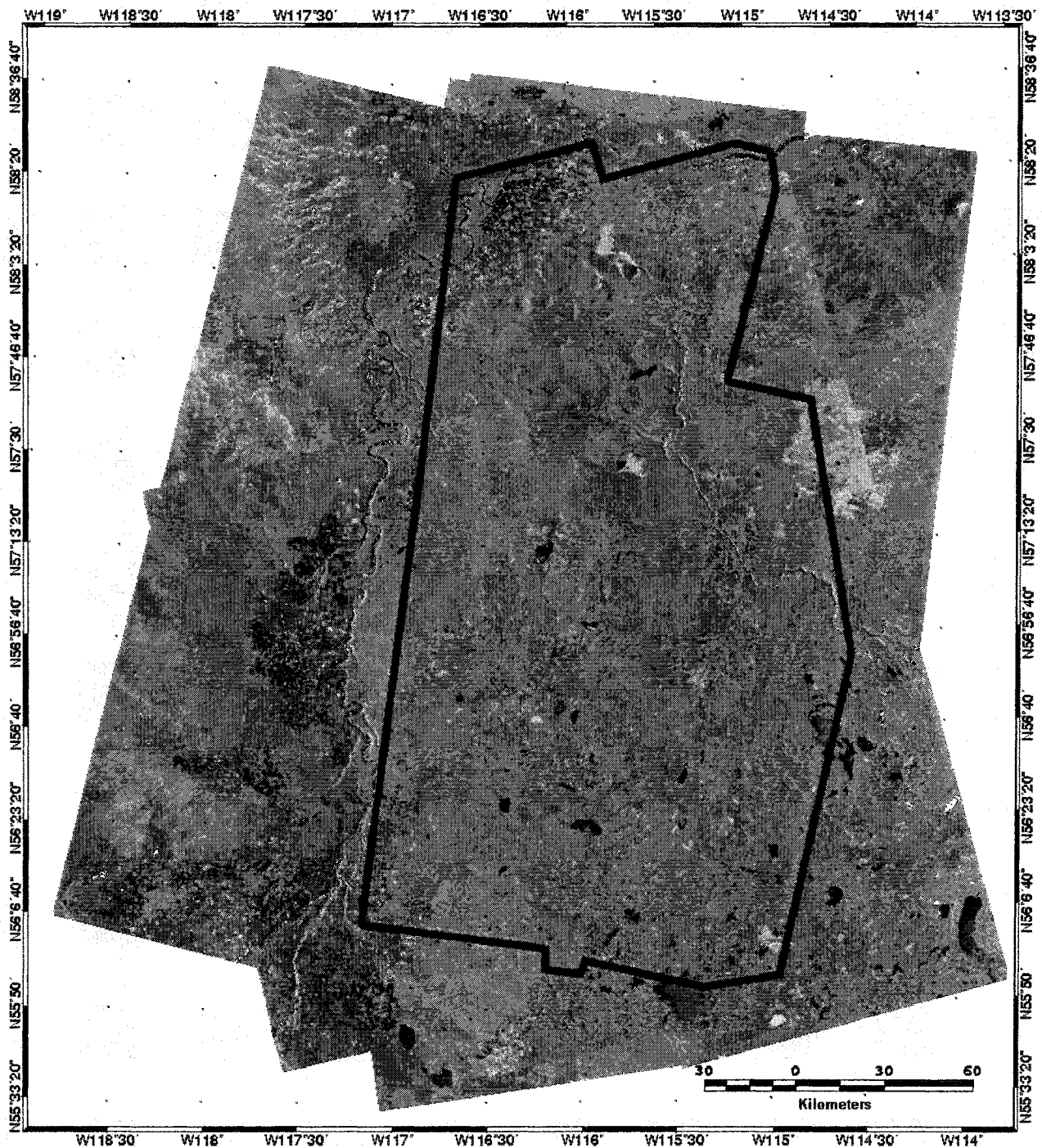
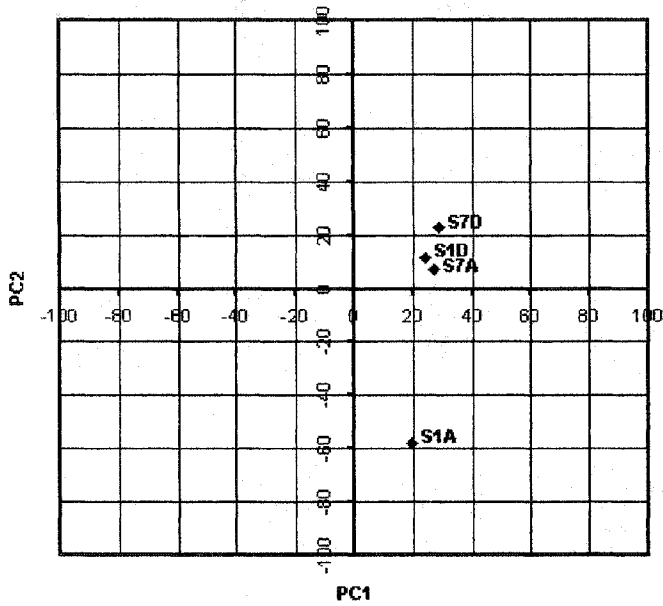


Figure 3.7. Mosaic of 6 filtered RADARSAT-1 S7 Descending scenes (MOSAIC_S7D): A, Buffalo Head Hills E-facing slope; B, Buffalo Head Hills NE-facing slope.

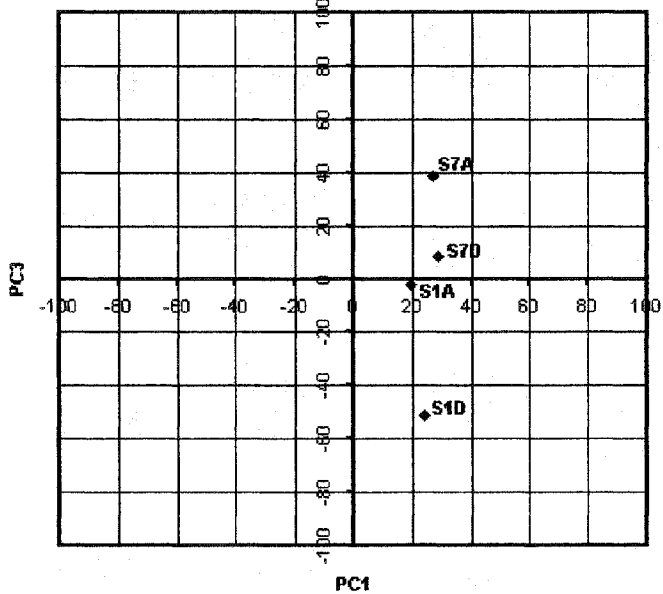


Figure 3.8. Outline of the resulting RADARSAT-PC image coverage of the Buffalo Head Hills study area.





- 1 **Figure 3.8A.** 1) Percentage loadings of multi-beam RADARSAT-1 input channels showing the relationships of each beam mode for the first two principal components, PC1 and PC2. S1A, S1D, S7A, and S7D contribute to the overall brightness of the first principal component. For the second principal component (PC2), S1A is inversely associated with S1D, S7A, and S7D. This suggests that scene brightness and variability is controlled by incidence angle and contrast in look direction, especially imposed by the contrast of S1D and S1A, which enhance terrain features. 2) The variability in the third component (PC3) is controlled by the contrast of beam mode and look direction. S7A and S7D are inversely related to S1A and S1D. The contrast between S7A and S1D determine enhancement for drainage and quaternary features although the dark tone variability. 3) The variability in the fourth component (PC4) is controlled by the contrast in look direction defined by the inverse correlation of S7A and S7D, and minor contribution of S1D and S1A.



3

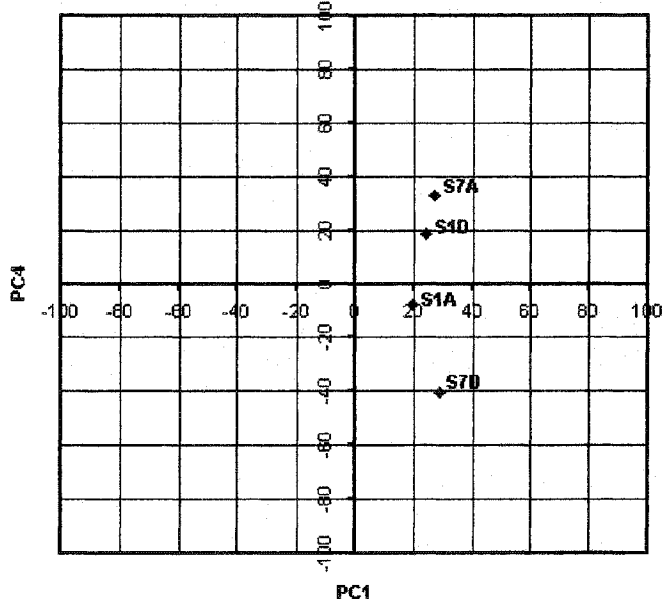


Figure 3.9. RADARSAT-1-PC1 image.

%loading PC1	PC1
S1A	19.74
S1D	24.18
S7A	27.16
S7D	28.92

54% scene
variance

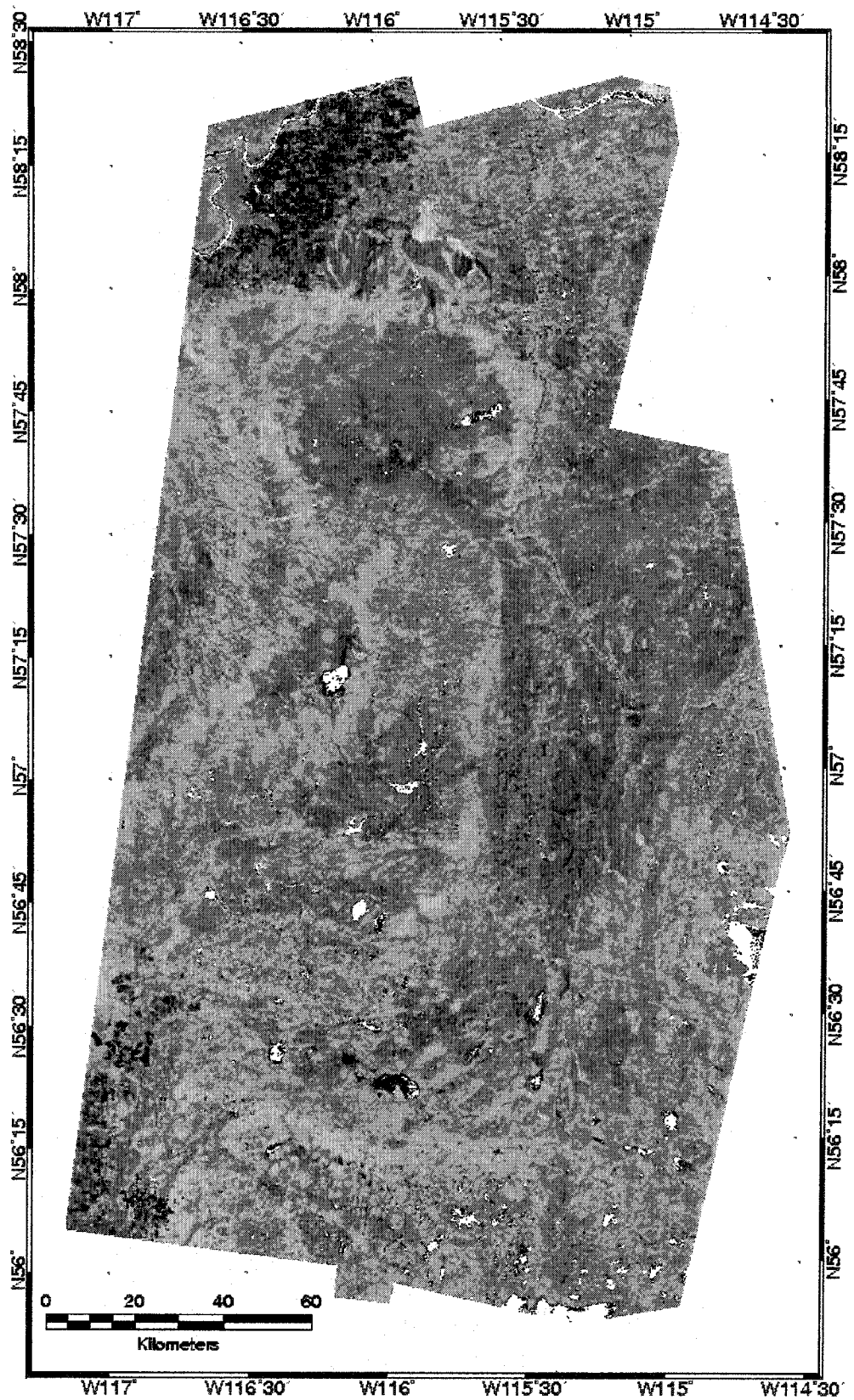


Figure 3.10. RADARSAT-1-PC2 image: A, Buffalo Head Hills E-facing slope; B, Buffalo Head Hills NE-facing slope; C, Peerless Uplands W-facing slope.

%loading	PC2
PC2	

S1A	-58.02
S1D	11.82
S7A	7.28
S7D	22.88

20% scene variance

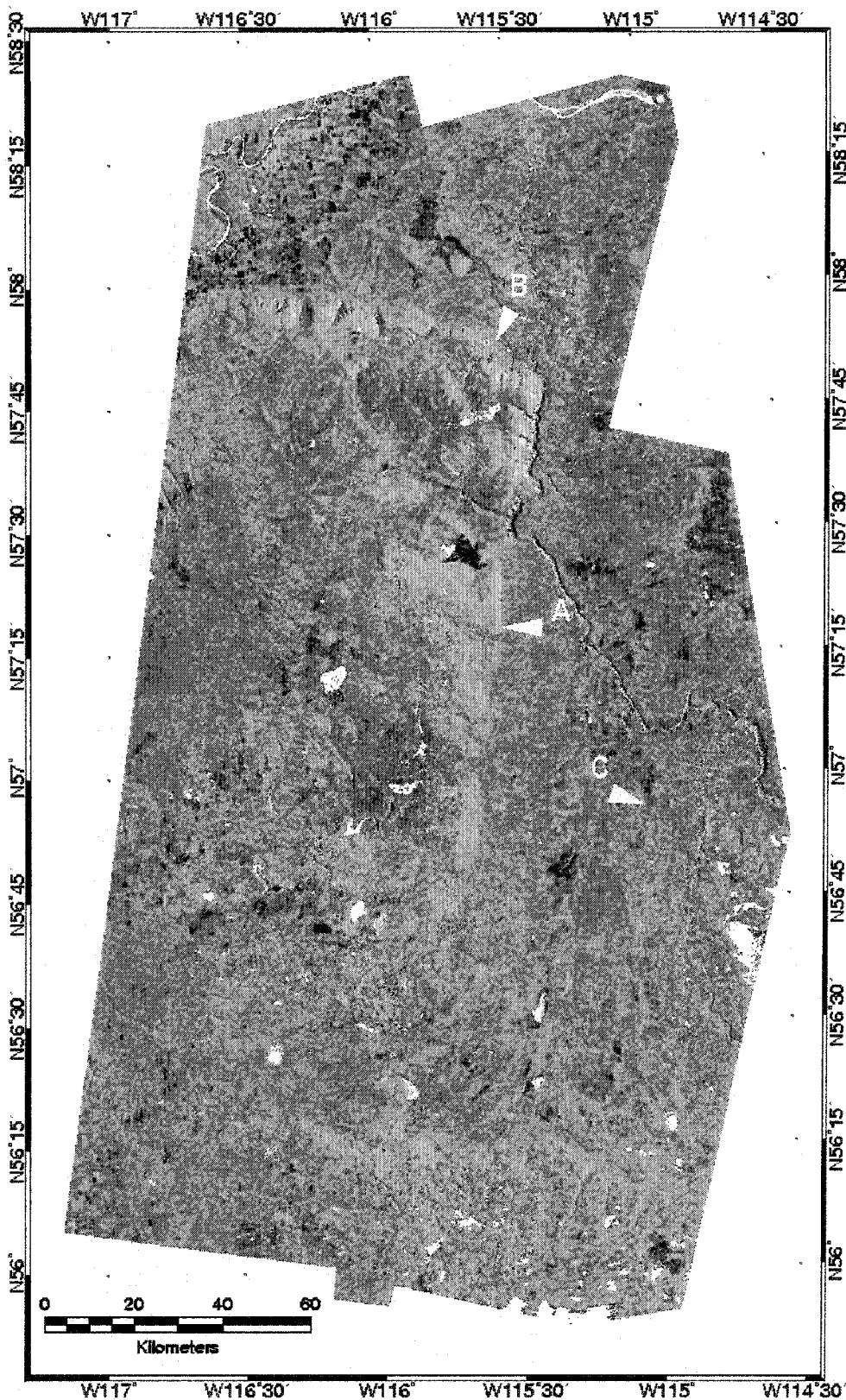


Figure 3.11. RADARSAT-1-PC3 image: A, Loon River Valley NNE-trend drainage; B, Loon River valley ENE-trend drainage; C, Buffalo Head Hills NW-trend drainage; D, Wabasca River NW-trend drainage.

%loading	PC3
PC3	

S1A	-2.32
S1D	-51.03
S7A	38.40
S7D	8.25

17% scene variance

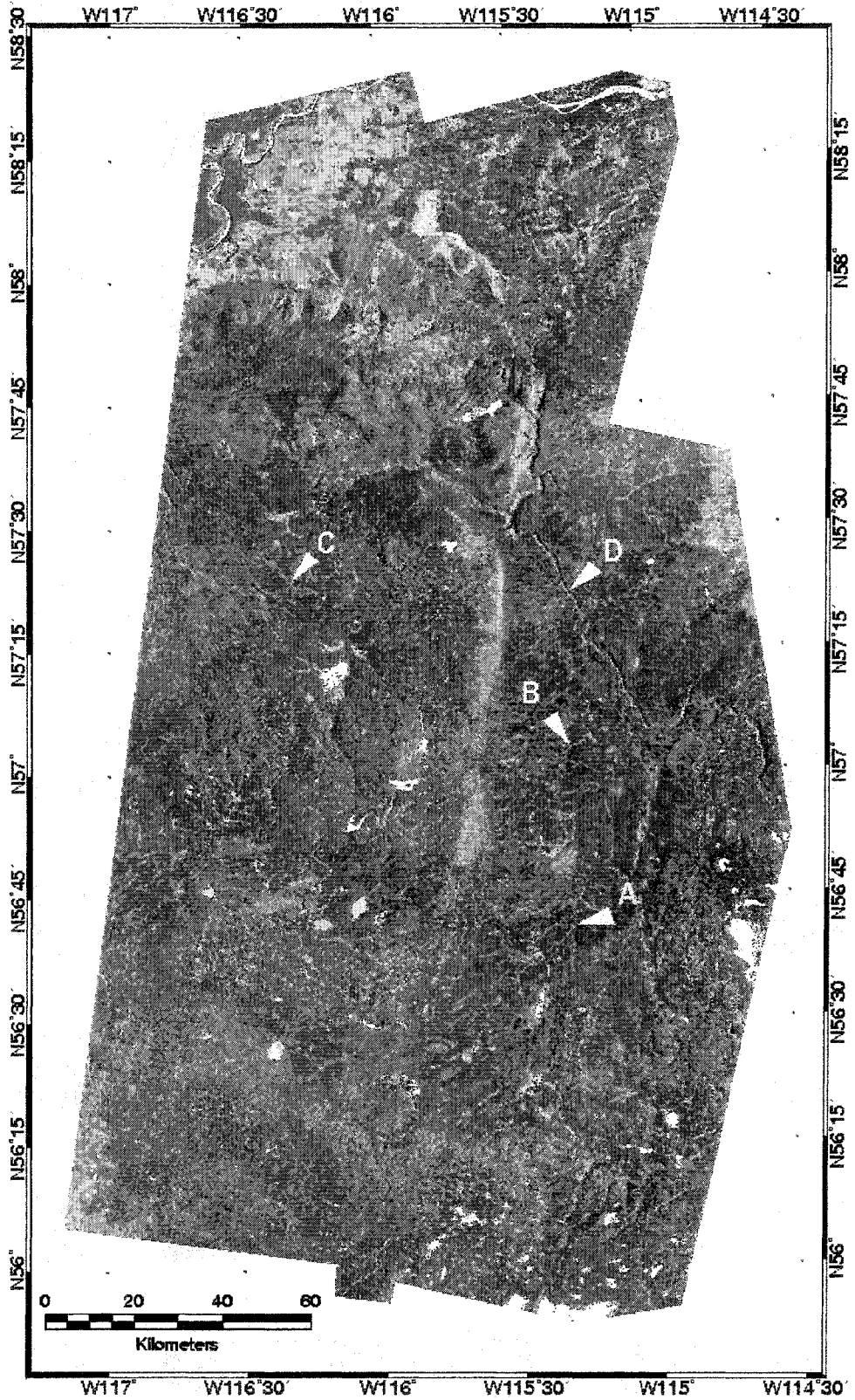


Figure 3.12. RADARSAT-1-PC4 image: A, artifact due to processing; B, Peerless Uplands ENE-trend feature; C. Buffalo Head Hills ENE-trend features.

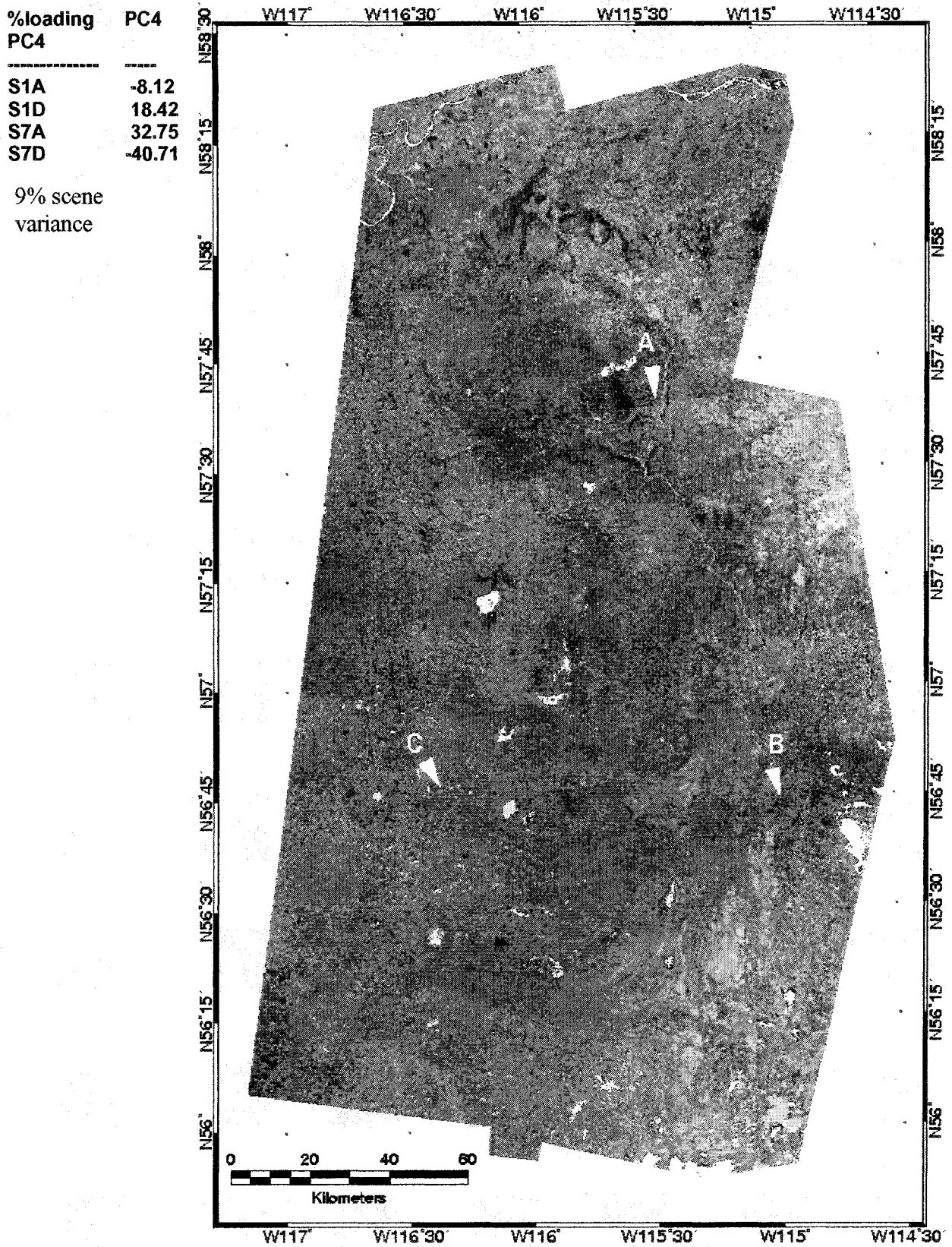
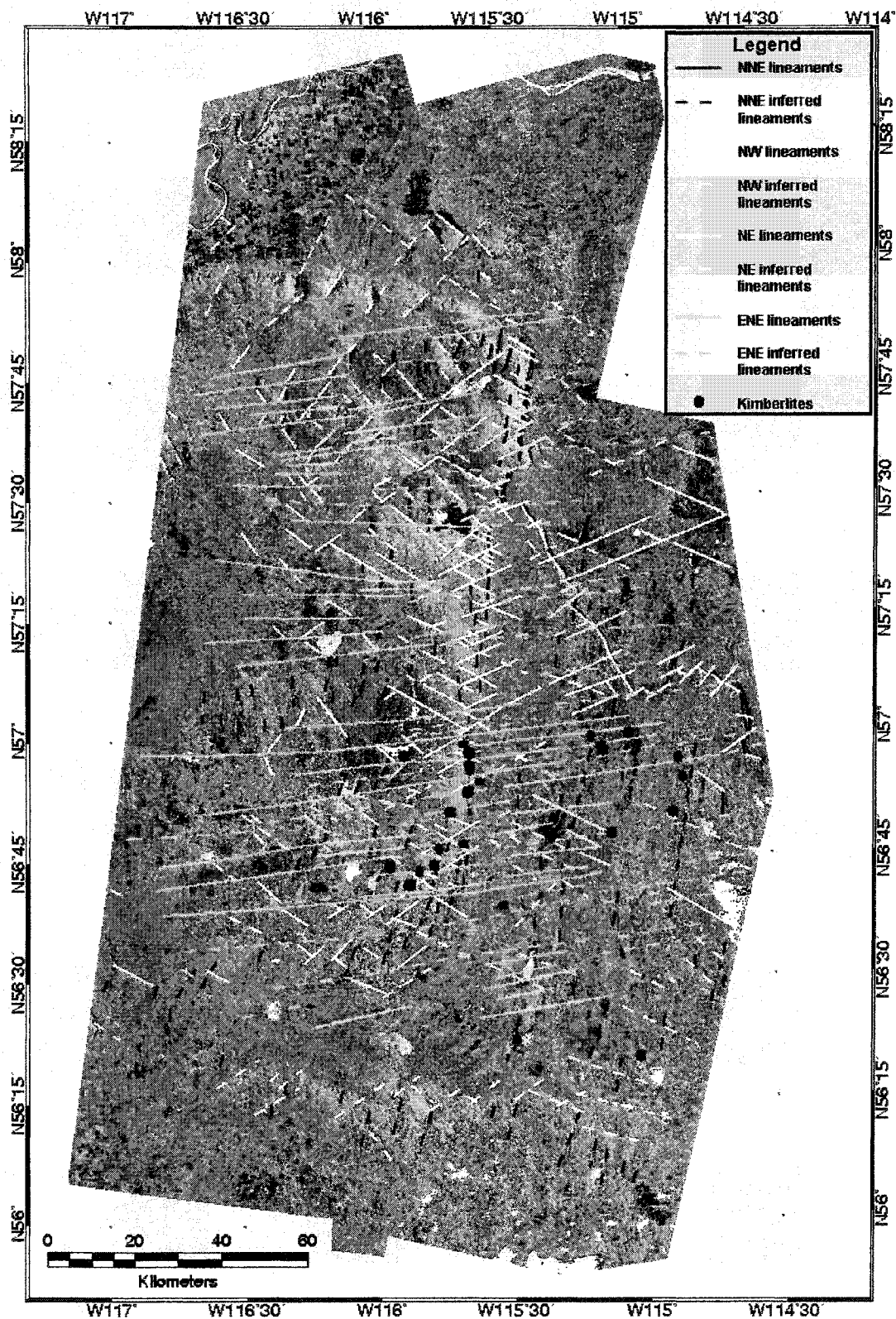


Figure 3.13. RADARSAT-1-PC2 structural interpretation and kimberlite locations.



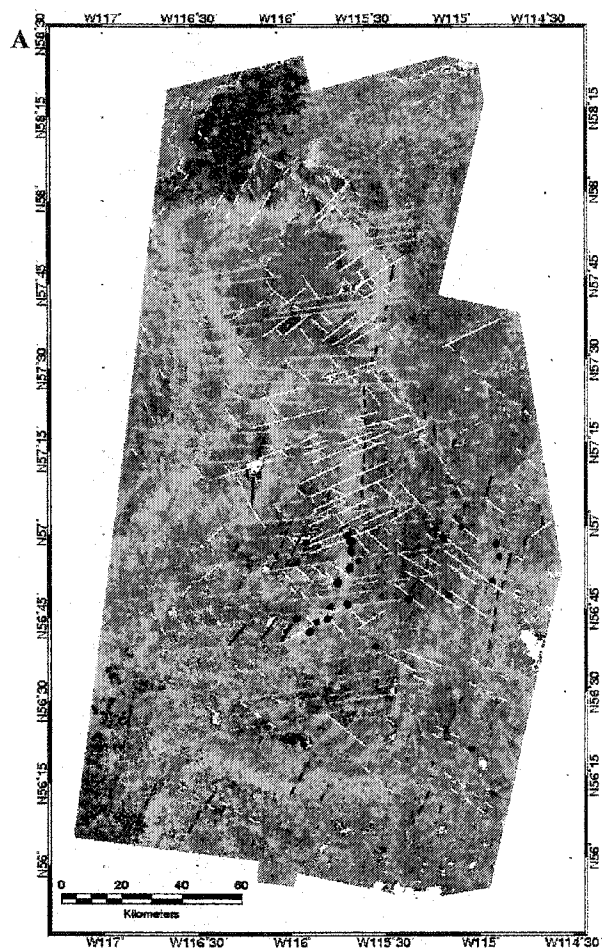


Figure 3.14. Structural interpretation and kimberlite locations of: A) RADARSAT-1-PC1; B) RADARSAT-1-PC3; C) RADARSAT-1-PC4.



Figure 3.15. RADARSAT-PC lineament compilation: **A)** NNE lineaments; **B)** NW lineaments; **C)** NE lineaments; **D)** ENE lineaments.

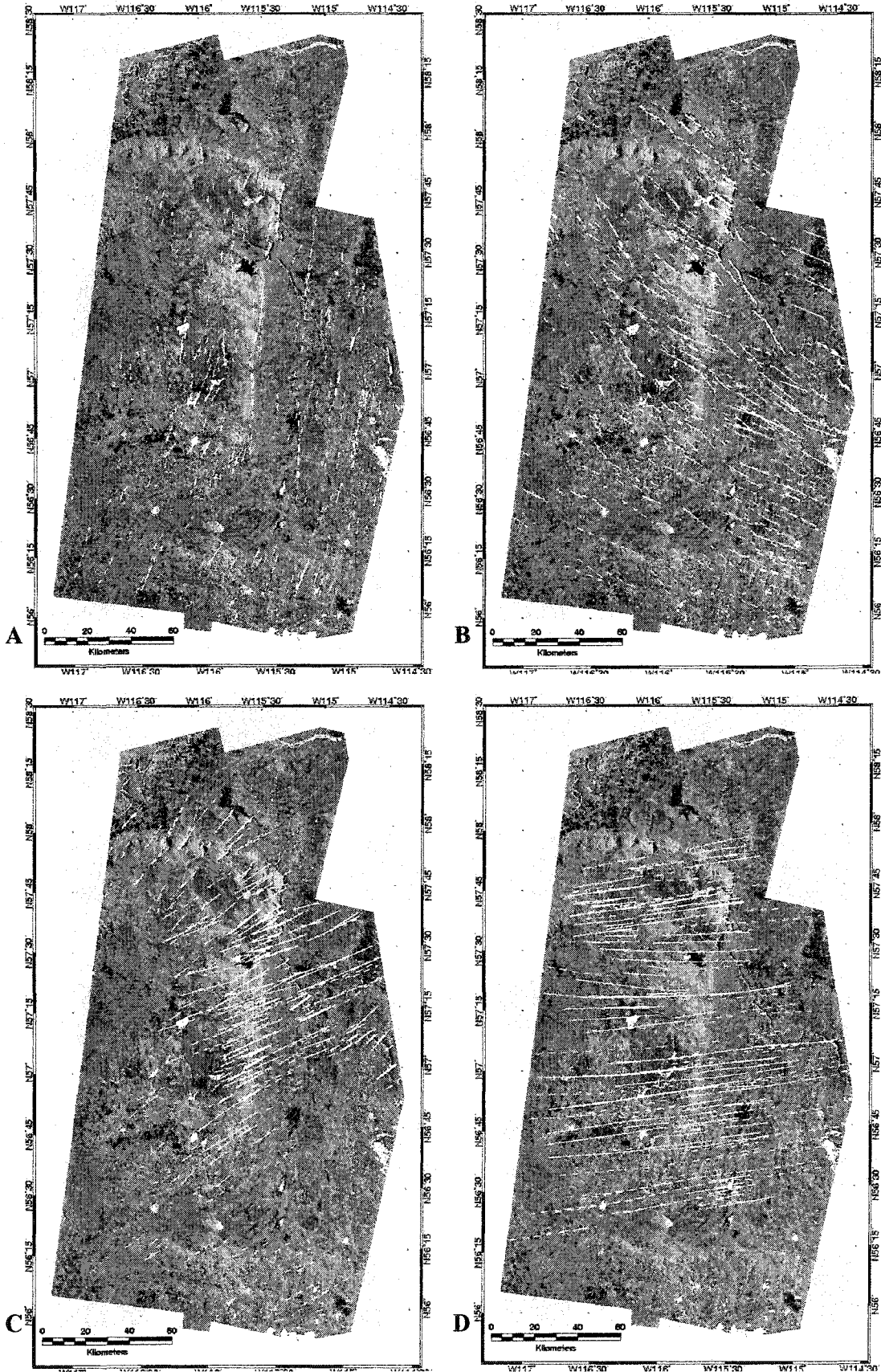
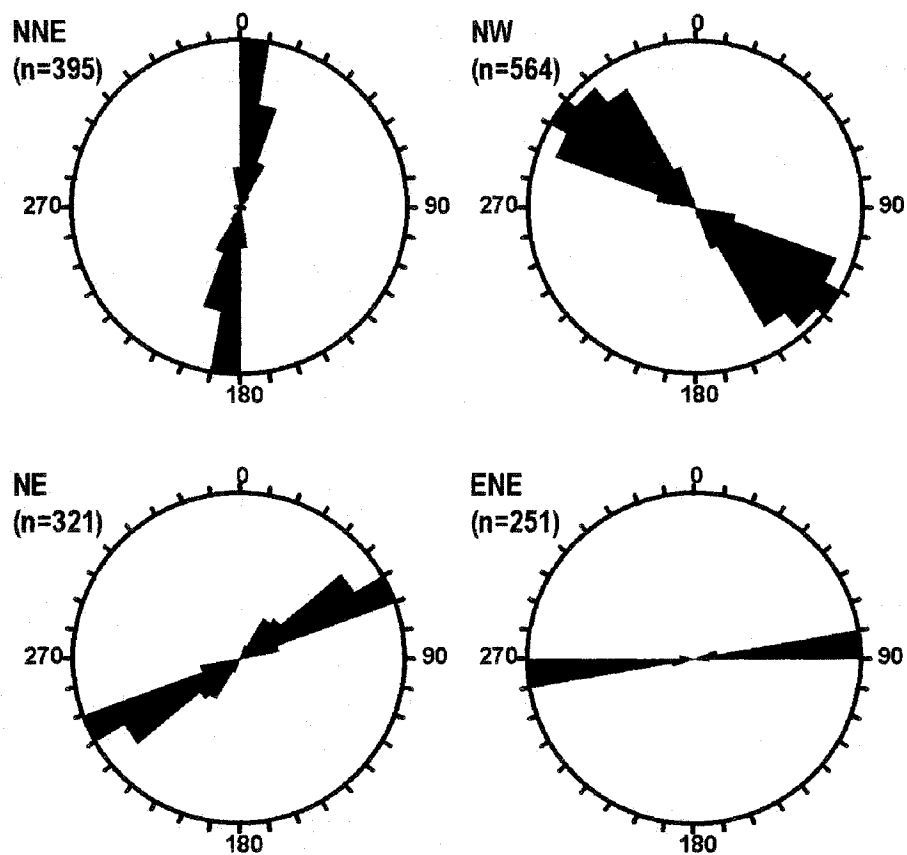
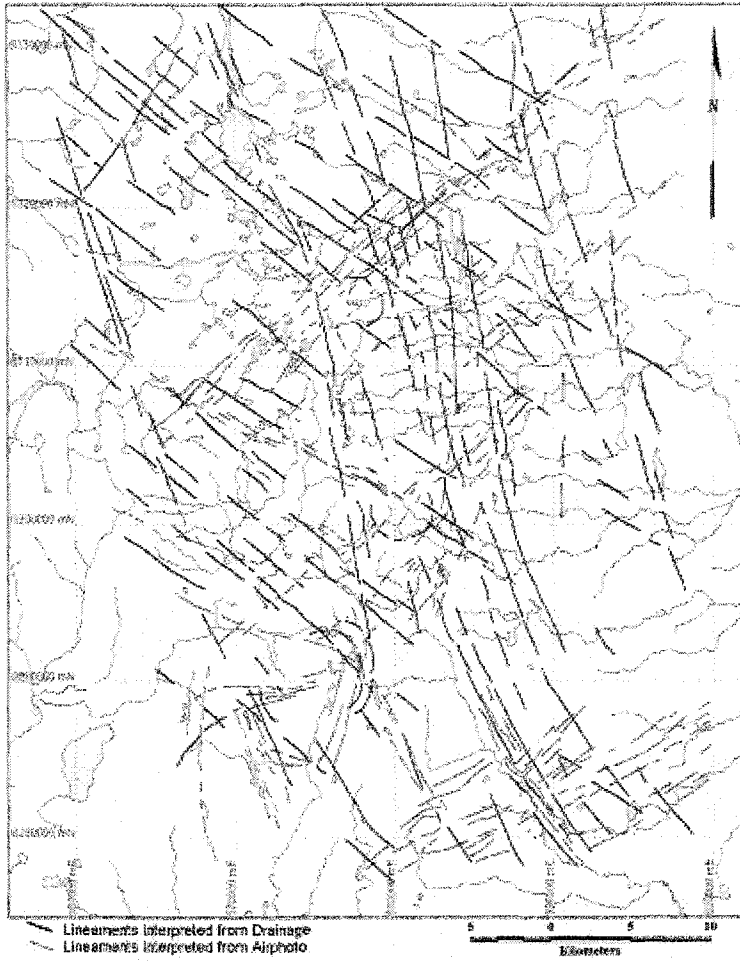
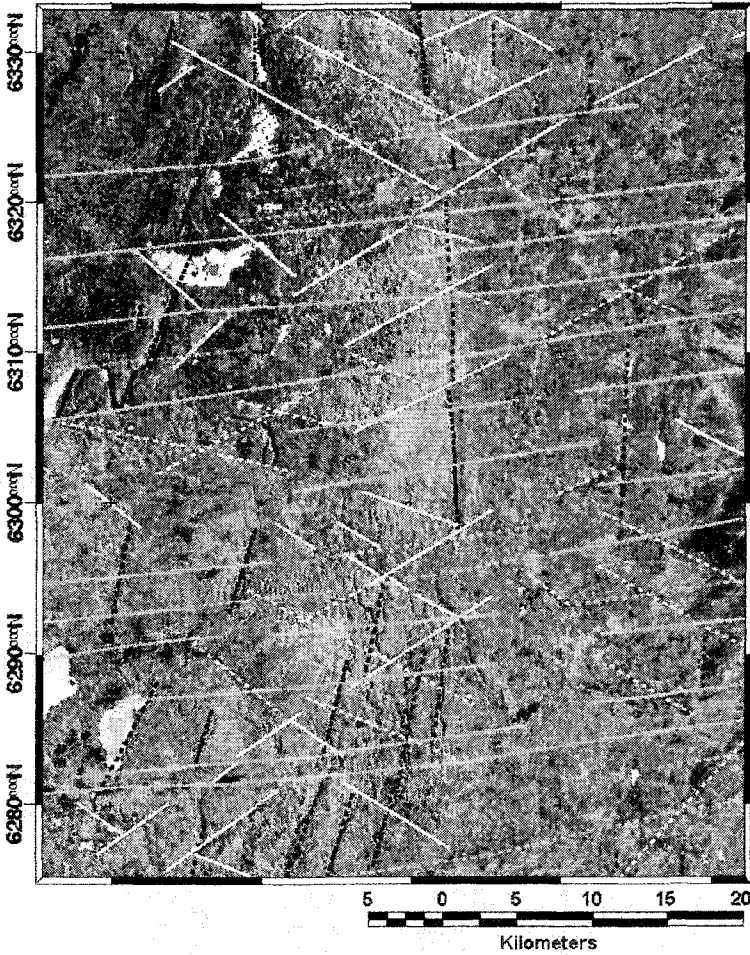


Figure 3.16. Rose diagrams of lineaments interpreted on RADARSAT-1-PC images.





A **Figure 3.17.** A) Ashton Mining of Canada Inc. (AMCI) structural interpretation map (Lockett, 1998); B) RADARSAT-1-PC2 subset structural interpretation map.



B

Figure 3.18A. Alberta Energy Company (AEC) structural interpretation map (Pryde, 2000).



Figure 3.18B. RADARSAT-1-PC2 subset structural interpretation map.



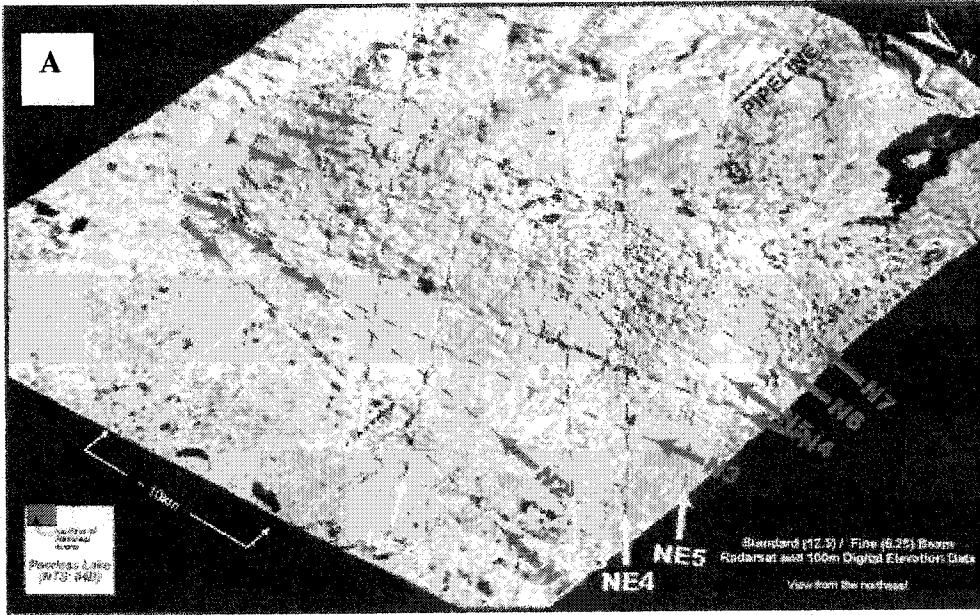
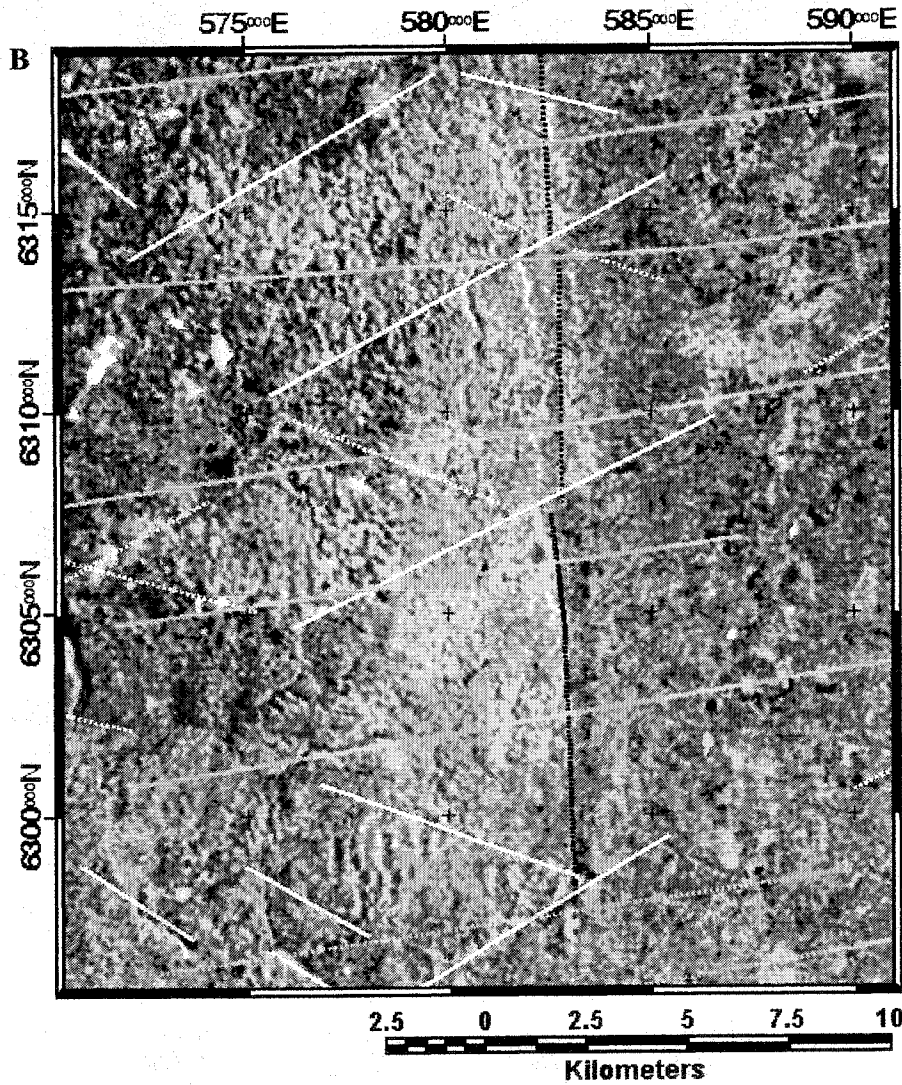


Figure 3.19. A) Alberta Geological Survey structural interpretation map (Eccles et al., 2000); B) RADARSAT-1-PC2 subset structural interpretation map.



Chapter 4

INTEGRATION OF STRUCTURAL, GRAVITY, AND MAGNETIC DATA USING THE WEIGHTS OF EVIDENCE METHOD AS A TOOL FOR KIMBERLITE EXPLORATION IN THE BUFFALO HEAD HILLS AREA, NORTHERN CENTRAL ALBERTA

4.1 INTRODUCTION

Worldwide, kimberlite occurrences have been found to be spatially related to regional scale structural lineaments (Woodzick and McCallum, 1982; Sarma and Verma, 2001). A structural study conducted in the Buffalo Head Hills area (Paganelli et al., 2001b) provided sufficient information to suggest a close interrelationship between kimberlite emplacement and structural features. The objective of this study is to assess the spatial relationship between the outlined lineament trends in Paganelli et al. (2001a, b) and the known kimberlite locations, to test this hypothesis in the Buffalo Head Hills area.

A geo-spatial quantitative assessment based on a Bayesian statistical approach of prior and posterior probability, in a loglinear form known as weights of evidence (Spiegelhalter, 1986), was used to analyze the spatial relationship between the lineament trends and the kimberlite locations. The results are illustrated on a favourability map, showing potential areas for exploration estimated using statistical weights assigned to the spatial datasets used as predictor maps (thematic maps) identifying spatial patterns such as lineaments, geology, and geophysical characteristics (Agterberg, 1989; Bonham-Carter, 1994). This method has been previously applied by Watson (1989), Agterberg et al. (1990), Bonham-Carter et al. (1988,1989), Wright et al. (1996), and Tangestani and

Moore (2001) for mineral potential mapping. However, the present study represents its first application to kimberlite exploration.

In the Buffalo Head Hills area, a first step in the application of the weights of evidence approach has been to test the hypothesis that known kimberlite locations are spatially related to the outlined structural lineaments in Paganelli et al. (2001a). Quantitative spatial correlation and verification of this hypothesis has been followed by the definition of four structural predictive maps integrated with three additional predictive maps defining: (1) the revised boundary of the Buffalo High and Buffalo Utikuma terranes from regional aeromagnetic data (provided by Dr. M. Pilkington, GSC, Ottawa; Pilkington et al., 2000); (2) the average aeromagnetic response of the Buffalo High and Buffalo Utikuma terranes (Pilkington et al., 2000); and (3) the Bouguer gravity anomaly characteristics of the Buffalo Head Hills basement. A total of seven predictor themes were therefore used in the weights of evidence model to define a favourability map for kimberlite exploration.

4.2 REGIONAL GEOLOGY

The Buffalo Head Hills in north-central Alberta (Figure 4.1) has been an area of intense oil and gas exploration, and recently also kimberlite exploration (Carlson et al., 1998). It is located northeast of the Peace River Arch within the Phanerozoic succession of the Western Canadian Sedimentary Basin. The Buffalo Head Hills is part of the cratonic platform whose tectonic evolution has been influenced by the uplift and

extensional episodes of the Peace River Arch (Cant, 1988; O'Connell et al., 1990). These episodes have resulted in the development of N-trending horst-graben block structures during the Phanerozoic. The Buffalo Head Hills is characterized by a sedimentary succession of platform carbonates, shale, and sandstone of Devonian and Cretaceous ages overlying a Precambrian crystalline metamorphic basement (Edwards et al., 1995). The Precambrian basement is here defined by the Buffalo Head High and Buffalo Head Utikuma terranes, whose differentiation is based on the high magnetic intensity response of the Buffalo Head High, and medium-low magnetic intensity response of the Buffalo Head Utikuma (Pilkington et al., 2000).

The Buffalo Head Hills area has recently attracted interest for kimberlite exploration (Carlson et al., 1998). Kimberlite pipes intrude the recessive Cretaceous sediments of the Smoky Group, Dunvegan Formation, and Shaftesbury Formation (Figure 4.2), and are characterized by crater facies lithologies, mainly of lapilli-bearing olivine crystal tuffs. Crustal xenoliths consist of shales of the Shaftesbury Formation, while mantle derived xenoliths include peridotite, pyroxenite, eclogite, and corundum-spinel-bearing lithologies. U-Pb perovskite dates of 86 ± 3 and 88 ± 5 Ma (Carlson et al., 1998) suggest that the pipes were emplaced in mid to late Cretaceous (Cenomanian to Campanian). The Buffalo Head Hills kimberlites contain mantle xenoliths that are classified as predominantly of lherzolitic type (Carlson et al., 1998), with the occurrence of G9 and minor G10 garnets suggesting the presence of a minor eclogitic component (Sobolev et al., 1973). Cr-Ti spinels exhibit atoll-texture, and Cr_2O_3 wt% vs. TiO_2 wt% composition typical of magmatic trend 1, associated with group I kimberlites (Mitchell, 1995). Microphenocrysts of phlogopitic mica display evolution towards aluminous

phlogopite, thus plotting along the “kimberlite” trend on the Al_2O_3 wt% vs. TiO_2 wt% discrimination diagram (Mitchell, 1995).

The diamondiferous intrusive events in the Buffalo Head Hills range between 86 ± 3 and 88 ± 5 Ma (Carlson et al., 1998) from U-Pb perovskite dates. In the Mountain Lake intrusion, northeast of Grande Prairie (approximately 100 km southwest of Buffalo Head Hills) apatite fission track analyses gave dates of 72 ± 7 to 78 ± 9 Ma (Leckie et al., 1997a). This age range is consistent with the 86 ± 2 Ma (U-Pb perovskite) of a kimberlite pipe located along the eastern margin on the Aylmer Lake map sheet (NTS 76C) in the Slave Province, Northwest Territories (Dredge et al., 1995). In contrast, Early Cretaceous to early Tertiary microfossils in mudstone xenoliths, and a Rb/Sr age of 52 ± 1.2 Ma (Eocene), delimit the age of two pipes between Exeter Lake and Lac de Gras (Ward et al., 1995). These age dates have constraint the association of the isolated Buffalo Head Hills kimberlite field within the western mixed age province defined by Heaman et al. (2002), which includes the kimberlite fields in the Wyoming and Slave craton, and fits the description of a Type 3 kimberlite Province as defined by Mitchell (1986).

4.3 WEIGHTS OF EVIDENCE METHOD

4.3.1 Weights of evidence modeling approach

The location of 58 known kimberlite pipes have been used as training points to assess the degree of spatial association with each of the obtained structural lineament

datasets. The locations include 38 sites from Ashton Mining Inc. Canada, and 20 from Montello, New Claymore, and Troymin (Skelton and Bursey, 1998). The study area characterizing the region of interest was defined by a raster map (250 m cell size) covering the Buffalo Head Hills area.

In the calculation of the weights and output favourability/response map, the study area map acts as a mask. This mask enable to ignore areas of evidential themes (predictor maps defining specific thematic patterns that express structural features, geology, geophysical data etc.), and training points (the known kimberlite occurrences used to derive the predictive power of the evidential themes) located outside the study area.

In the spatial analysis each kimberlite/training point is assumed to occupy a small unit area, defining the "unit cell area". In order to calculate the probability of a point occurrence, a unit area must be selected so that the prior probability can be estimated. The prior probability that a unit cell contains a point is assumed to be constant over the study area, which using Baye's Rule gives the posterior probability that each cell contains a point (Bonham-Carter, 1994). The selected unit cell area was set at 1 km² (Bonham-Carter et al., 1988). The unit cell area is unrelated to the physical size of points, and is independent of the grid size used in the raster datasets. The values of weights are relatively independent of the unit cell area, if the unit area is small (Bonham-Carter, 1994; Kemp et al., 1999).

In the weights of evidence model the calculated weights are estimated from the measured association between known kimberlite occurrences and predictor themes using the overlap relationships of the known kimberlite points, and the classes of the theme (one weight per class). Using binary themes (thematic maps defined by two classes, i.e.

for a lineament theme, one class would define the area with lineaments, the other defines the area without lineaments) two weights are assigned, one for presence of a lineament, and one for absence of a lineament. The above hypothesis is then repeatedly evaluated for all possible locations in the study area using the calculated weights.

In the spatial analysis, a unit cell (u) of 1 km x 1 km (nominal area for kimberlite occurrences) was used. The total number of unit cells (1 km^2) containing a kimberlite is represented by $N(O)$, where $N()$ is the count of unit cells and O refers to the presence of kimberlites. Defining the total area of the region of interest as $A(T)$, where T identifies the study area map, then $N(T) = A(T)/u$ defines the total count of unit cells area in the study area map. The average density of known kimberlites in the area defines the prior probability $P(O)$ that a cell contains a kimberlite:

$$P(O) = \frac{N(O)}{N(T)}$$

The assumption that the prior probability $P(O)$ that a unit cell contains a kimberlite is constant in the whole study area is essential for the application of Bayes' Rule (Bonham-Carter, 1994), which gives the posterior probability for each cell containing a kimberlite. For a given binary map E , in which the presence of a pattern is denoted by E , and the absence of a pattern as \bar{E} , the conditional probability for the presence of a pattern will be given by:

$$P(O|E) = \frac{N(O \cap E)}{N(E)}$$

while for the pattern absent as:

$$P(O|\bar{E}) = \frac{N(O \cap \bar{E})}{N(\bar{E})}$$

Using Venn notation, $N(O \cap E)$ and $N(O \cap \bar{E})$, summarizes respectively the number of kimberlites on E present, $N(E)$, and on E absent, $N(\bar{E})$, obtained as spatial overlap relationships between kimberlite pattern O (unit cell containing kimberlite) and the map pattern present $N(E)$, and absent $N(\bar{E})$. By Baye's Rule we can express the posterior probability of a kimberlite in terms of the prior probability (Bonham-Carter, 1994) as:

$$P(O|E) = P(O) * \frac{P(E|O)}{P(E|\bar{O})}$$

It is convenient to transform the expression from probability units to logits $L()$, where logits are the natural logarithms of odds, and odds are related to probability as $OD = P/(1 - P)$. Then the loglinear form of the posterior probability, posterior logit of kimberlite per unit cell area given the E binary theme is:

$$L(O|E) = L(O) + W^+$$

if the pattern is present or:

$$L(O|\bar{E}) = L(O) + W^-$$

if the pattern is absent, where W^+ defines the positive weight of evidence as:

$$W^+ = \ln \frac{P(E|O)}{P(E|\bar{O})}$$

and W^- defines the negative weight of evidence as:

$$W^- = \ln \frac{P(\bar{E}|O)}{P(\bar{E}|\bar{O})}$$

The measure of the spatial association/correlation of binary patterns and kimberlite occurrence points has been assessed using the contrast C , defined as:

$$C = W^+ - W^-$$

which is the best estimator in a large area and when a large number of known occurrences are considered (Bonham-Carter, 1994).

The final posterior probability P_{post} for the favourability map is calculated using the conversion of odds (OD) to probability (P) as:

$$OD_{\text{post}} = \exp(\ln OD_{\text{prior}} + \sum_{j=1}^m W_j^k)$$

where k superscript identifies the sign of the weight values for the j -th pattern present (+) or absent (-), and:

$$P_{\text{post}} = OD_{\text{post}} / (1 + OD_{\text{post}})$$

The weights of evidence modeling (Spiegelhalter, 1986; Agterberg et al., 1990; Bonham-Carter et al., 1988; Bonham-Carter, 1994) applied in this paper uses the method implemented in the Arcview Geographic Information System (Arcview-GIS) package, extension Arc-WofE (Weights of Evidence) by Kemp et al.(1999).

4.3.2 Data processing and binary map generation

Binary raster predictor maps were produced for each structural dataset defined as compiled vector maps for the NNE-, NW-, NE-, and ENE-trending lineaments. First, buffer maps with cumulative distance of 5 km, with intervals at 250 m, were created and

weights were calculated to determine the best cutoff defining the best spatial relationship (specific distance) of the structural predictor theme from the kimberlites. Different interval widths were tested, and the 250 m width provided the best estimate of the cutoff distance, and enabled therefore the maximum prediction power for the lineament themes (Bonham-Carter, 1994). The cutoff distance was determined by the analysis of the contrast (C), and as can be observed in Table 4.1, a cutoff at 250 m was chosen for the NNE lineaments theme, cutoffs of 750 m were chosen for the NW lineaments (Table 4.2) and NE lineaments (Table 4.3), and a cutoff of 1.000 km was defined for the ENE lineaments theme (Table 4.4). A reclassification was then applied to create the final lineament binary maps with a buffer width of 250 m for the NNE lineaments (Figure 4.3, A), 750 m for the NW lineaments (Figure 4.3, B) and NE lineaments (Figure 4.3, C), and 1.000 km for the ENE lineaments theme (Figure 4.3, D).

The recalculated weights for the final lineament binary maps are summarized in Table 4.5. It can be observed that the strongest spatial correlations have been found for the NNE lineaments, where a very strong affinity (a total of 9 kimberlite occurrences in the region within 250 m from the NNE lineaments), is defined by the total effect of the upweighting (positive weight, $W^+ = 1.719$) and downweighting (negative weight, $W^- = -0.1404$), resulting in a maximum positive contrast (C) of 1.8590. The second strongest spatial correlation is defined for the NE lineaments, with a total of 18 kimberlites within a distance 750 m. Although the greater number of kimberlites the effect of upweighting and downweighting is diluted because of the greater number of area units (i.e., greater surface area occupied by the lineament class buffer ≤ 750 m; however, the W^+ (0.9260) indicates a strong spatial association and defines a positive C of 1.1663. The ENE

lineaments show positive spatial correlation coefficients with a total of 24 kimberlite occurrences within 1.000 km from the lineaments. The 1.0 km buffer of the ENE lineaments characterizes the maximum distance defined in the spatial correlation of kimberlite occurrences and lineaments. The least spatial correlation is found for the NW lineaments, for which 14 kimberlite occurrences lie within 0.750 km, but over a greater area units proportion if compared with the NE lineaments that are characterized by the same buffer distance.

Three additional predictor maps were integrated in the final weights of evidence model, which included the Buffalo High and Buffalo Utikuma terrane boundary (Figure 4.4, A), the average magnetic response of the Buffalo High and Buffalo Utikuma terranes (Figure 4.4, B), and the reclassified Bouguer gravity anomaly map (Figure 4.4, C). The Buffalo High and Buffalo Utikuma terrane boundary was derived from the re-definition of terrane boundaries in the Western Canadian Sedimentary Basin obtained from aeromagnetic data interpretation (Pilkington et al., 2000). The data set, in point form, was provided by Dr. M. Pilkington (Geological Survey of Canada, Ottawa) and was used to create a polyline theme to define the terrane boundary and derive the buffer zone of influence of the basement transition between the Buffalo High and Buffalo Utikuma terranes. A buffer map with cumulative width of 20 km, and intervals at 1 km, was created and weights were calculated to determine the best cutoff defining the best spatial relationship of the terrane boundary predictor theme and the kimberlites. In this case, a wavelength or buffer width of 1 km was applied in consideration of the structural importance of this major basement transition between the Buffalo High and Buffalo Utikuma terranes at regional scale within the study area. The highest C value resulted

from a class distance of 10 km (Table 4.6). This distance was used to reclassify the buffer zone in a binary map as shown in Figure 4.4 (A), whose weights attributes are summarized in Table 4.7. The Buffalo High and Buffalo Utikuma terrane boundary defines a strong predictor factor as 27 of the kimberlite occurrences lie within 10 km distance, as expressed by the combined effect of $W^+(0.9092)$ and $W^-(0.4188)$ resulting in a strong positive C (1.328).

A polygon theme was derived from the terrane boundaries (Pilkington et al., 2000) to define the Buffalo High and Buffalo Utikuma terrane extents, and create a binary theme defining the Buffalo High and Buffalo Utikuma terranes based on their average magnetic response (Table 1 in Pilkington et al., 2000). This map characterizes the geophysical basement characteristics, and their possible effect in relation to kimberlite occurrences. The average magnetic response of the Buffalo High is defined at 294 nT, while the Buffalo Utikuma is defined by 72 nT. The binary map of the Buffalo High and Buffalo Utikuma terranes average magnetic response is shown in Figure 4.4 (B), and the weights attributes are shown in Table 4.8. Most of the kimberlite occurrences are within the Buffalo Utikuma terrane (51), which is characterized by the lower magnetic response with 72 nT. The spatial association is defined by $W^+(0.3974)$, which is not particularly high because of the large unit area proportion covered by the Buffalo Utikuma terrane. However, this is compensated by a strong negative $W^-(-1.2206)$ due to very small number of kimberlites (7) present in the Buffalo High terrane, which results in a good positive C of 1.6181.

The original Bouguer gravity map of the Buffalo Head Hills has been reclassified into four main classes to create the Bouguer gravity anomaly theme as shown in Figure

4.4 (C). The original gravity data are derived from a regional airborne gravity survey with grid spacing at 4 km and were provided for this work by the Alberta Geological Survey. The dataset was resampled to a 1 km grid spacing resolution. The main characteristics observable in the Bouguer gravity theme are the northeastward termination of the Peace River Arch Bouguer gravity anomaly (Ross, 1990) in the SW portion of the study area, and the gravity high characterizing a N-S trend within the Buffalo Utikuma terrane along the Loon River valley (parallel to the Buffalo High and Utikuma terrane boundary). The latter, is probably associated with low density sediment accumulation in what has been defined as "Loon River graben" by Eccles et al. (2000). This feature extends northwards within an E-W zone, characterized by the same high gravity values, which is parallel to the Peace River in the north of the study area.

The Bouguer gravity anomaly is a multi-class predictor theme, and has not been reduced to a binary form in order to preserve the real picture of favourable or unfavourable evidence with more precision (Bonham-Carter, 1994). It also provides a representation of basement characteristics in relation to kimberlite occurrences. The relative weights and C values of the Bouguer gravity theme are shown in Table 4.9, in which each class has been identified by the central value of the Bouguer gravity range. The relative weights and C values of the Bouguer gravity theme clearly outline a strong spatial correlation with Bouguer gravity class -63 mgal (-67 to -58 mgal), in which 37 kimberlite occurrences are present. An inverse spatial correlation seems to be present with the Bouguer gravity class -46 mgal (-57 to -35 mgal), despite the occurrence of 20 kimberlites, probably due to the high area units proportion covered by this gravity class, with respect to the number of kimberlite occurrences.

Table 4.10 reports the weights of evidence for the 7 themes used for modeling the final favourability map which is shown in Figure 4.5A. A pairwise test (Bonham-Carter, 1994) using χ^2 of conditional independence (CI) between all possible pairings of the binary and multi-class predictor/theme maps has been computed to outline dependencies. The χ^2 is based on squared deviations and enables to test the statistics of pairwise frequency distributions. This method is generally applied because it does not require a distribution to be normal, bimodal, or even uni-modal (Smith, 1966). The χ^2 test is based on the number of degrees of freedom (df) assigned in the model to each theme-pair, which depends on the number of classes, excluding missing data, that occur in both evidential themes being tested, as:

$$\text{df} = (\text{number classes in theme1} - 1) \times (\text{number classes in theme2} - 1).$$

This approach results in a $\text{df} = 1$ for the binary lineament themes, Buffalo High and Buffalo Utikuma terrane boundary theme, and Buffalo High and Buffalo Utikuma terranes average magnetic theme, whereas a $\text{df} = 3$ results for the Bouguer gravity theme. Table 4.11 shows the relative df for each theme-pair, and Table 4.12 contains the χ^2 values used for testing CI between all possible pairings. The hypothesis of CI was not rejected and resulted in a $\text{CI} = 0.73$. The CI value is below 1, and therefore implies a possible dependence between theme pairings. With a probability level of 98% and $\text{df} = 1$, the tabled $\chi^2 = 5.4$ (Smith, 1966). A source of dependency is observable between the Buffalo High and Buffalo Utikuma boundary theme and the lineament binary themes, showing all χ^2 values above 5.4. This is probably induced by the composite nature of the

Buffalo High and Buffalo Utikuma boundary theme, with portions characterized by similar trend to the lineament themes. Similarly, another source of dependency can be observed between the gravity map and the ENE lineament theme, shown by a χ^2 value of 9.42, possibly induced by a ENE-trend in the transition of the gravity class -46 and -63 mgal. This could be an artifact due to the triangulation of the 4km original gravity data grid, and its reclassification.

4.4 RESULTS OF THE WEIGHTS OF EVIDENCE MODEL IN THE BUFFALO HEAD HILLS

The final favourability map for kimberlite occurrence in a 1 km² area according to structural predictor patterns and terrane characteristics is shown in Figure 4.5A. The prior probability is 0.0017 with standard deviation of 0.0002. The posterior probabilities were classified in five classes. Values less than or equal to 0.048 were considered as background values (unfavourable), whereas values above 0.048 characterize combined evidence that is favourable for kimberlite occurrences.

The ranking of regions by posterior probability defines a favourability map that is based on a statistical model assuming that the known kimberlites are an adequate sample of kimberlites in the region. The final kimberlite potential is obviously a reflection of the quality and quantity of the original input data. Most of the known kimberlite occurrences in the central Buffalo Head Hills have been predicted, showing that the model is well constrained in this area by the higher data input and distribution, especially in relation to

the lineament density, and the role of the geological/geophysical boundary of the Buffalo High and Buffalo Utikuma terrane. This boundary, is parallel to the east-facing scarp of the Buffalo Head Hills, and intersects its SE-corner, where most of the known kimberlites are located. The poor prediction observed in the southern portion of the Buffalo Head Hills study area, Loon River Valley, and Peerless Uplands is probably due to the lower density of lineaments and kimberlite occurrences in these areas.

From the favourability map draped on the basement Digital Elevation Model (DEM), gravity field, and the boundary of the Buffalo High and Buffalo Utikuma terranes shown in Figure 4.5B, it is clear that the predicted potential kimberlite areas are, with few exceptions, all located in the Buffalo Utikuma terrane, but very close to its boundary with the Buffalo High terrane. In general, they show an approximately N-S trend, which derives from the high correlation with the NNE-trending lineaments and intersections with the NE- and ENE-trending lineaments.

The use of the basement DEM (derived from a subset of 871 picks of the Precambrian basement surface from oil wells, with average grid spacing of 8 km, compiled by the Alberta Energy and Utility Board, and resample to a 1 km grid spacing resolution) reveals important characteristics of the Buffalo High and Buffalo Utikuma terranes, such as the dome defining the northeastwards termination of the Peace River Arch in the Buffalo High terrane, and the dome with NE-SW trend defining the central portion of the Buffalo Utikuma terrane. In the southeast flank of the Buffalo Utikuma terrane dome, known kimberlite occurrences trace a NE-SW trend, but few favourability areas occur in this section. The NE-SW lineaments from RADARSAT-PC2, integrated with the model (Figure 4.5B), mirror this NE-SW dome structure defined in the Buffalo

Utikuma terrane. Although aeromagnetic data are not complete for this area, a magnetic low characterizes the area in which the Buffalo Utikuma terrane indents the Buffalo High terrane, showing a possible basement anomaly with NE-SW trend (Figure 4.6).

4.5 DISCUSSION AND CONCLUSIONS

The kimberlitic magmatism in the Buffalo Head Hills occurred during the Late Cretaceous, which suggests a possible relationship between extensional ENE-trending lineaments (Late Cretaceous), and their intersection with deep-seated basement faults, and kimberlite emplacement in the upper crust. This hypothesis has been supported by a statistical model which outlines the occurrence of favourable areas for kimberlite exploration as mainly defined along the Buffalo High and Buffalo Utikuma terrane boundary. This boundary parallels a set of NNE-trending lineaments, and kimberlite favourability areas occur at the intersection of NNE, NE, and ENE lineaments. The Buffalo High and Buffalo Utikuma terrane boundary defines a magnetic susceptibility contrast between the two terranes and a deep-seated basement discontinuity in the Buffalo Head Hills area. This geological context is similar to the association of basement shear zones characterized by low magnetic susceptibility, intersecting ENE-WSW and E-W lineaments, and kimberlite occurrences showing a conspicuous ENE-WSW, and E-W orientation, illustrated by Sarma and Verma (2001) in the Wajrakarur kimberlite field (India).

The aeromagnetic data reported in Figure 4.6, indicate a low magnetic susceptibility zone along the transition between the Buffalo High and Buffalo Utikuma terranes. Speculatively, a magnetic low could be defined along a NE-SW trend, which is parallel to the dome structure observed in the basement DEM (Figure 4.5B). However, due to the lack of a complete aeromagnetic data coverage in the NE portion of the Buffalo Head Hills this hypothesis will remain to be proven. The basement dome structure is mirrored by NE-SW lineaments, and characterizes a kimberlite occurrence trend in this sector of the Buffalo Head Hills area. In this area, a more accurate and complete definition of the Buffalo Utikuma terrane provided by aeromagnetic data would probably introduce additional predictive constraints in the statistical model, which would enable a more complete picture of the kimberlite potential where the prediction model seems poor.

The statistical approach of weights of evidence method enabled the quantitatively characterization of the degree of spatial relationship between structural lineaments and kimberlite locations, which shows a higher correlation with the NNE-trending lineaments, followed by the NE, ENE, and NW trends. The integration of the derived predictor lineament maps with the Buffalo High and Utikuma terrane boundary, and their magnetic and gravity characteristics, enabled the development of a suitable favourability map for kimberlite exploration. This statistical model outlines higher favourability within the Buffalo Utikuma terrane and along the major basement discontinuity between the Buffalo High and Buffalo Utikuma terranes.

The favourability areas are mainly located along a N-S trend, which reflects the predominant spatial correlation with the Buffalo High and Utikuma terrane boundary, the

parallel strike of the NNE-trending lineaments, and intersections with the NE- and ENE-trending lineaments.

Within the Buffalo Head study area the transition between the Buffalo High and Buffalo Utikuma terranes divides the area into two different domains. This boundary roughly underlies the eastern edge of the Buffalo Head Hills throughout the area. From the structural data analysis (Paganelli et al., 2001b) and its spatial correlation with kimberlite occurrences as analyzed in the weights of evidence model, this terrane transition is a key element in the formulation of a kimberlite emplacement model for the area.

Although the formulation of a kimberlite emplacement model is not in the objective of this paper, the structural element characterizing the Buffalo High and Buffalo Utikuma terranes boundary defines an important zone of weakness at the upper crustal level, and as shown by the prediction model, a locus and favourable corridor for the final stage of kimberlite emplacement whose source material derives from mantle depths.

REFERENCES

- Agterberg, F.P. (1989). Systematic approach to dealing with uncertainty of geoscience information in mineral exploration. *Proceedings of the 21st Symposium on the Application of Computers in the Mineral Industries*, Las Vegas, pp. 165-178.
- Agterberg, F.P., Bonham-Carter, G.F. and Wright, D.F. (1990). Statistical pattern integration for mineral exploration. In: *Computer Applications in Resource Estimation Prediction and Assessment for Metals and Petroleum*. Editors: Gaál, G. and Merriam, D.F., Pergamon Press, Oxford, pp.1-21.
- Bonham-Carter, G.F. (1994). *Geographic Information Systems for Geoscientists: Modeling with GIS*. Pergamon Press, Oxford.
- Bonham-Carter, G.F., Agterberg, F.P., and Wright, D.F. (1988). Interpretation of Geological datasets for gold exploration in Nova Scotia. *Photogrammetric Engineering and Remote Sensing*, Vol. 54, No. 11, pp. 1585-1592.
- Bonham-Carter, G.F., Agterberg, F.P., and Wright, D.F. (1989). Weights of evidence modeling: a new approach to mapping mineral potential. In: Agterberg F.P. and Bonham-Carter G.F. Eds. *Statistical Applications in Earth Sciences*, pp. 171-183. Geological Survey of Canada Paper 89-9.
- Burgess, P., Gurnis, M., Moresi, L. (1997). Formation of sequences in the cratonic interior of North America by interaction between mantle, eustatic, and stratigraphic processes. *Geological Society of America Bulletin*, Vol. 108, No. 12, pp. 1151-1535.
- Cant, D.J. (1988). Regional structure and development of the Peace River Arch, Alberta: a Paleozoic failed-rift system? *Bulletin of Canadian Petroleum Geology*, Vol. 36, pp. 284-295.
- Carlson, S.M., Hillier, H.D., Hood, C.T., Pryde, R.P., and Skelton, D.N. (1998). The Buffalo Head Hills kimberlite province, north central Alberta, Canada. In: *Seventh International Kimberlite Conference: Extended Abstracts*. Cape Town, April 1998, pp. 138-140.
- Chen, D. and Bergman, K.M. (1999). Stratal reorientation, depositional processes, and sequence evolution of the Cretaceous in the Peace River Arch region of the Western Canada Sedimentary Basin. *Bulletin of Canadian Petroleum Geology*, Vol. 47, No. 4, pp. 594-620.
- Dredge, L.A., Kjarsgaard, I.M., Ward, B.C., Kerr, D.E., Stirling, J.A.R. (1995). Distribution and chemistry of kimberlite indicator minerals, Aylmer Lake map area (76C), Northwest Territories. Geological Survey of Canada, Open File 3080.
- Eccles, D.R., Grunsky, E.C., Grobe, M. and Weiss, J. (2000). *Structural emplacement model for kimberlitic diatremes in northern Alberta*. Report, Alberta Energy and Utilities Board, Alberta Geological Survey, March 2000, p. 116. (in press).
- Edwards, D.J., Lyatsky, H.V. and Brown, R.J. (1995). Basement fault control on Phanerozoic stratigraphy in the Western Canada Sedimentary Province; integration

- of potential-field and lithostratigraphic data. In: G.M. Ross Ed., *Alberta Basement Transects Workshop, Lithoprobe Report 47*, pp. 181-224.
- Grunsky, E.C. (2001). The Application of Principal Components Analysis to Multi-beam RADARSAT-1 Satellite Imagery – A Tool for Terrain Mapping. *Canadian Journal of Remote Sensing*, (in press).
- Kemp, L.D., Bonham-Carter, G.F. and Raines, G.L.(1999). Arc-WofE: Arcview extension for weights of evidence mapping. <http://ntserv.gis.nrcan.gc.ca/wofe> (October 2001).
- Leckie, D.A., Kjarsgaard, B.A., Pierce, J.W., Grist, A.M., Collins, A., Sweet, A., Stasiuk, L., Tomica, M.A., Eccles, R., Dufresne, M., Fenton, M.M., Pawlowicz, J.G., Blazer, S.A., McIntyre, D., McNeil D. (1997a). Geology of Late Cretaceous possible kimberlite at Mountain Lake, Alberta – Chemistry, petrology, indicator minerals, aeromagnetic signature, age, stratigraphic position and setting. Geological Survey of Canada, Open File 3441.
- Leckie, D.A., Kjarsgaard, B.A., and Bloch, J., McIntyre, D., McNeil D., Stasiuk, L., Heaman, L. (1997b). Emplacement and reworking of Cretaceous, diamond-bearing, crater facies kimberlite of central Saskatchewan, Canada. *Geological Society of America Bulletin*, Vol. 109, No. 8, pp. 1000-1020.
- Lemieux, S. (1999). Seismic reflection expression and tectonic significance of the Late Cretaceous extensional faulting of the Western Canada Sedimentary Basin in Southern Alberta. *Bulletin of Canadian Petroleum Geology*, Vol. 47, No. 4, pp. 375-390.
- Lenhert-Thiel, K., Loewer, R., Orr, R.G., and Robertshaw, P. (1992). Diamond-bearing kimberlites in Saskatchewan, Canada: The Fort à la Corne case history. *Exploration and Mining Geology*, Vol. 1, pp. 391-403.
- Mitchell, R.H. (1986). *Kimberlites*. Plenum Press, New York.
- Mitchell, R.H. (1995). *Kimberlites, Orogeneites and Related Rocks*. Plenum Press, New York.
- O'Connell, S.C., Dix, G.R. and Barclay, J.E. (1990). The origin, history and regional structural development of the Peace River Arch, Western Canada. *Bulletin of Canadian Petroleum Geology*, Vol. 38A, pp. 4-24.
- Paganelli, F. and Rivard, B. (2001). Contribution of the synergy of RADARSAT-1 and seismic imagery interpretation in the structural geology of the Central Alberta Foothills, Canada, as aid for oil and gas exploration. *Canadian Journal of Remote Sensing* (in press).
- Paganelli, F., Grunsky, E.C., and Richards, J.P (2001a). Structural interpretation of RADARSAT-1 Principal Component imagery and its potential application to kimberlite exploration in the Buffalo Head Hills area, Northern Central Alberta. Alberta Geological Survey, Earth Science Report 2001-03. Edmonton, Alberta, Canada: Alberta Energy and Utilities Board, (in press).

- Paganelli, F., Grunsky, E.C., and Richards, J.P. (2001b). Use of RADARSAT-1 Principal Component imagery for structural mapping: a case study in the Buffalo Head Hills area, northern central Alberta, Canada. *Canadian Journal of Remote Sensing*, (in press).
- Pilkington, M., Miles, W.F., Ross, G.M., and Roest, W.R. (2000). Potential-field signatures of buried Precambrian basement in the Western Canada Sedimentary Basin. *Canadian Journal of Earth Sciences*, Vol. 37, pp. 1453-1471.
- Ross, G.M. (1990). Deep crust and basement structure of the Peace River Arch: constraints on mechanism of formation. *Bulletin of Canadian Petroleum Geology*, Vol. 38A, pp. 25-35.
- Ross, G.M., Parrish, R.R., Villeneuve, M.E., and Bowring, S.A. (1991). Geophysics and geochronology of the crystalline basement of the Alberta Basin, Western Canada. *Canadian Journal of Earth Sciences*, Vol. 28, pp. 512-522.
- Ross, G.M., Eaton, D.W. (1999). Basement reactivation in the Alberta Basin: Observational constraints and mechanical rationale. *Bulletin of Canadian Petroleum Geology*, Vol. 47, No. 4, pp. 391-411.
- Sarma, B.S.P. and Verna, B.K. (2001). Aeromagnetic lineaments, basement structure and kimberlite emplacement in Andhra Pradesh, India. *Geophysical Research Letters*, Vol. 28, No. 22, pp. 4307-4310.
- Skelton, D. and Bursey, T. (1998). *Assessment Report, Buffalo Head Hills Property (AL01)*. Ashton Mining of Canada Inc., p. 16.
- Smith, F.G. (1966). *Geological Data Processing*. Harper and Row, New York.
- Sobolev, N.V., Lavrentiev, Yu.G., Pokhilenko, N.P. and Usovo L.V. (1973). Chrome-rich garnets from the kimberlite of Yakutia and their paragenesis. *Contribution Mineralogy and Petrology*, Vol. 40, pp. 39-52.
- Spiegelhalter, D.J. (1986). Uncertainty in expert systems. In: *Artificial Intelligence and Statistics*, Editor: Gale, W.A., Addison-Wesley, Reading, Massachusetts, pp. 17-55.
- Tangestani, M.H. and Moore, F. (2001). Porphyry copper potential mapping using the weights of evidence model in a GIS, northern Shahr-e-Babak, Iran. *Australian Journal of Earth Sciences*, Vol. 48, No. 22, pp. 695-701.
- Theriault, R.J. and Ross, G.M. (1991). Nd isotopic evidence for crustal recycling in the ca.2.0 Ga subsurface of western Canada. *Canadian Journal of Earth Sciences*, Vol. 28, pp. 1140-1147.
- Villeneuve, M.E., Ross, G.G., Parrish, R.R., Theriault, R.J., Miles, W., and Broome, J. (1993). Geophysical subdivision, U-Pb geochronology and Sm-Nd isotope geochemistry of the crystalline basement of the Western Canadian Sedimentary Basin, Alberta and Northeastern British Columbia. Geological Survey of Canada, Bulletin 447.
- Ward, BC., Kjarsgaard, I.M., Dredge, L.A., Kerr, D.E., Stirling, J.A.R. (1995). Distribution and chemistry of kimberlite indicator minerals, Lac de Gras map area (76D), Northwest Territories. Geological Survey of Canada, Open File 3080.

- Watson, G.P., Rencz, A.N, and Bonham-Carter, G.F. (1989). Computers assist prospecting, *Geostationary Operational Environmental Satellites - GOES*, Vol. 18, No. 1, pp. 8-15.
- Wright, D.F. and Bonham-Carter, G.F. (1996). VHMS favourability mapping with GIS-based integration models, Chisel Lake-Anderson Lake area. In: Bonham-Carter G.F., Galley A.G. and Hall G.E. Eds. *EXTECHI: A Multidisciplinary Approach to Massive Sulfide research in the Rusty Lake-Snow Lake Greenstone Belts*, Manitoba, pp. 339-376. Geological Survey of Canada, Bulletin 426.
- Woodzick, T.L. and Mc Callum, M.E. (1982). A teledetective study of kimberlite regions in North America Colorado-Wyoming), East Africa (Mwadui) and Siberia (MIR). In: J. Kornprobst Ed., *Third International Kimberlite Conference*, Vol.1, pp. 5-19.

Table 4.1. Summary of RADARSAT-1-PC NNE total lineaments weights at variable distance from kimberlite locations.

CLASS DISTANCE [km]	AREA SQ KM	AREA UNITS	NO_POINTS	W+	W-	C	STUDENTIZED C [C/S(C)]
0.250	980.5625	980.5625	9	1.0652	-0.1206	1.1858	3.2401
0.500	926.3750	926.3750	4	0.3062	-0.0205	0.3267	0.6278
0.750	948.5625	948.5625	4	0.2824	-0.0191	0.3015	0.5795
1.000	961.2500	961.2500	2	-0.4262	0.0203	-0.4464	-0.6191
1.250	970.8750	970.8750	4	0.2591	-0.0177	0.2768	0.5320
1.500	959.5000	959.5000	2	-0.4243	0.0201	-0.4445	-0.6164
1.750	937.5000	937.5000	4	0.2942	-0.0198	0.3140	0.6035
2.000	927.7500	927.7500	1	-1.0848	0.0370	-1.1218	-1.1109
2.250	920.0000	920.0000	1	-1.0764	0.0365	-1.1129	-1.1021
2.500	909.0625	909.0625	5	0.5494	-0.0414	0.5908	1.2562
2.750	895.5625	895.5625	3	0.0514	-0.0029	0.0542	0.0912
3.000	875.5625	875.5625	1	-1.0269	0.0338	-1.0606	-1.0503
3.250	855.1250	855.1250	4	0.3866	-0.0248	0.4114	0.7905
3.500	842.9375	842.9375	0				
3.750	811.6875	811.6875	3	0.1500	-0.0080	0.1581	0.2657
4.000	776.7500	776.7500	0				
4.250	740.3750	740.3750	2	-0.1645	0.0068	-0.1712	-0.2374
4.500	713.8125	713.8125	3	0.2790	-0.0140	0.2930	0.4924
4.750	678.5625	678.5625	3	0.3299	-0.0161	0.3460	0.5814
5.000	649.2500	649.2500	0				
> 5.000	17694.5000	17694.5000	3				

Table 4.2. Summary of RADARSAT-1-PC NW total lineaments weights at variable distance from kimberlite locations.

CLASS DISTANCE [km]	AREA SQ KM	AREA UNITS	NO_POINTS	W+	W-	C	STUDENTIZED C [C/S(C)]
0.250	1843.7500	1843.7500	3	-0.2819	0.0201	-0.3020	-0.5074
0.500	1713.5000	1713.5000	4	0.0798	-0.0064	0.0861	0.1653
0.750	1672.1875	1672.1875	7	0.6656	-0.0729	0.7385	1.8141
1.000	1667.3125	1667.3125	4	0.1071	-0.0084	0.1156	0.2218
1.250	1636.7500	1636.7500	4	0.1257	-0.0098	0.1355	0.2600
1.500	1601.9375	1601.9375	5	0.3710	-0.0324	0.4035	0.8564
1.750	1523.3125	1523.3125	3	-0.0906	0.0058	-0.0965	-0.1620
2.000	1407.5000	1407.5000	4	0.2770	-0.0200	0.2969	0.5698
2.250	1322.7500	1322.7500	2	-0.3554	0.0172	-0.3726	-0.5163
2.500	1224.5000	1224.5000	4	0.4167	-0.0280	0.4447	0.8531
2.750	1137.9375	1137.9375	2	-0.2047	0.0091	-0.2138	-0.2962
3.000	1060.4375	1060.4375	0				
3.250	997.2500	997.2500	0				
3.500	932.3750	932.3750	0				
3.750	861.8125	861.8125	1	-0.6205	0.0170	-0.6375	-0.6309
4.000	804.3125	804.3125	3	0.5498	-0.0256	0.5753	0.9656
4.250	752.3750	752.3750	3	0.6168	-0.0278	0.6446	1.0817
4.500	697.2500	697.2500	2	0.2863	-0.0099	0.2962	0.4102
4.750	653.5000	653.5000	0				
5.000	609.6875	609.6875	1	-0.2739	0.0062	-0.2801	-0.2772
> 5.000	10855.1250	10855.1250	6				

Table 4.3. Summary of RADARSAT-1-PC NE total lineaments weights at variable distance from kimberlite locations.

CLASS DISTANCE [km]	AREA_SQ_KM	AREA_UNITS	NO_POINTS	W+	W-	C	STUDENTIZED C [C/S(C)]
0.250	1596.4375	1596.4375	7	0.6936	-0.1104	0.8040	1.9116
0.500	1394.5000	1394.5000	4	0.2677	-0.0281	0.2958	0.5579
0.750	1319.9375	1319.9375	7	0.8847	-0.1284	1.0131	2.4079
1.000	1240.0000	1240.0000	5	0.6094	-0.0689	0.6783	1.4079
1.250	1151.5625	1151.5625	3	0.1712	-0.0138	0.1849	0.3067
1.500	1077.7500	1077.7500	2	-0.1688	0.0106	-0.1794	-0.2465
1.750	997.2500	997.2500	0				
2.000	922.4375	922.4375	1	-0.7071	0.0290	-0.7361	-0.7257
2.250	853.8125	853.8125	0				
2.500	793.1875	793.1875	4	0.8341	-0.0663	0.9004	1.6967
2.750	754.8750	754.8750	2	0.1881	-0.0097	0.1978	0.2717
3.000	689.3125	689.3125	0				
3.250	632.3125	632.3125	0				
3.500	575.6875	575.6875	0				
3.750	541.3125	541.3125	0				
4.000	508.6250	508.6250	0				
4.250	482.8125	482.8125	0				
4.500	464.0000	464.0000	0				
4.750	439.3750	439.3750	2	0.7312	-0.0292	0.7604	1.0436
5.000	411.8750	411.8750	0				
> 5.000	18128.5000	18128.5000	21				

Table 4.4. Summary of RADARSAT-1-PC ENE total lineaments weights at variable distance from kimberlite locations.

CLASS DISTANCE [km]	AREA_SQ_KM	AREA_UNITS	NO_POINTS	W+	W-	C	STUDENTIZED C [C/S(C)]
0.250	2427.8125	2427.8125	3	-0.5313	0.0527	-0.5839	-0.9757
0.500	2140.9375	2140.9375	8	0.5778	-0.0931	0.6709	1.7134
0.750	2028.8125	2028.8125	4	-0.0633	0.0066	-0.0699	-0.1331
1.000	1889.5625	1889.5625	9	0.8215	-0.1346	0.9561	2.5529
1.250	1694.5625	1694.5625	4	0.1171	-0.0110	0.1281	0.2440
1.500	1495.6875	1495.6875	4	0.2423	-0.0213	0.2635	0.5019
1.750	1332.0625	1332.0625	6	0.7654	-0.0811	0.8465	1.9229
2.000	1176.9375	1176.9375	3	0.1941	-0.0128	0.2069	0.3456
2.250	1029.3750	1029.3750	0				
2.500	853.6250	853.6250	0				
2.750	754.5000	754.5000	0				
3.000	667.0000	667.0000	0				
3.250	590.2500	590.2500	1	-0.2152	0.0056	-0.2208	-0.2181
3.500	530.4375	530.4375	0				
3.750	497.5625	497.5625	1	-0.0441	0.0010	-0.0451	-0.0446
4.000	458.6875	458.6875	0				
4.250	403.6250	403.6250	0				
4.500	361.6250	361.6250	1	0.2758	-0.0056	0.2814	0.2778
4.750	329.0625	329.0625	0				
5.000	288.2500	288.2500	0				
> 5000	14025.1875	14025.1875	14				

Table 4.5. Summary of weights of the RADARSAT-1-PC lineaments for modeling posterior probability of a kimberlite occurring in a 1 km² area.

LINEAMENTS	CLASS DISTANCE [km]	AREA SQ_KM	AREA UNITS	NO_POINTS	W+	W-	C	STUDENTIZED C [C/S(C)]
NNE	0.250	980.5625	980.5625	9	1.7186	-0.1404	1.8590	5.1056
NW	0.750	5229.4375	5229.4375	14	0.4800	-0.1145	0.5945	1.9350
NE	0.750	4310.8750	4310.8750	18	0.9260	-0.2404	1.1663	4.1026
ENE	1.000	8487.1250	8487.1250	24	0.5349	-0.2565	0.7914	2.9652

Table 4.6. Summary of the Buffalo High and Buffalo Utikuma terranes boundary weights at variable distance from kimberlite locations.

CLASS DISTANCE [km]	AREA SQ_KM	AREA UNITS	NO_POINTS	W+	W-	C	STUDENTIZED C [C/S(C)]
1	657.5625	657.5625	2	0.0102	-0.0005	0.0108	0.0148
2	656.1250	656.1250	1	-0.6823	0.0261	-0.7083	-0.6986
3	657.6875	657.6875	0				
4	656.3750	656.3750	2	0.0120	-0.0006	0.0127	0.0174
5	659.1875	659.1875	0				
6	658.1250	658.1250	5	0.9302	-0.0853	1.0155	2.1129
7	657.1875	657.1875	1	-0.6839	0.0262	-0.7100	-0.7003
8	658.4375	658.4375	3	0.4159	-0.0280	0.4438	0.7370
9	657.1875	657.1875	1	-0.6839	0.0262	-0.7100	-0.7003
10	657.1875	657.1875	12	1.8179	-0.3165	2.1344	6.1108
11	656.2500	656.2500	5	0.9331	-0.0855	1.0186	2.1191
12	654.9375	654.9375	2	0.0142	-0.0008	0.0150	0.0206
13	650.1250	650.1250	1	-0.6731	0.0256	-0.6986	-0.6891
14	645.5000	645.5000	1	-0.6659	0.0252	-0.6911	-0.6817
15	639.6875	639.6875	1	-0.6568	0.0247	-0.6816	-0.6723
16	636.1875	636.1875	1	-0.6513	0.0245	-0.6758	-0.6665
17	630.8125	630.8125	0				
18	625.0625	625.0625	1	-0.6337	0.0236	-0.6572	-0.6482
19	621.8750	621.8750	0				
20	618.3750	618.3750	0				
>20	22021.6875	22021.6875	19				

Table 4.7. Weights of the Buffalo High and Buffalo Utikuma terrane boundary reclassified binary theme used in the weights of evidence model.

BH/BU boundary [km]	AREA SQ_KM	AREA UNITS	NO_POINTS	W+	W-	C	STUDENTIZED C [C/S(C)]
10	6575.0625	6575.0625	27	0.9092	-0.4188	1.3280	5.0380
> 10	28400.5000	28400.5000	31	-0.4188	0.9092	-1.3280	-5.0380

Table 4.8. Weights of the Buffalo High and Buffalo Utikuma terrane magnetic signature for modeling posterior probability of a kimberlite occurring in a 1 km² area.

BH/BU magnetic [nT]		AREA_SQ_KM	AREA_UNITS	NO_POINTS	W+	W-	C	STUDENTIZED C [C/s(C)]
BU	72	20595.9375	20595.9375	51	0.3974	-1.2206	1.6181	4.0129
BH	294	14228.5000	14228.5000	7	-1.2206	0.3974	-1.6181	-4.0129

Table 4.9. Weights of the Bouguer gravity anomaly for modeling posterior probability of a kimberlite occurring in a 1 km² area.

Bouguer gravity [mgal]		AREA_SQ_KM	AREA_UNITS	NO_POINTS	W+	W-	C	STUDENTIZED C [C/s(C)]
[-97 to -78]	-88	1358.8750	1358.8750	0				
[-77 to -68]	-73	4237.3750	4237.3750	1	-1.9545	0.1124	-2.0669	-2.0488
[-67 to -58]	-63	15810.7500	15810.7500	37	0.3418	-0.4121	0.7539	2.7572
[-57 to -35]	-46	13451.5625	13451.5625	20	-0.1127	0.0648	-0.1775	-0.6421

Table 4.10. Weights for modeling posterior probability of a kimberlite occurring in a 1 km² area.

THEME		AREA_SQ_KM	AREA_UNITS	NO_POINTS	W+	W-	C	STUDENTIZED C [C/s(C)]
NNE lineaments (0.25 km)		980.5625	980.5625	9	1.7186	-0.1404	1.8590	5.1056
NW lineaments (0.75 km)		5229.4375	5229.4375	14	0.4800	-0.1145	0.5945	1.9350
NE lineaments (0.75 km)		4310.8750	4310.8750	18	0.9260	-0.2404	1.1663	4.1026
ENE lineaments (1.0 km)		8487.1250	8487.1250	24	0.5349	-0.2565	0.7914	2.9652
BH-BU boundary (10 km)		6575.0625	6575.0625	27	0.9092	-0.4188	1.3280	5.0380
BH/BU magnetic [nT]								
	BU 72	20595.9375	20595.9375	51	0.3974	-1.2206	1.6181	4.0129
	BH 294	14228.5000	14228.5000	7	-1.2206	0.3974	-1.6181	-4.0129
Bouguer gravity [mgal]								
	-88	1358.8750	1358.8750	0				
	-73	4237.3750	4237.3750	1	-1.9545	0.1124	-2.0669	-2.0488
	-63	15810.7500	15810.7500	37	0.3418	-0.4121	0.7539	2.7572
	-46	13451.5625	13451.5625	20	-0.1127	0.0648	-0.1775	-0.6421

Table 4.11. Table of degree of freedom between all pairs of 7 binary and multi-class themes assigned in the weights of evidence model.

ETHEME	BH_BFPCNWT	BH_BFPCNET	BH_BFPCENET	BH_BFBHBU	BH_BU	GRAVITY_BH
Bh-bfpcnnet	1	1	1	1	1	3
Bh-bfpcnwt		1	1	1	1	3
Bh-bfpcnet			1	1	1	3
Bh-bfpcenet				1	1	3
Bh-bfbhbu					1	3
Bh-bu						3

Table 4.12. χ^2 values for testing conditional independence between all pairs of 7 binary and multi-class themes of the weights of evidence model.

THEME	BH_BFPCNWT	BH_BFPCNET	BH_BFPCENET	BH_BFBHBU	BH_BU	GRAVITY_BH
Bh-bfpcnnet	0.32	4.50	0.03	5.79	0.43	3.41
Bh-bfpcnwt		3.56	2.84	6.11	1.26	0.33
Bh-bfpcnet			0.07	5.50	0.34	0.96
Bh-bfpcenet				6.24	1.31	9.42
Bh-bfbhbu					1.01	2.09
Bh-bu						3.35

Figure 4.1. Buffalo Head Hills study area and NTS coverage. GSLSZ, Great Slave Lake Shear Zone; STZ, Snowbird Tectonic Zone. The inset shows the Precambrian basement terrane boundaries (after Pilkington et al., 2000).

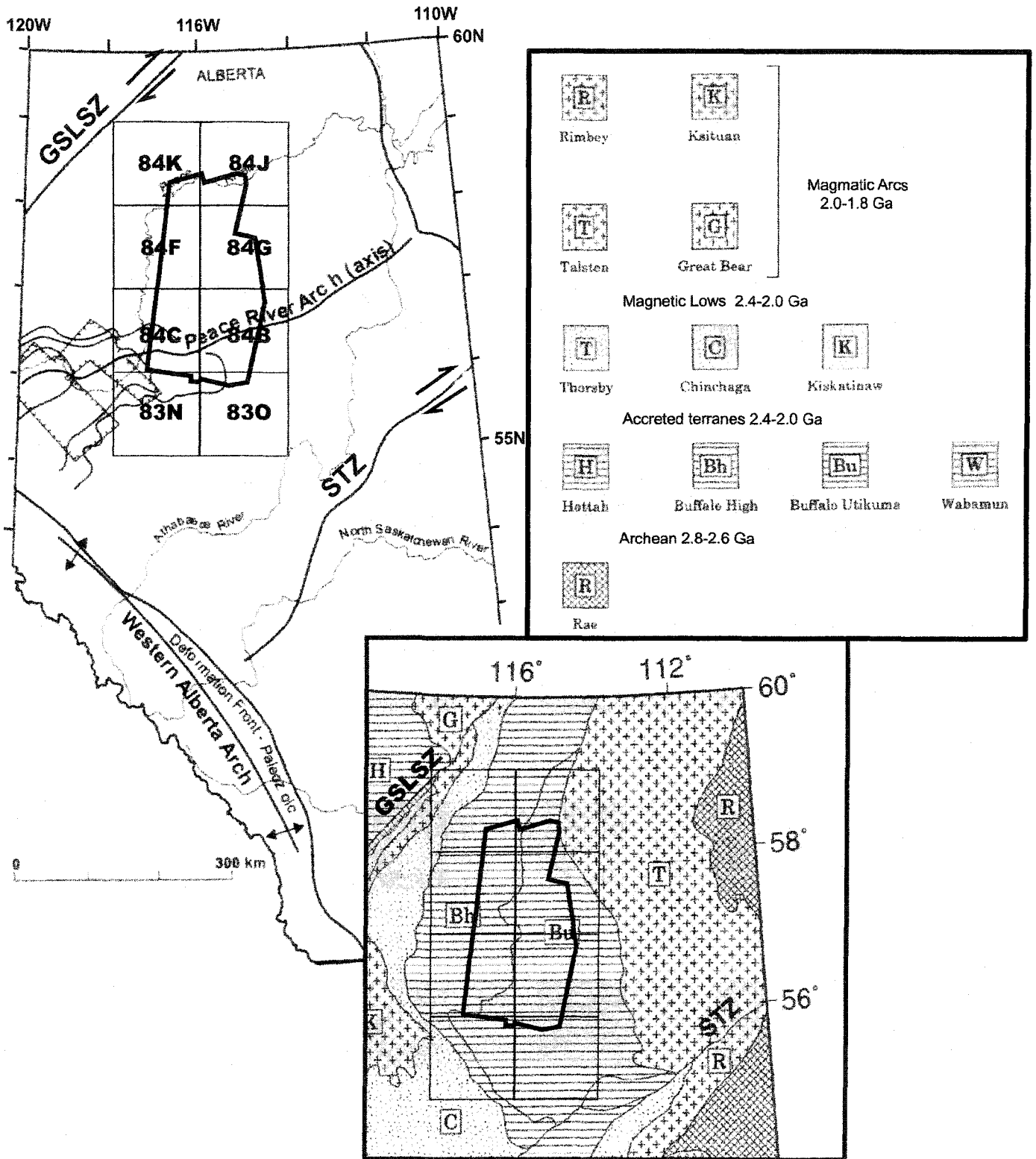


Figure 4.2. Buffalo Head Hills geology and kimberlite locations: K1, Loon River Formation (Lower Cretaceous); Kp, Peace River Group (Lower Cretaceous); Ksh, Shaftesbury Formation (Lower-Upper Cretaceous); Kd, Dunvegan Formation (Upper Cretaceous); Ks, Smoky Group (Upper Cretaceous); kimberlite, black circles.

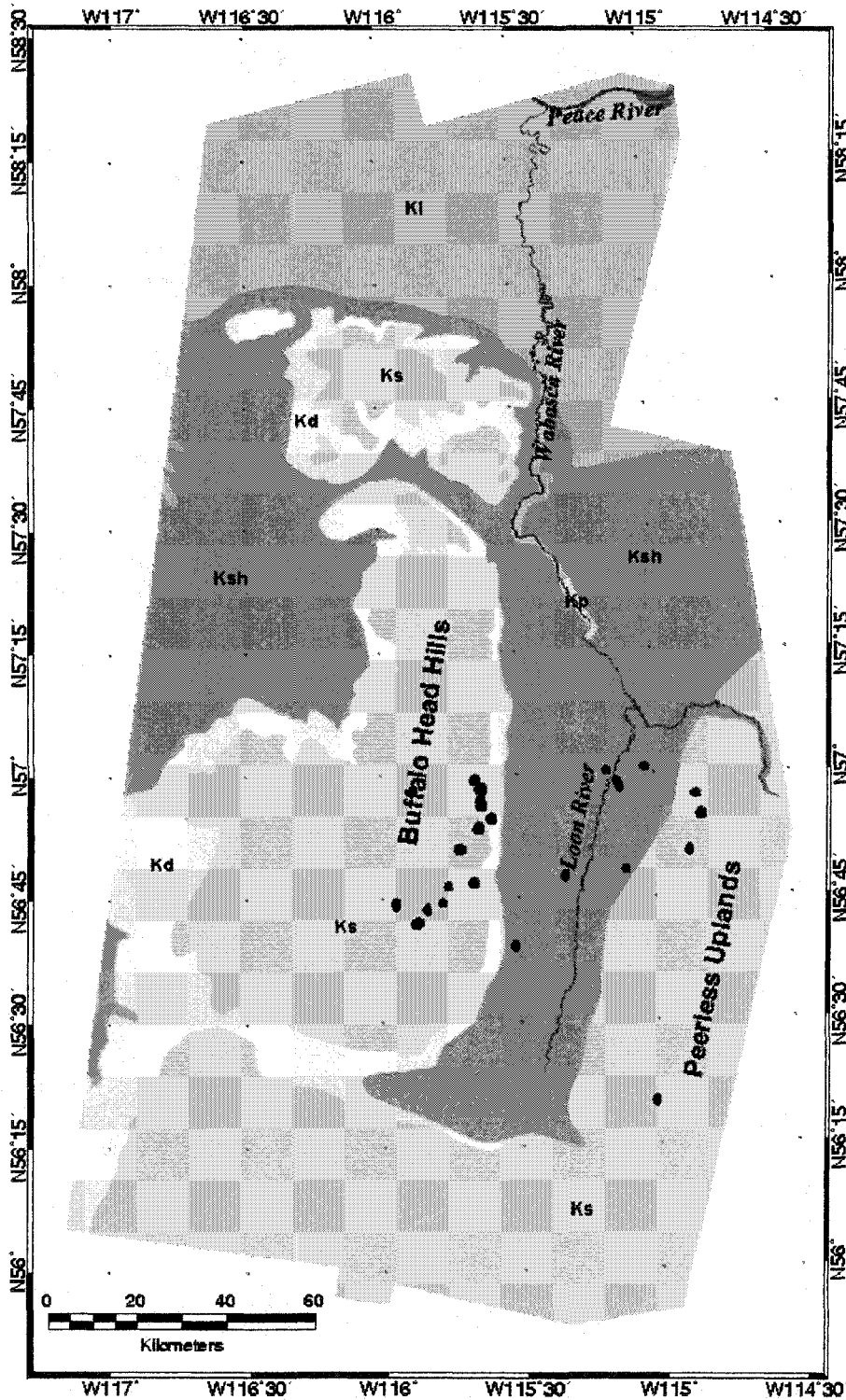
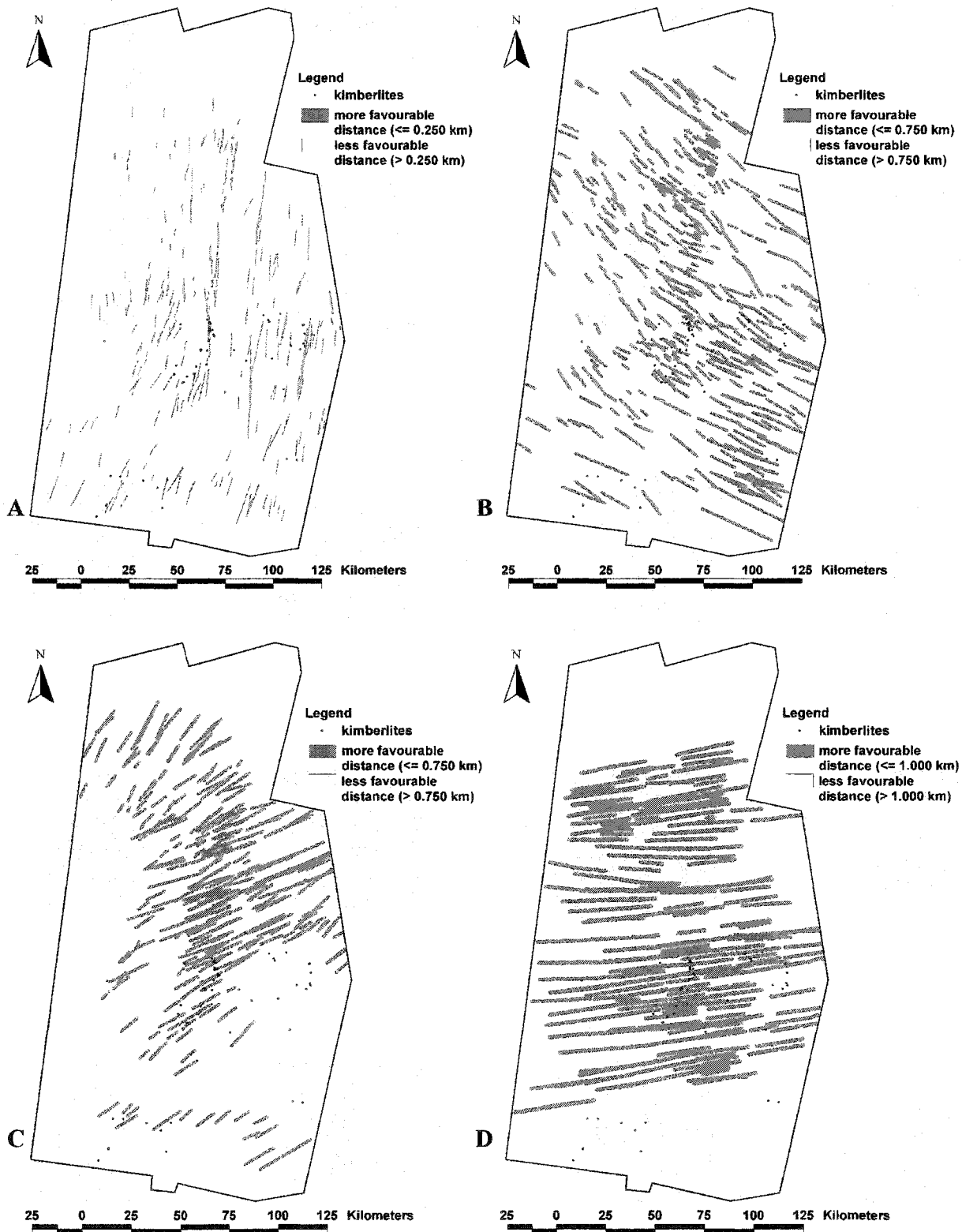


Figure 4.3. Lineament binary maps used in weights of evidence modeling: **A)** NNE lineaments; **B)** NW lineaments; **C)** NE lineaments; **D)** ENE lineaments.



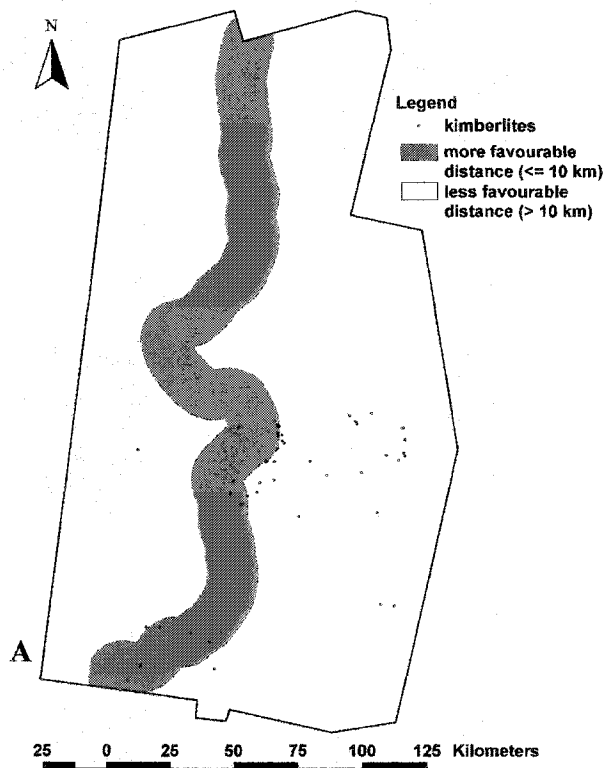


Figure 4.4. Additional predictor binary themes used in weights of evidence modeling: **A)** Buffalo High and Buffalo Utikuma terrane contact binary theme; **B)** Buffalo High and Buffalo Utikuma terranes average magnetic response; **C)** Buffalo Head Hills Bouguer gravity.

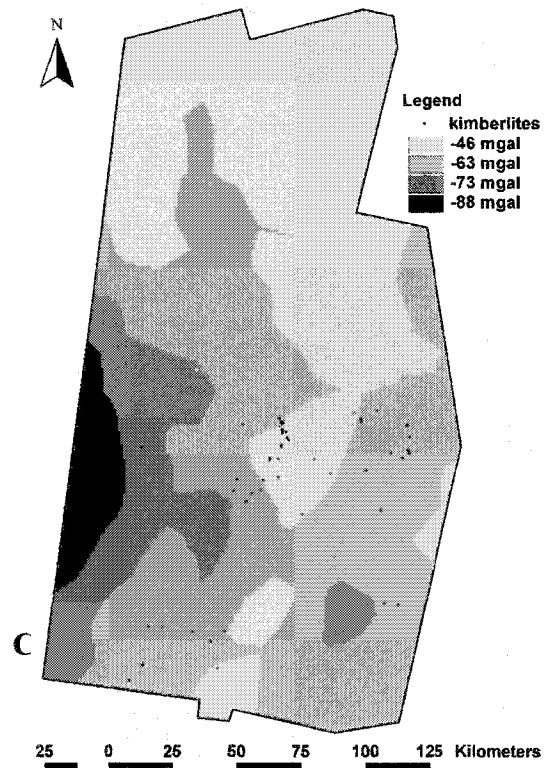
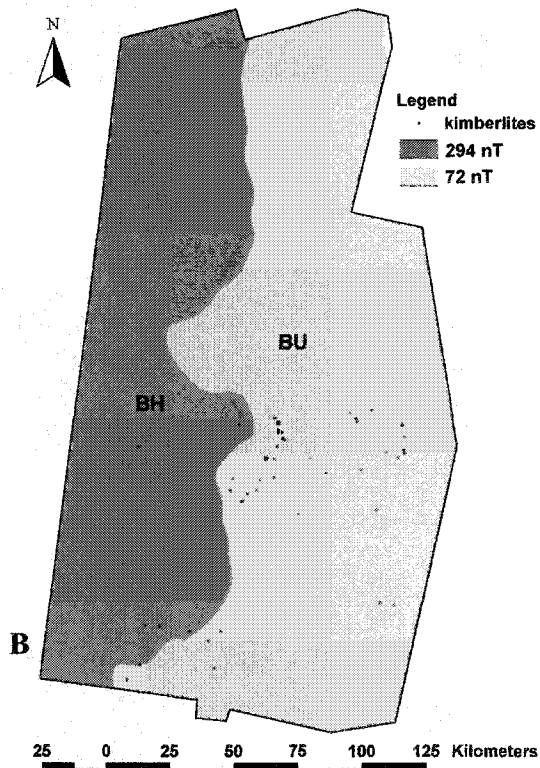


Figure 4.5A. Buffalo Head Hills kimberlite favourability map.

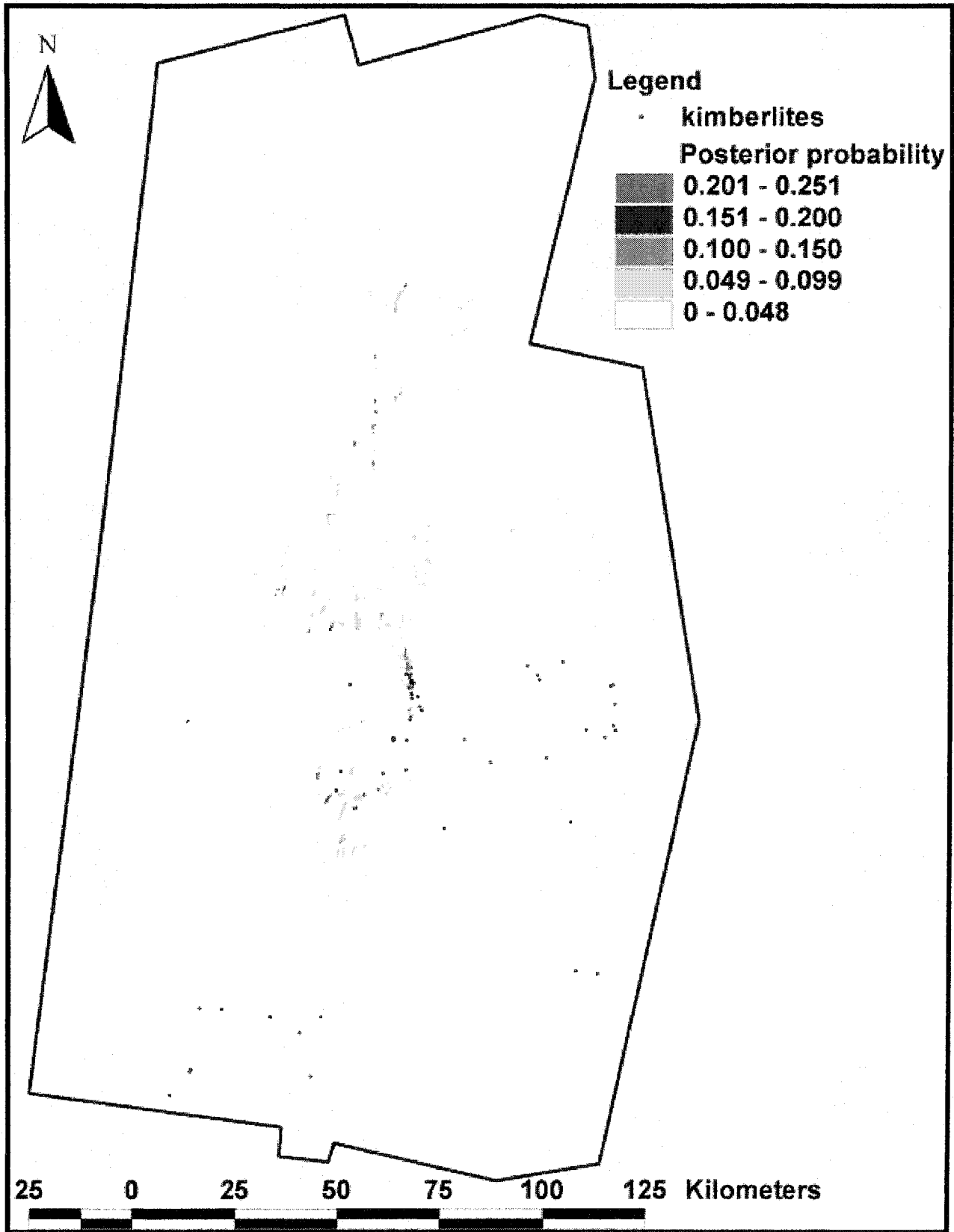


Figure 4.5B. Buffalo Head Hills kimberlite favourability map over the Bouguer gravity field draped on the Precambrian basement DEM shading (illumination azimuth 45°, elevation 70°) with structural trend from RADARSAT-1-PC2 (legend of posterior probability as in 4.5A).

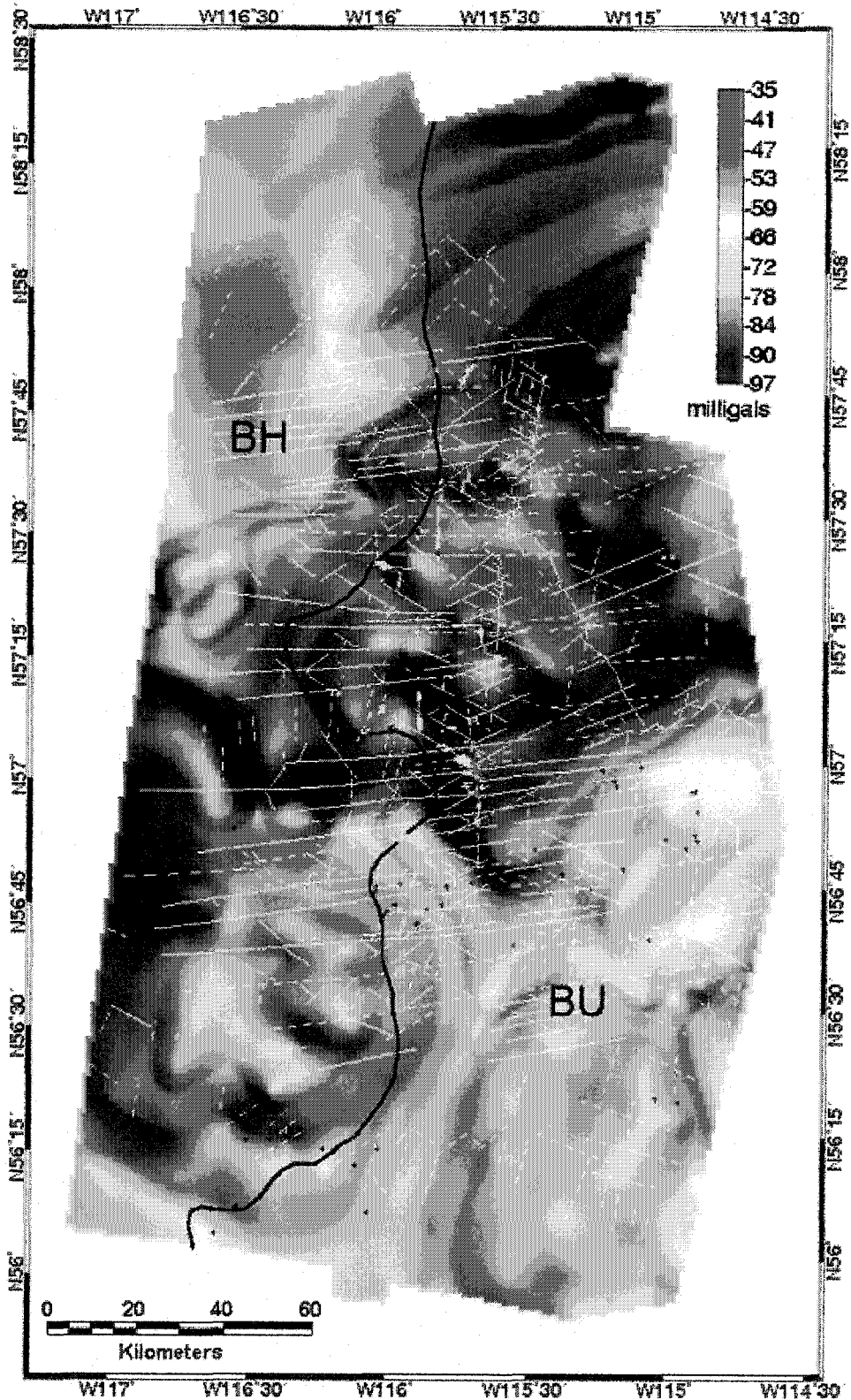
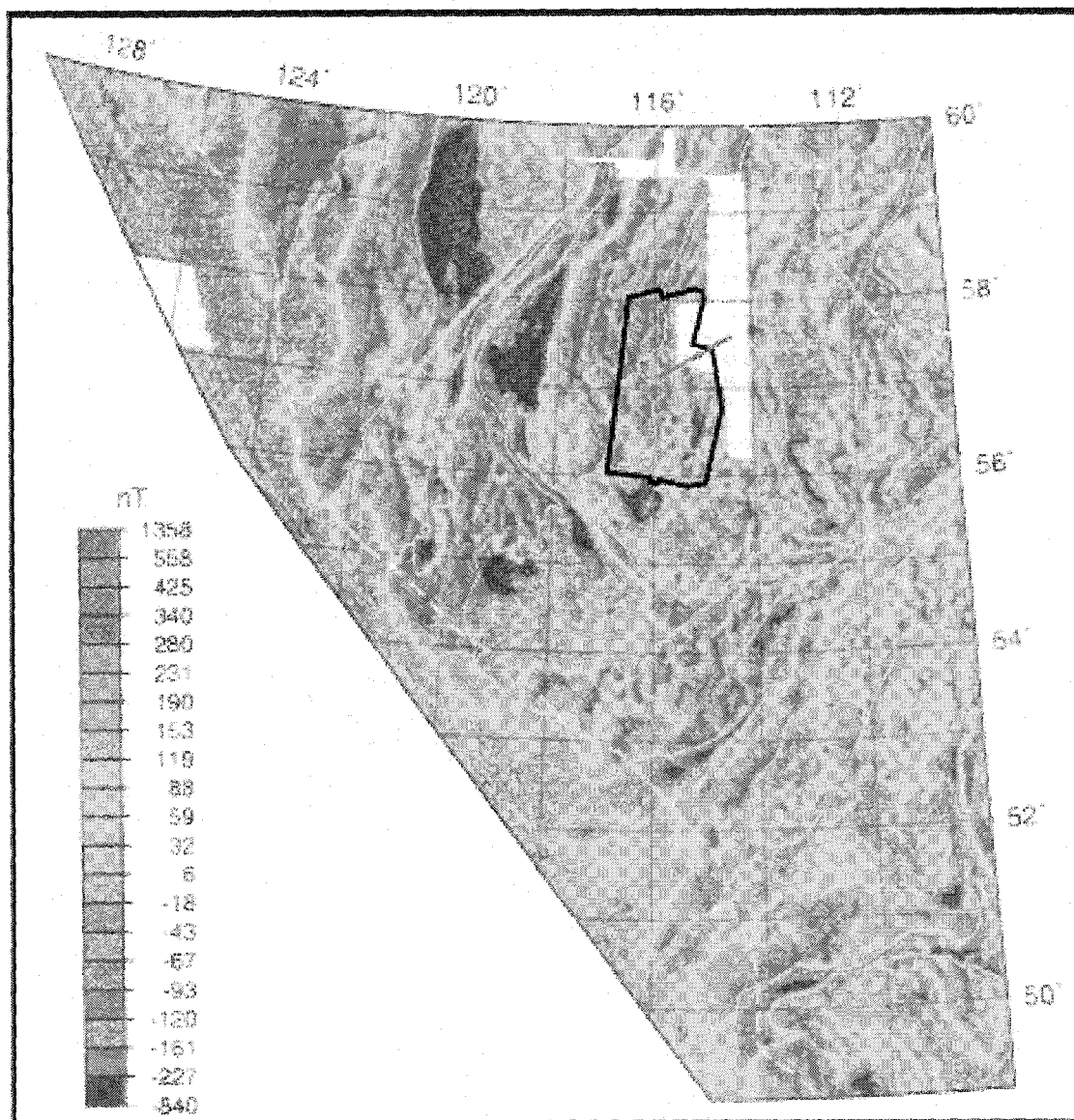


Figure 4.6. Buffalo Head Hills magnetic anomaly field. The dark-grey line indicates the possible susceptibility low with NE-SW trend (basement magnetic anomaly field from Pilkington et al., 2000).



Chapter 5

GENERAL DISCUSSION AND CONCLUSIONS

5.1 RADARSAT-1 CONTRIBUTION TO STRUCTURAL MAPPING AND EXPLORATION

In this thesis the approach in data selection, processing and interpretation of RADARSAT-1 imagery has been explored, and its contribution to structural mapping applications as an aid to oil/gas and kimberlite exploration has been demonstrated in two different study areas characterized by diverse geological setting, topography, and vegetation coverage. Integration with geophysical data, where available, has furthermore confirmed the suitability in the use of RADARSAT-1 imagery for structural mapping at a regional scale.

In the Blackstone area, radar imaging filtering techniques and integration with seismic data interpretation in a GIS environment enabled mapping of the continuity of geological structures in the central Alberta foothills. RADARSAT-1 imaging for regional scale mapping provides a complementary tool to traditional seismic data used in the foothills environment, which is of particular importance for oil and gas exploration.

In the Buffalo Head Hills study, structural data have been obtained from the interpretation of RADARSAT-1 principal component imagery. The structural data have been integrated with geological and geophysical data for the assessment and development of a statistical model for kimberlite exploration using GIS methods.

5.1.1 Blackstone study area, Foothills Canadian Cordillera

The synergy of RADARSAT-1 and seismic image interpretation has been applied in the Blackstone area of the central Alberta foothills in the Canadian Cordillera thrust and fold belt to map the continuity of geological structures, which are of importance for oil and gas exploration.

The surface features located on the radar images have been confirmed through seismic imaging, which helped in the definition of the deep expression of thrusts and related fold structures. RADARSAT-1 imaging provided important information for the connection along strike of geological structures with subtle surface expression.

The reconstruction of the continuity of thrust-fold-related major structures known in the area has been successful. Moreover, transverse faults and lineaments with ENE-WSW, NE-SW, and NNE-SSW trends have been delineated on the radar images. The ENE-WSW transverse faults have an extensional character, cut across the inner and outer Foothills, and are persistent at the regional scale. The NE-SW and NNE-SSW transverse faults are wrench-type faults, and are mainly localized in the inner Foothills. These structures have been identified for the first time in the area and are possibly a third generation fault-play type for oil and gas exploration.

The results of this work show that satellite radar imagery can greatly contribute to the structural and geological mapping of the foothills terrain, and are therefore a valuable aid for oil and gas exploration in analogous tectonic environments.

5.1.2 Buffalo Head Hills study area, Western Canada Sedimentary Basin

The study analyzed the suitability of Principal Component Analysis (PCA) of RADARSAT-1 images (Grunsky, 2001) to enhance interpretability of surface features for structural mapping applications. Four Principal Components (PCs) were extracted from the RADARSAT-1 Standard Beam Mode S1/S7 scenes acquired in ascending and descending orbit. The use of PCA minimizes the data redundancy inherent in the RADARSAT-1 scenes and creates component images that are characterized by a linear combination of the input data. These images emphasize the unique information contained in the source data as a response of the radar backscattering to surface roughness, soil dielectric properties, slope attitude, and vegetation canopy variations. The Feature Oriented Principal Components Selection (FPCS) method of Crosta and McMoore (1989) has been applied to examine the PCA eigenvector loadings, and to understand which principal component images will concentrate and enhance information directly related to the theoretical backscattering response of specific targets.

The application of the method to the Buffalo Head Hills, north central Alberta, a region of active kimberlite exploration, has shown that the RADARSAT-1-PC2 image optimizes topographic perception inherent in the RADARSAT-1 scenes, and retains information related to radar backscattering response to surface targets. This image therefore provides sufficient detail to outline the major lineaments characterizing the meso- and mega-scale structures of the Buffalo Head Hills (Paganelli et al., 2001a, b).

North and NNE-trending lineaments that bound the eastern edge of the Buffalo Head Hills along the Loon River valley were delineated, and are interpreted to be related

to Precambrian basement structures. A younger conjugate set of NW- and NE-trending lineaments that form block fault structures within the Buffalo Head Hills area and its eastern boundary has been outlined. These structures appear to be associated with Precambrian basement structures and the development of the Devonian Peace River Arch structures. ENE-trending lineaments have been identified as the latest structures, offsetting the N-, NNE-, and NW-trending structures and extending throughout the Buffalo Head Hills area. These lineaments have been attributed to extensional tectonics during the Laramide Orogeny (Late Cretaceous). Positive constraints on the outlined structural trends and history reconstruction have been provided by independent structural studies conducted by Ashton Mining Canada Inc. (AMCI), Alberta Energy Company (AEC), and the Alberta Geological Survey (AGS).

The statistical approach of weights of evidence method was used to determine the spatial relationship of the NNE-, NE-, NW-, and ENE-trending lineaments to known kimberlite locations (Paganelli et al., 2001c). The method revealed that the kimberlites have different degrees of spatial correlation with the analyzed lineaments, and that the highest correlations occur with the NNE, NE, and ENE lineaments. A weights of evidence model was then constructed using the structural lineament maps, the Buffalo High and Buffalo Utikuma terrane boundary, the Bouguer gravity anomaly, and magnetic characteristics of the Buffalo High and Buffalo Utikuma terranes. The model revealed maximum favourability for kimberlite exploration along the Buffalo High and Buffalo Utikuma terrane boundary in correspondence with NNE-trending lineaments and their intersections with NE and ENE lineaments.

From the statistical model, the relationship of the kimberlite occurrences along the Buffalo High-Buffalo Utikuma terrane boundary and structural lineaments seems to favour the hypothesis of kimberlite emplacement through a major zone of weakness within the basement, here characterized by the boundary between the Buffalo High and Buffalo Utikuma terranes.

5.1.3 Structural similarities at regional scale and their implications

In the Blackstone area, ENE-WSW transverse extensional faults, which cut across the inner and outer foothills, have been clearly identified and show similarities with the ENE-trending lineaments identified in the Buffalo Head Hills area. Although the two areas are characterized by completely different tectonic environments, these ENE-WSW lineaments/faults probably reflect the evidence of a common extensional tectonic event that occurred during the Late Cretaceous, which could be attributed to the onset of the Laramide Orogeny. The mechanism for the Late Cretaceous extensional faulting is interpreted to be flexural subsidence of the foreland plate and forebulge migration, generated by thrust loading along the continental margin of western North America during the Laramide Orogeny. This process is probably related to the subduction of the Farallon plate beneath North America. The Farallon plate was subducted beneath the length of the North American western seaboard (Figure 5.1, A) during the Laramide orogeny (Burgess (1997)). Mantle density contrasts and mass remobilization produced an effect of dynamic topography and forebulge migration, with E-W wavelength of thousands of km within the North American craton (Figure 5.1, B).

Late Cretaceous extensional faulting in the Buffalo Head Hills finds analogy in the Late Cretaceous differential sedimentation, stratal reorientation, and forebulge migration postulated in the Peace River Arch region by Chen and Bergman (1999).

At regional scale, the evidence of ENE-WSW lineaments in the Blackstone area, at the edge of the inner and outer Foothills of central Alberta, would be consistent with the regional scale tectonic event that affected all the continental margin of western Canada during the Laramide Orogeny. Evidence for ENE- and NE-trending lineaments has been outlined by Misra et al. (1991) throughout the transition of the Rocky Mountains region and the Foothills, and within the Western Canada Sedimentary Basin (WCSB).

Late Cretaceous extensional faulting, although characterized by general NW-SE strike, has been identified in southern Alberta, through the Lithoprobe Southern Alberta Lithospheric Transect (SALT1995) which extends from the triangle zone in the Foothills, to the Plains of southeastern Alberta within the WCSB by Lemieux (1999). These faults have been interpreted to be induced by flexural subsidence of the foreland plate, generated by thrust loading along the continental margin of western North America during the Laramide Orogeny.

5.2 KIMBERLITES IN CANADA

A recent compilation of locations and dates related to kimberlite magmatism in North America (Heaman et al., 2002) is reported here to illustrate the new

characterization of kimberlite occurrences within Canada. The Phanerozoic kimberlite magmatism in Canada has been divided into three main regions: (1) an eastern province (kimberlites in Ontario, New York, and Pennsylvania) dominated by Jurassic (180-140 Ma) magmatism (Heaman and Kjarsgaard, 2001); (2) a Cretaceous central province or corridor in Saskatchewan and Northwest Territories which includes the 103-94 Ma Somerset Island and 101-95 Ma Fort à la Corne fields (Kjarsgaard, 1996b; Leckie et al., 1997; Heaman and Kjarsgaard, 2002); (3) a western mixed age province defined by kimberlite fields of the Slave and Wyoming cratons. In the Slave craton, the ages of kimberlite emplacement range between ~50 and ~540 Ma (Heaman et al., 1997), including Eocene, Cretaceous, Jurassic, and Cambrian ages in relatively close spatial proximity (Heaman et al. 2002, and references therein). The western mixed age province fits with the description of a Type 3 kimberlite province (Mitchell, 1986) as suggested in Heaman et al. (2002). Type 3 provinces are characterized by kimberlite fields of different age and petrological character (Mitchell, 1986). Within the western mixed province, the Buffalo Head Hills kimberlites are characterized by a discrete magmatic event at 86-88 Ma (Carlson et al., 1999; Heaman et al, 2002).

Previous studies from Heaman and Kjarsgaard (2001, and references therein) have identified a correlation between the local and global timing of kimberlite magmatism in the eastern Jurassic province with a mantle plume model. A corridor of kimberlite magmatism younging from northwest to southeast, is precisely coincident with independent estimates for timing and location of continental extension related to the Great Meteor hotspot track (Heaman and Kjarsgaard, 2001). However, other Jurassic kimberlite occurrences in North America are not related to this hotspot, such as the

Jericho kimberlite pipes (173 Ma) in Nunavut, northern Slave Craton (Heaman et al., 2002).

In the Slave craton, the five dated kimberlites in the Ekati cluster have Rb-Sr phlogopite ages of 47.5 to 53.9 Ma (Heaman et al., 2002). Late Cretaceous-Eocene magmatism is common in western North America, and includes the 48 Ma Williams kimberlite (central Montana, Marvin et al., 1980). Eocene extension and associated magmatism is common throughout the Cordillera of North America and is generally attributed to steepening of the eastward-dipping Farallon plate subduction zone and concomitant upwelling of mantle asthenosphere (e.g., Lipman et al., 1972; Bird, 1992; O'Brien et al., 1995; Beitsprecher and Thorkelson, 2001). Although unclear at this stage, it is however possible that the Eocene kimberlite magmatism in the Lac de Gras region could be linked to distal mantle perturbations caused by changes in geometry of the Farallon plate subduction and ensuing Eocene crustal extension with upwelling of mantle asthenosphere as suggested by Heaman et al. (2002).

5.2.1 Buffalo Head Hills kimberlite emplacement model

This thesis has provided information in relation to the possible implications of basement structures and extensional fault systems that, at a crustal level, could have played a role for kimberlite emplacement in the Buffalo Head Hills. The structural controls at the high crustal level of kimberlite emplacement have been defined by the structural data and statistical models, and indicate that Late-Cretaceous ENE-trending extensional faulting, which represents a local and regional fracture pattern, may have an

important control. At deeper crustal levels, the structural analysis and a statistical model suggests that a major terrane boundary structure may control the ascent of the kimberlitic magma from the upper mantle. This structure is interpreted to be a deep-seated transition zone defined by the Buffalo High and Buffalo Utikuma terrane boundary. The Late-Cretaceous reactivation of this major zone of weakness, through the intersection with ENE-trending extensional faults, appears to play a role in the kimberlite emplacement in the Buffalo Head Hills area, which are located along a corridor with approximately N-S trend. However, a NE-SW trend is also defined by a cluster of kimberlites located across the Loon River Valley and the Peerless Uplands, which seems to follow another major magnetic low within the Buffalo Utikuma terrane (Figure 4.6). The author is not aware of any age determinations for this kimberlite cluster, and their disposition, at an angle with the major N-S trend observed along the Buffalo Head Hills, might indicate a different timing and feeder system for this kimberlite cluster. In the Buffalo Head Hills area there are no elements to clearly define the deep feeder system of the kimberlite field. Only one kimberlite (K14), along the Buffalo Head Hills eastern edge, has been sufficiently drilled to permit a near surface (0-200 m) geometric configuration, which is characterized by a flared, bowl-shaped structure with a central neck and marginal apron deposits of limited thickness (Carlson et al., 1999). Seismic profiles of other kimberlites in the area show similar near-surface flaring, and also suggest that kimberlites are vertically persistent at depth. The kimberlite pipes appear to be in the order of 40 to 150 m across at or near basement, at approximately 1600 m depth, suggesting a disruptive feeder system (Carlson et al., 1999). Deeper drilling would be required to clarify these relationships and constrain pipe geometry.

5.3 RECOMMENDATIONS FOR FUTURE STUDIES

The growing amount and accessibility of geophysical data, geological remote sensing information, and field geological data are leading to the more common use of GIS and IPS tools for qualitative and quantitative interpretation methods and studies. The main advantages in the use of remotely sensed data and digital integration methods are shown in this thesis to be cost-effective approaches to improving the understanding of structural features at a regional scale.

The optimization of remotely sensed data interpretation and integration requires a systematic approach in survey methodologies to establish interrelationships between the remotely sensed physical measurements and field observed geological features.

In the use of radar data, a useful approach would be the verification of the backscatter characteristics for specific surface targets, in order to outline differences in the effect of different conditions of exposure, soil moisture, and vegetation coverage. This approach would have been extremely useful for the analysis and interpretation of the RADARSAT-1-PC imagery, in which a statistical combination of N components (where N defines the number of input images) of the backscattering characteristics of the original RADARSAT-1 images is represented, and merged in the resulting RADARSAT-1-PC- i (with $i = 1$ to N) image.

The use of principal component analysis is new in the use of RADARSAT-1 images with variable look directions. Therefore, a problem of non co-planarity of the RADARSAT-1 images in ascending and descending mode integrated in the procedure

may exist. This should be a point for further study, in order to verify how this might affect the interpretation of surface features.

In the integration approaches using spatial analysis tools to determine spatial correlation of geological features, the results are obviously affected by the accuracy and quality of the interpretations. Visual interpretation is subject to the interpreter's knowledge and skill, and automatic feature extraction is a product that has yet to be verified and filtered of processing artifacts. However, the two approaches should eventually produce comparable results. Comparative analysis of the two methods should be applied in improving the capability of automatic feature extraction tools.

Thematic maps derived from interpreted remotely sensed data introduce a source of error when integrated and analyzed in a GIS environment to determine exploration strategies and or exploration target areas. Although, it has not been a topic developed in this study, it is however emphasized that such models are not absolute representations, and are dependent upon the number of datasets used as input maps, and the conditions imposed by the user. As well in this case, possible re-calibration of the model could be obtained through field tests, in order to verify the accuracy in the outlined favourable target areas, and therefore as a consequence to modify the initial conditions in the model to meet the field evaluations.

With the advanced technology in radar data acquisition, radar image characteristics will furthermore meet the user requirements for diverse applications in geology, and other geoscience disciplines to analyze the earth surface. The new RADARSAT-2 scheduled for launch in 2002, will be the first satellite to carry a fully polarimetric synthetic aperture radar (SAR) while providing continuity of acquisition

modes with RADARSAT-1. RADARSAT-2 will offer new capabilities such as selectable polarization, dual polarization, and quad polarimetric modes, as well as some higher resolution modes (RSIC, 2000). These new-generation of SAR systems, also called polarimeters, can measure the amplitude and phase of the reflected wave for the four available transmit and receive linear antenna polarizations [Horizontal-Horizontal (HH), Horizontal-Vertical (HV), Vertical-Horizontal (VH), and Vertical-Vertical (VV)], that will enable improved characterization of the physical properties of surface targets illuminated by the radar antenna.

REFERENCES

- Allegre, C.J. and Turcotte, D.L. (1985). Geodynamic mixing in the mesosphere boundary layer and the origin of oceanic islands. *Geophysical Research Letters*, Vol. 12, pp. 207-210.
- Breitsprecher, K., and Thorkelson, D.J. (2001). Spatial coincidence of the Kula-Farallon slab window with trench-distal volcanism of the Eocene Magmatic Belt in the southern Cordillera. SNORCLE Workshop, Lithoprobe Report 79, pp. 178-183.
- Bird, P. (1992). Deformation and uplift of North America in the Cenozoic era, in: K. R. Billingsley, H. U. Brown, III, and E. Derohanes (eds.), *Scientific Excellence in Supercomputing: the IBM 1990 Contest Prize Papers*, Baldwin Press, Athens, Georgia, Vol. 1, pp. 67-105.
- Burgess, P., Gurnis, M., Moresi, L. (1997). Formation of sequences in the cratonic interior of North America by interaction between mantle, eustatic, and stratigraphic processes. *Geological Society of America Bulletin*, Vol. 108, No. 12, pp. 1151-1535.
- Carlson, J.A., Kirkley, M.B., Thomas, E.M., and Hillier, W.D. (1999). Recent Canadian kimberlite discoveries. Seventh International Kimberlite Conference 1, pp. 81-89.
- Chen, D. and Bergman, K.M. (1999). Stratal reorientation, depositional processes, and sequence evolution of the Cretaceous in the Peace River Arch region of the Western Canada Sedimentary Basin. *Bulletin of Canadian Petroleum Geology*, Vol. 47, No. 4, pp. 594-620.
- Crosta, A.P. & McM. Moore, J. (1989). Enhancement of Landsat Thematic Imagery for residual soil mapping in SW Minas Gerais State, Brazil: a prospecting case history in Greenstone Belt Terrain. *Proceedings of the 7th (ERIM) Thematic Conference: Remote Sensing for Exploration Geology 2-6th October*, Calgary, Vol. II, pp. 1173-1187.
- Eccles, D.R., Grunsky, E.C., Grobe, M. and Weiss, J. (2000). *Structural emplacement model for kimberlitic diatremes in northern Alberta*. Report, Alberta Energy and Utilities Board, Alberta Geological Survey, March 2000, p. 116. (in press).
- Eggler, D.H. (1986). Kimberlites: How do they form?. In: *Kimberlites and Related Rocks. Their composition, occurrence origin and emplacement*. Geological Society of Australia Special Publication No. 14.
- Fraser, K.J., Hawkesworth, C.J., Erlank, A.J., Mirchell, R.H., and Scott-Smith, B.H. (1985). Sr, Nd and Pdisotopes and minor element geochemistry of lamproites and kimberlites. *Earth and Planetary Science Letters*, Vol. 76, pp. 57-70.
- Grunsky, E.C. (2001). The Application of Principal Components Analysis to Multi-beam RADARSAT-1 Satellite Imagery – A Tool for Terrain Mapping. *Canadian Journal of Remote Sensing*, (in press).
- Heaman, L.M., Kjarsgaard, B.A., Creaser, R.A., Cookenboo, H.O. and Kretschmar, U. (1997). Multiple episodes of kimberlite magmatism in the Slave Province, North America. Lithoprobe Workshop Report 56, pp. 14-17.

- Heaman, L.M., and Kjarsgaard, B.A. (2001). Timing of eastern North American kimberlite magmatism: continental extension of the Great Meteor hotspot track? *Earth and Planetary Science Letters*, Vol. 178, pp. 253-268.
- Heaman, L.M., and Kjarsgaard, B.A. (2002). A Cretaceous corridor of kimberlite magmatism: U-Pb results from the Fort à la Corne field, central Saskatchewan. Geological Association of Canada. Mineralogical Association of Canada Meeting in Saskatoon, Saskatchewan.
- Heaman, L.M., Kjarsgaard, and Craser, R.A. (2002). The timing of kimberlite magmatism and implications for diamond exploration: a global perspective. *Lithos*, (in press).
- Kjarsgaard, B.A. (1996b). Somerset Island kimberlite field, District of Franklin, N.W.T., In: *Searching for diamonds in Canada*, A.N. LeCheminant, D.G. Richardson, R.N.W. DiLabio and K.A. Richardson (eds.), Geological Survey of Canada Open File 3228, pp. 61-66.
- Leckie, D.A., Kjarsgaard, B.A., Bloch, J., McIntyre, D., McNeil, D., Stasiuk, L.S., and Heaman, L.M. (1997). Emplacement and reworking of Cretaceous, diamond-bearing, crater facies kimberlite of central Saskatchewan, Canada. *Geological Society of America Bulletin*, Vol. 109, pp. 1000-1020.
- Lemieux, S. (1999). Seismic reflection expression and tectonic significance of the Late Cretaceous extensional faulting of the Western Canada Sedimentary Basin in Southern Alberta. *Bulletin of Canadian Petroleum Geology*, Vol. 47, No. 4, pp. 375-390.
- Lipman, P.W., Prostka, J.J., and Christiansen, R.L. (1972). Cenozoic volcanism and plate tectonic evolution of the western United States. *Philosophical Transactions*, Royal Society of London Series A 271, pp. 217-248.
- Marvin, R.F., Hearn, B.C.Jr., Mehnert, H.H., Naeser, C.W., Zartman, R.E., and Lindsay, D.A. (1980). Late Cretaceous-Paleocene-Eocene igneous activity in north central Montana. *Isochron West*, Vol. 29, pp. 5-25.
- McKenzie, D.P. and O'Nions, R.K. (1983). Mantle reservoirs of ocean island basalts. *Nature*, Vol. 301, pp. 229-231.
- Misra, K.S., Slaney, V.R., Graham, D., Harris, J. (1991). Mapping of Basement and other tectonic features using SEASAT and Thematic Mapper in hydrocarbon-producing areas of the Western Sedimentary Basin of Canada. *Canadian Journal of Remote Sensing*, Vol. 17, No. 2, pp. 137-151.
- Mitchell, R.H. (1986). *Kimberlites*, Plenum Press, New York, 442 pp.
- Mitchell, R.H. (1995). *Kimberlites Orogenites and Related Rocks*. Plenum Press, New York.
- Mitchell, R.H., and Platt, R.G. (1984). The Freemans Cove volcanic suite: field relations, petrochemistry and tectonic setting of nephelinite-basanite volcanism associated with rifting in the Canadian Arctic Archipelago. *Canadian Journal of Earth Sciences*, Vol. 21, pp. 428-436.
- O'Brien, H.E., Irving, A.J., MaCallum, I.S., and Thirwall, M.F. (1995). Strontium, neodymium and lead isotopic evidence for interaction of post-subduction asthenospheric potassic mafic magmas of the Highwood Mountains, Montana,

- USA, with ancient Wyoming craton lithospheric mantle. *Geochimica et Cosmochimica Acta*, Vol. 59, pp. 4539-4562.
- Paganelli, F., Grunsky, E.C., and Richards, J.P. (2001b). Use of RADARSAT-1 Principal Component imagery for structural mapping: a case study in the Buffalo Head Hills area, northern central Alberta, Canada. *Canadian Journal of Remote Sensing*, (in press).
- Paganelli, F., Richards, J.P., and Grunsky, E.C. (2001c). Integration of structural, gravity, and magnetic data using the weights of evidence method as a tool for kimberlite exploration in the Buffalo Head Hills area, northern central Alberta, Canada. *Canadian Journal of Remote Sensing*, (in prep.).
- Plint, H.E. and Ross, G.M. (1993). ^{40}Ar - ^{39}Ar geochronology of selected crystalline basement samples from Alberta Basin: the timing of Proterozoic assembly of the subsurface of western Canada. In: *Radiogenic Age and Isotopic Studies: Report 7*. Geological Survey of Canada, Paper 93-2, p. 71-82.
- Pysklywec, R.N. and Mitrovica, J.X. (2000). Mantle flow mechanism of epeirogeny and their possible role in the evolution of the Western Canada Sedimentary Basin. *Canadian Journal of Earth Sciences*, Vol. 37, pp. 1535-1548.
- Ringwood, A.E. (1982). Phase transformations and differentiation in subducted lithosphere: implications for mantle dynamics, basalt petrogenesis, and crustal evolution. *Journal of Geology*, Vol. 90, pp. 611-643.
- RSIC (2000). Remote Sensing in Canada, Vol. 28, No.1. <http://www.ccrs.nrcan.gc.ca/ccrs/comvnts/rsic/2801/2801inde.html>(January 2002)
- Skinner, E.M.W. (1986). Contrasting group 1 and group 2 kimberlite petrology: towards a genetic model for kimberlites. In: *Fourth International Kimberlite Conference, Perth, Extended abstracts*. Geological Society of Australia, Abstract Series, Vol. 16, pp.202-204.
- Sleep, N.H. (1990). Montereian hotspot track: a long-lived mantle plume. *Journal of Geophysical Research*, Vol. 95, pp. 21983-21990.
- Smith, C.B. (1983). Pb, Sr, and Nd isotopic evidence for sources of southern African Cretaceous kimberlites. *Nature*, Vol. 304, pp. 51-54.
- Theriault, R.J. and Ross, G.M. (1991). Nd isotopic evidence for crustal recycling in the ca.2.0 Ga subsurface of western Canada. *Canadian Journal of Earth Sciences*, Vol. 28, pp. 1140-1147.

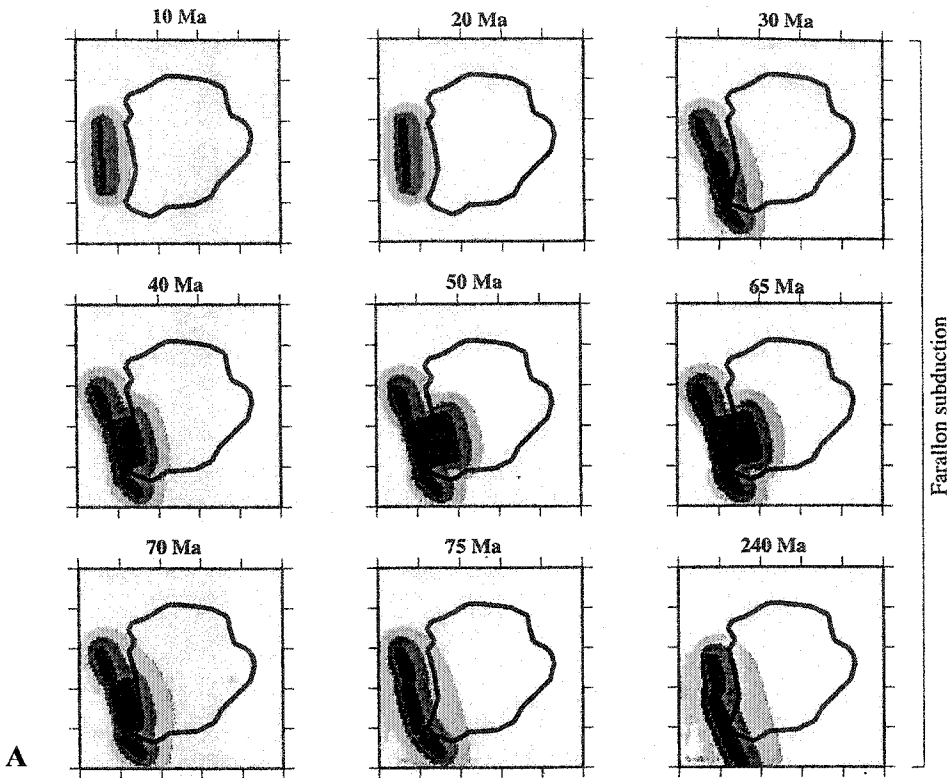
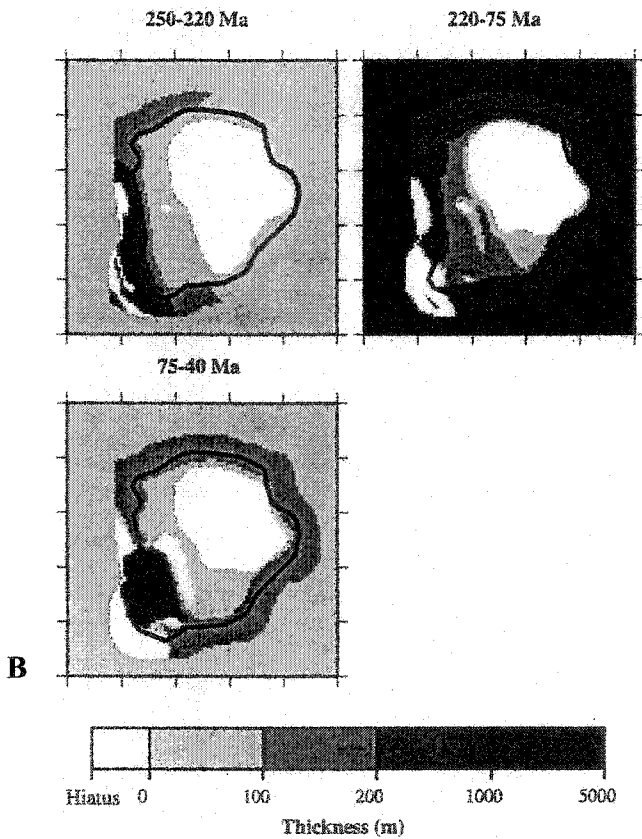


Figure 5.1. A) Farallon subduction sequence; B) model of Farallon subduction induced dynamic topography. The model is simulated within a confined area of 5000 km x 5000 km, defining a grid of 1000x1000 km² (from Burgess et al., 1997).



BIBLIOGRAPHY

Journal publications

- Paganelli F., Compagnoni R., Nervo R., Tallone S. (1995) - Il lembo Austroalpino di Eaux Rousses e le sue relazioni con la Zona Ophiolitica Piemontese nell'alta Valle di Cogne, Valle d'Aosta Meridionale. *Accademia Nazionale delle Scienze XL, Scritti e Documenti XIV. Atti del Convegno Rapporti Alpi-Appennino e guida alle escursioni*, p. 335-348.
- Paganelli F. and Rivard B. (2001) - Contribution of the integration of RADARSAT-1 and seismic imagery interpretation in the structural geology of the Central Alberta Foothills, Canada, as aid for oil and gas exploration. *Canadian Journal of Remote Sensing* (in press).
- Paganelli, F., Grunsky, E.C., and Richards, J.P. (2001b). Use of RADARSAT-1 Principal Component imagery for structural mapping: a case study in the Buffalo Head Hills area, northern central Alberta, Canada. *Canadian Journal for Remote Sensing* (in press).
- Paganelli, F., Richards, J.P., and Grunsky, E.C. (2001c). Integration of structural, gravity and magnetic data using the weights of evidence method as a tool for kimberlite exploration in the Buffalo Head Hills area, northern central Alberta, Canada. *Natural Resources Research* (submitted).

Conference proceedings and reports

- Paganelli F., Compagnoni R., Nervo R., Tallone S. (1994) - Assetto geologico-strutturale ed evoluzione metamorfica del lembo austroalpino delle Eaux Rousses e relazioni con le unita' della Falda Ophiolitica Piemontese (Cogne, Valle D'Aosta). *Convegno della Societa' Geologica Italiana sul tema: "Rapporti tra Alpi e Appennino"*, Riassunti, p.97-98.
- Paganelli F. (1996) - Synergy of RS data for geo-botanic applications: "Monitoring spectral characteristics of vegetation canopies influenced by anthropogenic dust deposition using integrated spectral and chemical data in Karvina forest ecosystem (Czech Republic). Report Human Capital and Mobility Program of the European Community "Synergy of Remotely Sensed Data": European Scientific Research Network, pp.90.
- Paganelli, F., Rivard B. (1999) - Tracking geological structures in the Central Alberta Foothills, Canada, using RADARSAT imagery (University of Alberta and Petro-Canada, unpublished)
- Paganelli F. and Rivard B. (1999) - Tracking geological structures in the Central Alberta Foothills, Canada, using RADARSAT imagery. *Proceeding 13th International*

- Conference and Workshops of Applied Geologic Remote Sensing, 1-3 March 1999, Vancouver, Canada, Vol. I, p.109.
- Paganelli, F. and Rivard B. (2000) - Reflectance and gamma-ray spectroscopy of carbonate rocks, Moose Mountain, Alberta, Canada. 1st Geomatics for Informed Decisions (GEOIDE) Conference, 25-26 May 2000, Calgary, Alberta, Canada.
- Paganelli, F. and Rivard B. (2000) - Reflectance and gamma-ray spectroscopy of carbonate rocks, Moose Mountain, Alberta, Canada. GeoCanada 2000 Geoscience Summit, 29 May-1 June 2000, Calgary, Alberta, Canada.
- Paganelli, F., Rivard B., Johnston S. (2000) - The Doornberg shear zone from RADARSAT-1 and Landsat7 TM, northeastern Namaqua Metamorphic Belt, South Africa. Geocongress 2000, 27th Earth Science Congress of the Geological Society of South Africa, 4-6 July 2000, Stellenbosh, South Africa.
- Paganelli, F. and Rivard B. (2000) - Reflectance spectroscopy of carbonate rocks, Moose Mountain, Alberta, Canada. 22nd Canadian Aeronautic and Space Institute Symposium (CASI), 21-25 August 2000, Victoria, British Columbia, Canada.
- Paganelli, F. and Rivard B. (2000) - Reflectance and gamma-ray spectroscopy of carbonate rocks, Moose Mountain, Alberta, Canada. Presented at the 14th International Conference and Workshops of Applied Geologic Remote Sensing, 6-8 November 2000, Las Vegas, Nevada, United States.
- Paganelli, F., Grunsky, E.C., and Richards, J.P (2001a). Structural interpretation of RADARSAT-1 Principal Component imagery and its potential application to kimberlite exploration in the Buffalo Head Hills area, Northern Central Alberta. Alberta Geological Survey, Earth Science Report 2001-03. Edmonton, Alberta, Canada: Alberta Energy and Utilities Board (in press).
- Paganelli, F., Grunsky, E.C., and Richards, J.P (2001d). RADARSAT and Landsat5 TM integration for kimberlite exploration in the Buffalo Head Hills area, northern central Alberta. Geological Association of Canada and Mineralogical Association of Canada, Joint Annual Meeting. Memorial University, St. John's, Newfoundland, May 27-30, p.110-111.
- Paganelli, F., Richards J.P., Grunsky E.C. (2001) - Structural Interpretation of RADARSAT-1 and Landsat5 TM images for kimberlite exploration in the Buffalo Head Hills area, North Central Alberta. 10th Calgary Mining Forum, Mineral Exploration Group (MEG), 18-19 April 2001, Calgary, Alberta, Canada.
- Paganelli, F., Richards J.P., Grunsky E.C. (2002) - Integration of structural, gravity and magnetic data using the weights of evidence method as a tool for kimberlite exploration in the Buffalo Head Hills area, Northern Central Alberta. *Proceedings of the 2002 International Geoscience and Remote Sensing Symposium - 24th Canadian Symposium on Remote Sensing*, 24-28 June, Toronto, Ontario, Canada (in press).

CURRICULUM VITAE

Flora Paganelli was born in Ruvo di Puglia (BA, Italy) on February 26, 1966. She completed secondary School at the Technical Institute for Informatics in Torino in 1986. She studied geology and completed a thesis in field-based lithological/structural mapping, and applied petrological/microstructural study of the polymetamorphic Austroalpine slice Eaux Rousses (Cogne-Valle D'Aosta, Western Alps, Italy) at the University of Torino (Torino, Italy), Faculty of Earth Sciences, where she received a B.Sc. degree in 1993. She did her M.Sc. research at the International Institute for Aerospace Survey and Earth Sciences (ITC), Geological Survey Division, of Enschede (The Netherlands), on the use of field spectral measurements (PIMA) and Landsat5 TM data modeling for environmental geo-botany investigation in the Ostrava-Karvina coal basin (Czech Republic), which led to her degree in 1996. In 1997 she held a one year internship as researcher at the Joint Research Centre of the European Commission (JRC), Space Advanced Techniques Institute (SAI; Ispra, Italy), working on SAR Differential Interferometry applied to ice flow dynamic and landslide monitoring. In 1998 she started her Ph.D. at the University of Alberta (Edmonton), Department of Earth and Atmospheric Sciences, where the research presented in this thesis was initiated.